



**HAL**  
open science

# From Short to Medium Range Order in Glasses and Melts by Diffraction and Raman Spectroscopy

James Drewitt, Louis Hennet, Daniel R. Neuville

► **To cite this version:**

James Drewitt, Louis Hennet, Daniel R. Neuville. From Short to Medium Range Order in Glasses and Melts by Diffraction and Raman Spectroscopy. *Reviews in Mineralogy and Geochemistry*, 2022, 87 (1), pp.55-103. 10.2138/rmg.2022.87.02 . hal-03857138

**HAL Id: hal-03857138**

**<https://hal.science/hal-03857138v1>**

Submitted on 17 Nov 2022

**HAL** is a multi-disciplinary open access archive for the deposit and dissemination of scientific research documents, whether they are published or not. The documents may come from teaching and research institutions in France or abroad, or from public or private research centers.

L'archive ouverte pluridisciplinaire **HAL**, est destinée au dépôt et à la diffusion de documents scientifiques de niveau recherche, publiés ou non, émanant des établissements d'enseignement et de recherche français ou étrangers, des laboratoires publics ou privés.

# From Short to Medium Range Order in Glasses and Melts by Diffraction and Raman Spectroscopy

**James W. E. Drewitt**

*School of Earth Sciences  
University of Bristol  
Wills Memorial Building  
Queens Rd  
Bristol, BS8 1RJ  
United Kingdom*

*james.drewitt@bristol.ac.uk*

**Louis Hennet**

*Conditions Extrêmes et Matériaux: Haute Température et Irradiation  
CEMHTI-CNRS, Université d'Orléans  
1d avenue de la Recherche Scientifique  
45071 Orléans cedex 2  
France*

*louis.hennet@cns-orleans.fr*

**Daniel R. Neuville**

*Géomatériaux  
CNRS-Institut de physique du globe de Paris  
Université de Paris  
1 rue Jussieu  
75005 Paris  
France*

*neuville@ipgp.fr*

## INTRODUCTION

The structure of glasses and the melts from which they are formed is intrinsically disordered, making their structural characterization difficult. Whilst the structure of solid minerals can be readily determined from the periodicity of the crystallographic unit cell, the absence of long-range symmetry in glasses and melts means their “unit cell” is essentially of infinite extent. However, although structurally disordered, the atomic-scale arrangements in glasses and melts are not strictly random. As detailed in chapter 2 by Henderson and Stebbins (2020, this volume), glasses typically exhibit a high degree of local short-range order (SRO) in the form of well-defined coordination polyhedra and chemical bond lengths, often similar to the corresponding crystal. This is illustrated in figure 1a for pure silica (SiO<sub>2</sub>) glass where, as for crystalline polymorphs of SiO<sub>2</sub>, every silicon atom is bonded to four oxygen atoms in tetrahedral units bonded to the next tetrahedron by a bridging oxygen atom.

In a glass, periodicity breaks down beyond the scale of a few atoms. Nevertheless, different patterns of medium range order (MRO), also called intermediate range order, may occur beyond the next nearest neighbour length-scale at  $\sim 5\text{-}20 \text{ \AA}$  ( $1 \text{ \AA} = 10^{-10} \text{ m}$ ) related to the topology of the glass network (Elliot 1991; Price 1996). Chemical ordering may also persist in some network glasses on extended length scales up to nanometer distances (Salmon and Zeidler 2013). In the silica glass example in figure 1a, substantial MRO arises from ring structures that enclose open regions in the network of corner shared  $\text{SiO}_4$  tetrahedra. Ring statistics (LeRoux and Jund 2010) or more recently persistent homology (Hiraoka et al. 2016; Hosokawa et al. 2019) techniques are commonly applied to characterize the nature of MRO arising from glass and melt network connectivity.

With the addition of other cations, the silicate network is disrupted with the formation of non-bridging oxygens (see chapter 2). Two models have been proposed to describe the structure of modified silicate glasses: the perturbed cation distribution (PCD) model (Lee and Stebbins 2003), and the modified random network (MRN) model (Greaves 1985). The PCD model assumes a relatively homogeneous distribution of modifier cations in the glass network. In contrast, the MRN model predicts the development of MRO formed by modifier cations in dynamic channels which percolate through the disrupted silicate tetrahedral network (figure 1b). While some evidence from experiments and simulations appears to substantiate the Greaves MRN model in alkali silicate glasses, the question of whether cation diffusion channels are a general feature of modified silicate glasses is yet to be resolved.

Diffraction (x-ray and neutron) and vibrational spectroscopies (Raman and IR) provide detailed information on SRO in glasses. Raman spectroscopy is also sensitive to MRO and can be exploited to identify ring structures in glasses. Pre-peaks observed in diffraction measurements of glasses can also be highly indicative of MRO. Combining the strengths of diffraction measurements, Raman spectroscopy, and computer simulation (Jahn 2020, this

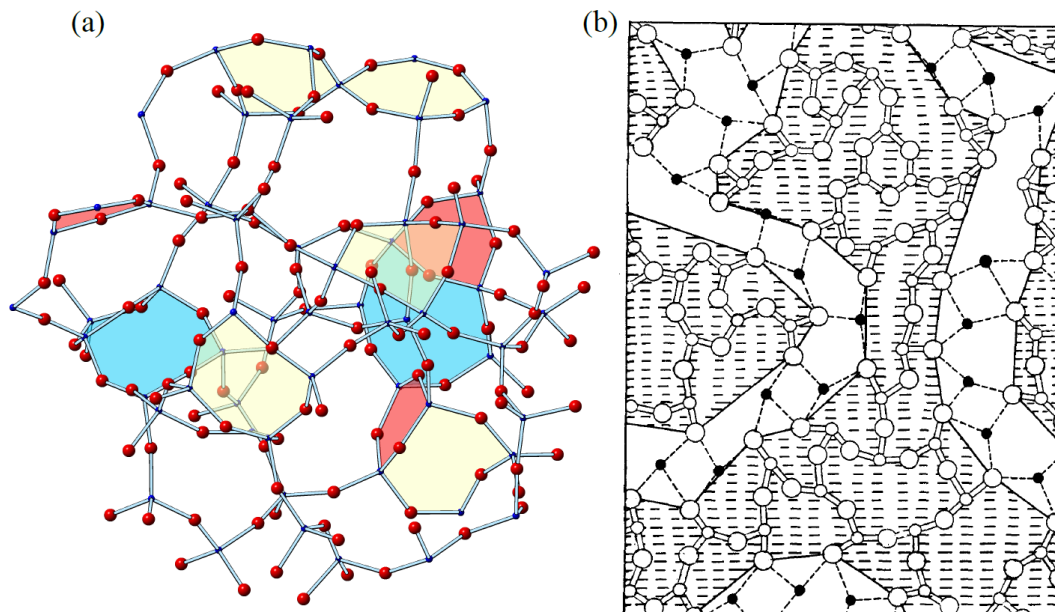


**Figure 1:** (a) Structural model of pure silica ( $\text{SiO}_2$ ) glass. 3-, 4-, and 5-membered rings of  $\text{SiO}_4$  tetrahedra are shown by the red, yellow, and blue shaded regions, respectively. Si = small blue spheres; O = large red spheres. Created using the  $\text{SiO}_2$  glass configuration from Le Roux and Petkov (2010). (b) The Greaves modified random network (MRN) model. Modifier cations (solid black circles with dashed lines denoting ionic bonds) form percolation channels in the covalently bonded glass network represented by open circles within the hatched region (Reprinted (permission pending) from Greaves 1985. © Elsevier.).

volume) enables detailed structural insight to be obtained on SRO and MRO in non-crystalline materials including glasses and their melts, offering a complementary perspective to the cationic environment probed by Nuclear Magnetic Resonance (NMR) or x-ray absorption spectroscopy.

In this chapter, we provide an overview of Raman spectroscopy and x-ray or neutron diffraction experiments to determine the SRO and MRO structure of geologically relevant silicate and aluminate glasses and their high-temperature ( $T$ ) melts under both ambient and high-pressure ( $p$ ) conditions.

## X-RAY, NEUTRON, AND RAMAN SCATTERING OF GLASSES AND MELTS

A brief overview of the theory of diffraction and Raman spectroscopy to obtain information on SRO and MRO in the atomic-scale structure in glasses and melts is provided in the following by reference to pure  $\text{SiO}_2$  (silica), one of the principal components of all-natural and most commercial silicate glasses. For more exhaustive theoretical treatment of x-ray and neutron diffraction studies of liquids and glasses we refer the reader to the reviews by Fischer et al. (2006), Hannon (2015), Benmore (2015), and Cormier (2019). For the theory of Raman scattering and required data treatment and normalization procedures for oxide glasses we recommend Rull (2012), Rossano and Mysen (2012), and Neuville et al. (2014).

### X-ray and neutron diffraction

X-ray diffraction (XRD), pioneered by M. von Laue, W. H. Bragg, and L. Bragg in the early 20<sup>th</sup> century, is a powerful tool for characterizing structure of materials at the atomic level. Although less widely available and requiring large-scale reactor or accelerator sources, diffraction by neutrons provides highly complementary information: while x-ray sensitivity increases with atomic number, the scattering power of neutrons varies between elements and

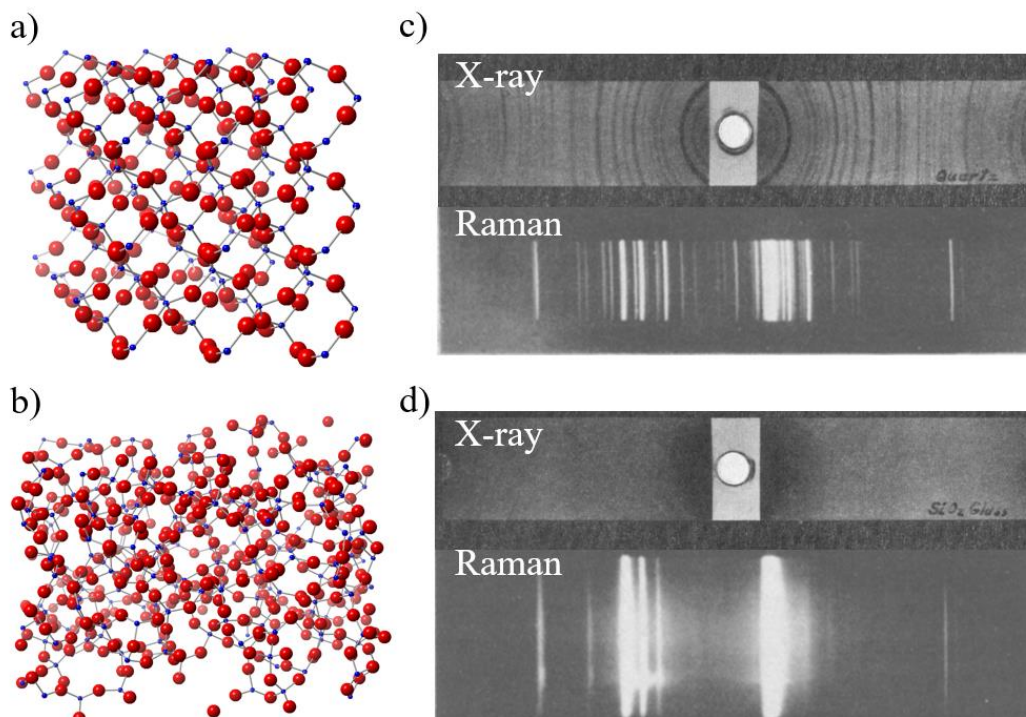


**Figure 2:** a) crystalline and b) amorphous structure of  $\text{SiO}_2$  (small blue spheres: Si atoms, large red spheres: O atoms) shown together with their corresponding x-ray diffraction (Warren 1934a) and Raman (Gross and Ramanova 1929) photographs in c) and d).

isotopes such that neutron diffraction is more sensitive to some light elements including oxygen.

Consider first a crystalline solid composed of atoms organized in a highly ordered repeating periodic arrangement in three dimensions (e.g. crystalline SiO<sub>2</sub>, figure 2a). The interatomic distances are of the order of Ångström, the same order of magnitude as x-ray wavelengths: a crystal thus constitutes a three-dimensional network which can diffract x-rays in accordance to Bragg's law, producing sharp constructive interference peaks associated with the crystalline lattice spacings. Similarly, inelastic light scattering from crystalline materials typically produces intense narrow bands corresponding to specific vibrational modes or chemical bonds. In the case of a non-crystalline solid (e.g. SiO<sub>2</sub> glass, figure 2b), the structure is disordered with no long-range translational periodicity such that diffraction patterns exhibit broad diffuse peaks. This is demonstrated by the first XRD patterns (Warren 1934a,b,c) measured for SiO<sub>2</sub> crystal (quartz) (figure 2c) and glass (figure 2d), with sharp intense peaks observed for the crystal diffuse features for the glass measurements. However, despite the structural disorder in glasses and melts, chemical bonding constraints give rise to a high degree of SRO which, together with MRO, is encoded in the diffuse scattering signal.

Diffraction provides information on liquid and glass structure by measurement of the structure factor,  $S(q)$ , obtained after processing the diffracted intensity, where the magnitude of the reciprocal space scattering vector  $q = 4\pi \sin \theta / \lambda$  for scattering angle  $\theta$  and x-ray or neutron beam wavelength  $\lambda$  (Fischer et al. 2006). The real space pair distribution function,  $G(r)$ , provides a measure of the probability of finding two atoms a distance  $r$  apart and is given by the Fourier transform relation

$$G(r) - 1 = \frac{1}{2\pi^2 r \rho_0} \int_0^\infty q [S(q) - 1] \sin(qr) dq, \quad (1)$$

where  $\rho_0$  denotes the atomic number density. For a glass containing  $n$  different chemical species, the  $S(q)$  and  $G(r)$  are comprised of a weighted sum of the Faber-Ziman partial structure factors  $S_{\alpha\beta}(q)$  (Faber and Ziman 1965) or partial pair distribution functions  $g_{\alpha\beta}(r)$  for  $n(n+1)/2$  atomic pairs for chemical species  $\alpha$  or  $\beta$ :

$$S(q) = \sum_{\alpha=1}^n \sum_{\beta=1}^n W_{\alpha\beta}^S S_{\alpha\beta}(q), \quad (2)$$

$$\text{and } G(r) = \sum_{\alpha=1}^n \sum_{\beta=1}^n W_{\alpha\beta}^G g_{\alpha\beta}(r). \quad (3)$$

For neutrons  $W_{\alpha\beta}^G = W_{\alpha\beta}^S = c_\alpha c_\beta b_\alpha b_\beta / (\sum_\alpha c_\alpha b_\alpha)^2$ , where  $c$  denotes concentration and  $b$  is the neutron scattering length (Sears 1992). X-ray form-factors are  $q$ -dependent and the  $S_{\alpha\beta}(q)$  weighting factors in XRD are  $W_{\alpha\beta}^S(q) = c_\alpha c_\beta f_\alpha(q) f_\beta^*(q) / (\sum_\alpha c_\alpha f_\alpha(q))^2$ , where  $f(q)$  and  $f^*(q)$  denote the complex atomic scattering factor and its conjugate (e.g. Waasmaier and Kirfel 1995). As such, the x-ray  $G(r)$  cannot be described in terms of simple weighted linear combination of  $g_{\alpha\beta}(r)$ . The Warren-Krutter-Morningstar (WKM) approximation (Warren 1936) in which  $W_{\alpha\beta}^S(q)$  is assumed to be independent of  $q$  such that the weighting factor  $W_{\alpha\beta}^G = W_{\alpha\beta}^S(q=0)$ , can be used to eliminate this complication. In most cases, the WKM is a good approximation, however an expansion to higher order can be made for improved accuracy (Masson and Thomas 2013). Alternatively, if a real-space peak of interest arises solely from

one distinct partial pair distribution function then its real-space weighting factor can be eliminated by division prior to Fourier transformation (Zeidler et al. 2009).

The average number of neighboring atoms in a coordination shell between  $r_1$  and  $r_2$  can be calculated by integrating the radial distribution function,  $RDF(r)$  (Fischer et al. 2006):

$$\bar{n}_\alpha^\beta = \int_{r_1}^{r_2} RDF(r) = 4\pi\rho_0 \int_{r_1}^{r_2} r^2 G(r). \quad (4)$$

The  $S(q)$  and  $G(r)$  functions measured for  $\text{SiO}_2$  (silica) glass by XRD are shown in figure 3 (Kohara and Suzuya 2005). The pronounced first sharp diffraction peak (FSDP) in  $S(q)$  at  $q_1=1.55 \text{ \AA}^{-1}$  is observed in many different glasses and is a signature of MRO in the glass with a periodicity  $2\pi/q_1$  (Price et al. 1989; Elliot 1991; Salmon 1994). The coherence length, which estimates the distance in real space over which the intermediate range ordering persists, is given by  $2\pi/\Delta q_1$ , where  $\Delta q_1$  full width at half maximum of the FSDP, estimates the distance in real space over which the MRO persists (Salmon 1994). Hence, a lower position  $q_1$  reflects increasingly longer-range order, and a sharper peak reflects MRO persisting for a longer distance in real space. The FSDP is highly sensitive to variations in MRO induced by  $p$ ,  $T$ , and compositional changes (discussed later).

Under ambient conditions, the FSDP observed in the  $S(Q)$  for  $\text{SiO}_2$  glass is attributed to tetrahedral units in ring arrangements (figure 1a). While information on the ring structure can potentially be extracted directly from its real-space representation (Shi et al. 2019), in practice simulation methods (Jahn 2020, this volume) are required to quantify the full nature of MRO and ring structure.

The oscillatory features in  $S(q)$  at high- $q$  relate to local structural ordering, as manifested in real-space peaks in  $G(r)$  at the characteristic interatomic distances of short-range chemical

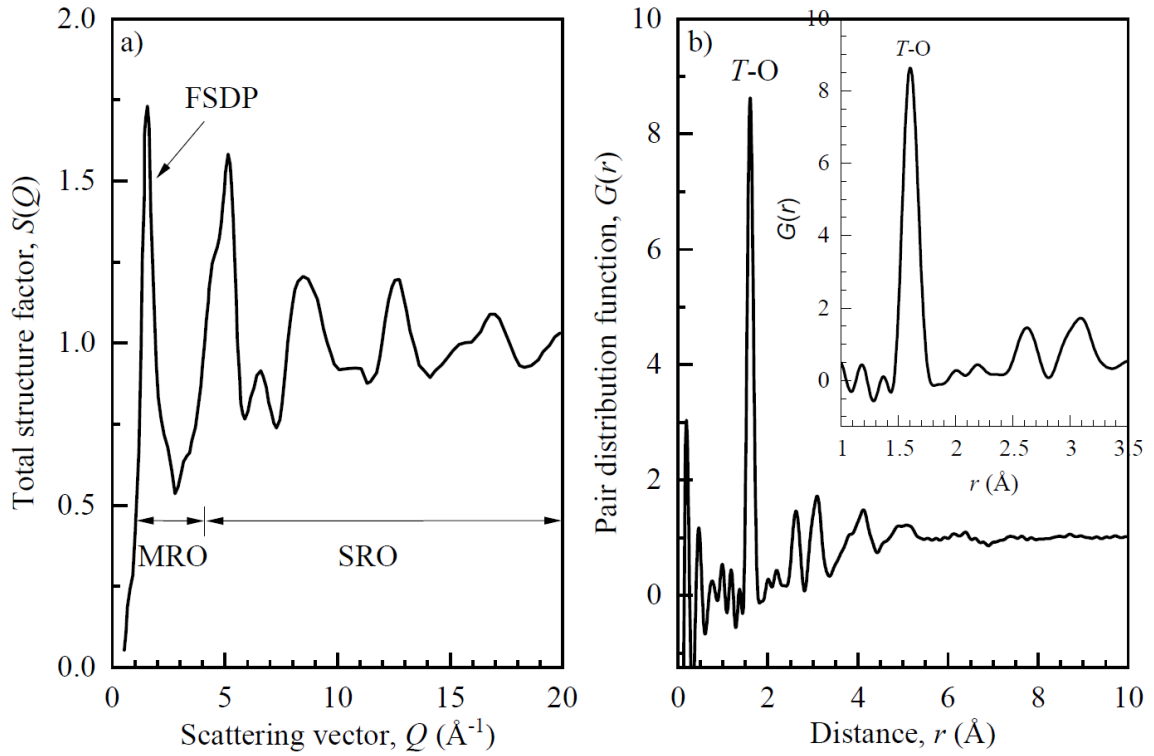


**Figure 3:** a) Total structure factor  $S(q)$  and b) pair distribution function,  $G(r)$ , for  $\text{SiO}_2$  glass, from synchrotron x-ray diffraction measurements reported by Kohara & Suzuya (2005). Regions of  $S(q)$  associated with SRO and MRO are indicated including the first sharp diffraction peak (FSDP).

bonds. The Fourier transform integral in equation 1 requires  $S(q)$  to be known to infinitely high  $q$  but in practice diffraction measurements have a finite maximum scattering vector,  $q_{\max}$ . While termination ripples can be minimized by multiplying  $S(q)$  by a smooth modification function that decays to zero at  $q_{\max}$  (Fischer et al. 2006), high-energy neutron or x-ray beams, and detectors that cover a wide range of scattering angles, are required to probe the bulk structure of glasses and melts with a sufficiently high  $q_{\max}$  for good resolution in  $G(r)$ . As such, these experiments are typically performed at large-scale spallation or reactor neutron sources, or synchrotron x-ray user facilities. The  $G(r)$  for pure silica glass (figure 3b) is dominated by the first peak at 1.60 Å, followed by a second peak at 2.61 Å, corresponding to the nearest neighbor Si-O and O-O bond distances in a SiO<sub>4</sub> tetrahedron, respectively. The angle O-Si-O calculated from these two distances using the law of cosines is very close to the perfect intra tetrahedral angle. The  $G(r)$  becomes increasingly featureless at distances greater than ~ 6 Å due to the lack of long-range ordering.

## Raman Spectroscopy

Raman spectroscopy, discovered by C. V. Raman and K. S. Krishnan in 1928 using filtered sunlight, relies on the inelastic scattering of light and provides information on the vibrational modes in the system. In principle, vibrational spectroscopy is possible using any source of monochromatic light, including x-rays. Raman spectroscopy in most modern laboratory settings typically employs laser light from near ultraviolet to visible and near infrared wavelengths in the order of  $10^{-6}$ - $10^{-7}$ m (energy ~ 1-10eV, frequency ~  $3 \cdot 10^{14}$ - $3 \cdot 10^{15}$  Hz).

In a Raman experiment, a sample is irradiated by a focused beam of monochromatic laser light with wavelength  $\lambda_0$  and energy  $E_0 = hc/\lambda_0$ , where  $h$  is Planck's constant and  $c$  the speed of light. Most of the incident photons undergo an elastic scattering process (Rayleigh scattering) with the energy of the scattered light  $E = E_0$ . A small fraction of the incident photons exchange energy with molecular bond vibrations producing very weak inelastic Raman scattering intensity with energy  $E = E_0 \pm E_m$ . Here  $E_m = hc/\lambda_m$  corresponds to the energy of an elementary excitation of a molecule measured in Raman spectroscopy relative to the incident energy  $E_0$ . If a photon is absorbed, exciting the molecule to a higher vibrational mode, then  $E < E_0$  and the measured intensities are referred to as 'Stokes' lines. Alternatively, if the molecule is de-excited into a lower vibrational mode then a photon with  $E > E_0$  is emitted giving rise to 'Anti-Stokes' lines. The 'Anti-Stokes' intensity is typically weaker and normally only the 'Stokes' side of the Raman spectrum is measured.

In practice, Raman spectra are expressed as a function of wavenumber (in  $\text{cm}^{-1}$ ) instead of the energy with the Raman shift of the vibrational mode given by:

$$\Delta\omega = \frac{1}{\lambda_0} - \frac{1}{\lambda_m}.$$

Raman active vibration modes are determined by selection rules, where only molecular excitations that result in a change in polarizability will produce a Raman signal (Rull 2012).

Raman spectroscopy provides a spectral signature of a given material. The position of the Raman lines or bands are characteristic of the composition and the intensities correlate with the concentration of the chemical species. The line width can provide information including the size of crystallites in polycrystalline materials or the degree of structural disorder. Like diffraction measurements, glasses and disordered materials yield broad diffuse Raman peaks (figure 2d). The Raman spectrum of SiO<sub>2</sub> glass and two crystalline polymorphs, quartz and cristobalite, are shown for comparison on figure 4. The Raman spectrum of silica glass has been



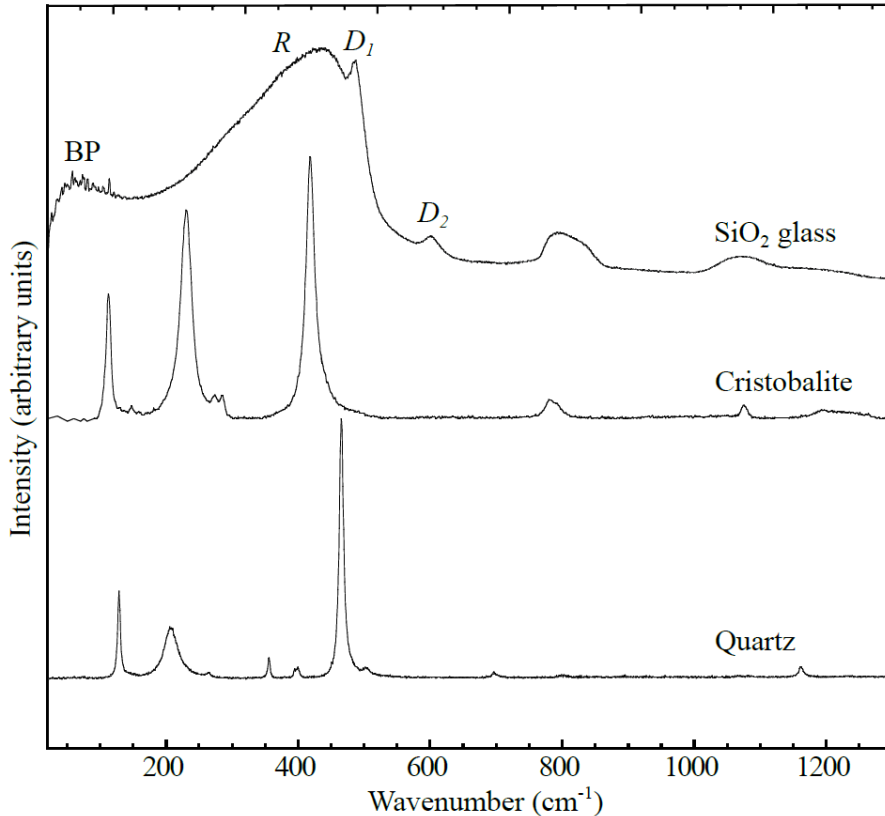


**Figure 4:** Raman spectra of SiO<sub>2</sub> polymorphs: quartz, cristobalite and glass (redrafted from Neuville et al. (2014)). See the text for the assignment of the BP, R, D<sub>1</sub>, D<sub>2</sub>, and other peaks in the glass spectrum.

well characterized and, as described in chapter 2 (Henderson and Stebbins 2020, this volume) the specific Raman bands annotated in figure 4 can be attributed to distinct vibrational features.

The Boson peak (BP) at  $\sim 80 \text{ cm}^{-1}$ , so-called because the temperature dependence of the peak intensity obeys Bose-Einstein statistics, is a ubiquitous yet controversial feature of glass Raman spectra (Nakayama 2002) which may be a signature of longer-range vibrational structure (discussed in more detail below). The Raman spectrum below  $\sim 1000 \text{ cm}^{-1}$  has a strong sensitivity to MRO, typically related to Si-O-Si breathing modes from SiO<sub>4</sub> tetrahedra in ring arrangements (Sharma et al. 1981; Galeener, 1982a,b; Galeener et al. 1983; Geissberger and Galeener 1983; Barrio et al. 1993; McMillan et al. 1994; Pasquerello and Car 1998; Umari & Pasquarello, 2002; Umari et al., 2003; Rahmani et al. 2003; Kalampounias et al. 2006). The broad peak at  $440 \text{ cm}^{-1}$  (R) corresponds to bending vibrations associated with the broad distribution of inter tetrahedral Si-O-Si angles in  $n$ -membered rings with  $n > 5$ . The narrow D<sub>1</sub> ( $\sim 495 \text{ cm}^{-1}$ ) and D<sub>2</sub> ( $\sim 606 \text{ cm}^{-1}$ ) bands are associated with the well-defined bending Si-O-Si modes in 4- and 3-membered rings, respectively. The asymmetric peaks centered at  $\sim 800 \text{ cm}^{-1}$  and  $\sim 1070 \text{ cm}^{-1}$  are attributed Si-O stretching vibrations in SiO<sub>4</sub> tetrahedra (McMillan 1984, Sarnthein et al. 1997, Kalampounias et al. 2006).

### ***The Boson Peak: A signature of SRO or MRO?***

The BP observed in Raman, inelastic neutron, and infrared spectroscopy arises from excess low frequency,  $\omega$ , contributions in THz range of the vibrational density of states (VDOS),  $g(\omega)$  compared to the Debye elastic continuum model [ $g(\omega) \propto \omega^2$ ] obeyed by crystalline materials. The BP appears to be a universal feature of inorganic glasses; however, its origin remains



controversial and several competing theories have been developed (Nakayama 2002; Greaves and Sen 2007; Brink et al. 2016; Wang et al. 2018; Baggiolo and Zaccone 2019).

The soft-potential model has been used to explain the BP (Buchenau et al. 1992; Gurevich et al. 1993; Parshin 1993), in which quasi-localised vibrational modes are associated with “defects” in the disordered structure (Laird and Schober 1991). Quasi-local vibrations caused by linked “rigid” SiO<sub>4</sub> tetrahedra which rotate against each other without distortion are offered as an explanation for the BP in the Raman spectrum of pure SiO<sub>2</sub> glass (Buchenau et al. 1986; Taraskin and Elliot 1999; Hehlen et al. 2000, 2002). However, the ubiquity of the BP in a wide range of glasses indicates the requirement for a more generalized interpretation.

Experimental evidence for a correlation between the positions of the FSDP and BP in some glasses is strongly suggestive of a connection to MRO (Novikov and Sokolov 1991; Sokolov et al. 1992; Börjesson et al. 1993; Price 1996). Several interpretations of the BP invoke a degree of MRO or extended range ordering, including nano-structured clusters (Duval 1986; Mermet et al. 1996), density fluctuations intrinsic to the disordered structure (Elliot 1992), or heterogeneity in the elastic constant producing “soft” regions in the material (Sokolov 1999; Schirmacher et al. 2007; Schirmacher 2013; Schirmacher et al. 2015; Marruzzo et al. 2013). Recent Raman measurements showing an increase in BP intensity on substitution of Na by K in aluminosilicate glasses indicates that the BP may be related to the development of nano-structured percolation channels (Le Losq et al. 2017).

Another explanation indicates there is a relationship between the BP and the glass transition temperature ( $T_g$ ) associated with marked changes in MRO at  $T_g$  (Levelut et al. 1995; Takahashi et al. 2009; Stavrou et al. 2010; Tomoshige et al. 2019), where theoretical interpretations predict a phonon-saddle transition (Grigera et al. 2003). Alternatively, it has been suggested that the BP simply originates from a broadening or shift of the lowest Van Hove singularity of the corresponding crystalline state (Taraskin et al. 2001; Chumakov et al. 2011) and as such relates to SRO in the glass.

## MULTICOMPONENT SILICATE GLASSES

Natural glasses and melts contain a variety of oxide components, typically including SiO<sub>2</sub>, Al<sub>2</sub>O<sub>3</sub>, MgO, CaO, FeO, and other metal oxides. A conventional structural model of a multi-component silicate glass is illustrated in figure 5a. Here, the small Si<sup>4+</sup> or Al<sup>3+</sup> cations are the network formers, denoted  $T$ , bonded to 4 oxygen atoms in tetrahedral units interlinked by bridging oxygen (BO) atoms to form the backbone of a network structure with three, four, five, and more membered rings. Larger lower-charged cations, denoted  $M$  (e.g. alkaline, alkaline-earth, other metal cations), adopt varying roles as either charge compensators or network modifiers forming larger structural motifs and perturbing the network structure via the formation of non-bridging oxygen (NBO) atoms.

An example of a pair distribution function  $G(r)$  for this silicate glass model is shown in figure 5b featuring three distinct peaks which can be attributed to local structural ordering; the first from nearest neighbour intra tetrahedral bonds ( $T$ -O), the second peak arising from cation-oxygen ( $M$ -O) or oxygen-oxygen (O-O) distances, and the third peak and features at higher distances due to tetrahedra-cation ( $T$ - $M$ ), tetrahedra-tetrahedra ( $T$ - $T$ ), cation-cation ( $M$ - $M$ ) correlations. As discussed earlier, for a glass containing  $n$  different chemical species the  $G(r)$  comprises a weighted sum of  $n(n+1)/2$  individual partial pair correlations. Due to the complexity of these overlapping atom-atom correlations it becomes increasingly difficult to assign peaks to specific structural features in higher-order coordination shells at length scales greater than  $\sim 3$  Å. However, information on these correlations may be obtained by making a systematic survey of simple systems, or individual partial pair correlations may be resolved directly by using specialist element selective techniques such as neutron diffraction with isotope

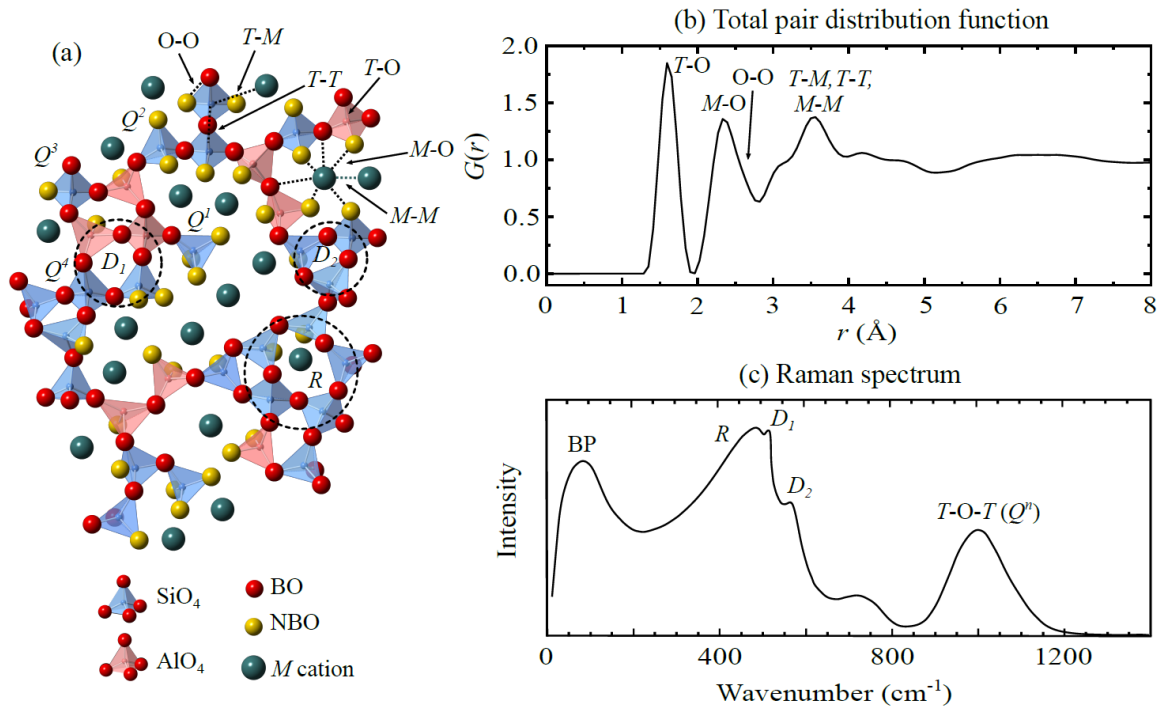


**Figure 5:** (a) Schematic of a model aluminosilicate glass structure, where network formers  $T=\text{Si}$ , Al are represented by the small blue spheres, bridging and non-bridging oxygen atoms by the red and gold spheres, and modifier cations  $M$  in green. (b) The corresponding pair distribution function  $G(r)$  and (c) Raman spectrum are shown with specific peaks corresponding to specific SRO and MRO structural features highlighted.

substitution (NDIS). This method exploits the contrast in neutron scattering length for isotopes of the same element by measuring the diffraction patterns of two or more samples that are identical in every respect, except for the isotopic enrichment of one or more element. Using different function methods, these patterns are subtracted to extract the correlations involving the substituted species. The resolution of structural information on a partial pair distribution function level using NDIS, as well as conventional total scattering measurements, offer a rigorous test of the efficacy of molecular dynamics (MD) simulations (Jahn 2020, this volume) which can provide a full-picture of glass and melt structure and properties.

An example Raman spectrum for the model multicomponent silicate glass structure is shown in figure 5c. The biggest difference compared to the spectrum of pure  $\text{SiO}_2$  glass (figure 4) is in the appearance of a strong peak in the high wavenumber region centered at around  $1100 \text{ cm}^{-1}$ . This intensity arises from  $T-O$  stretching vibrations in different tetrahedral species with  $n$  BO and  $4-n$  NBO: i.e. the  $Q^n$  units, from isolated ( $Q^0$ ) to fully polymerized tetrahedra ( $Q^4$ ) (see chapter 2 by Henderson and Stebbins (2020, this volume) and discussion therein).

## Binary silicate glasses

In the following, we present some x-ray diffraction (XRD) and Raman measurements of binary silicate glass compositions in the system  $(\text{MO})_x(\text{SiO}_2)_{1-x}$  for  $M = \text{Li}_2, \text{Na}_2, \text{K}_2, \text{Mg}, \text{Ca}, \text{Ba}, \text{Pb}$ , with mole fraction  $x$  from 0 to 0.7 and discuss the effect of the network modifier on the silicate glass network. The results presented illustrate all of the salient features observed in the  $G(r)$  functions and Raman spectra of binary silicate glasses and melts. Specific compositions are denoted by concatenating the element  $M$  with the mole fraction in per cent  $X$  ( $\text{MX}$ , e.g.  $\text{Ca50} = (\text{CaO})_{0.5}(\text{SiO}_2)_{0.5}$ ).

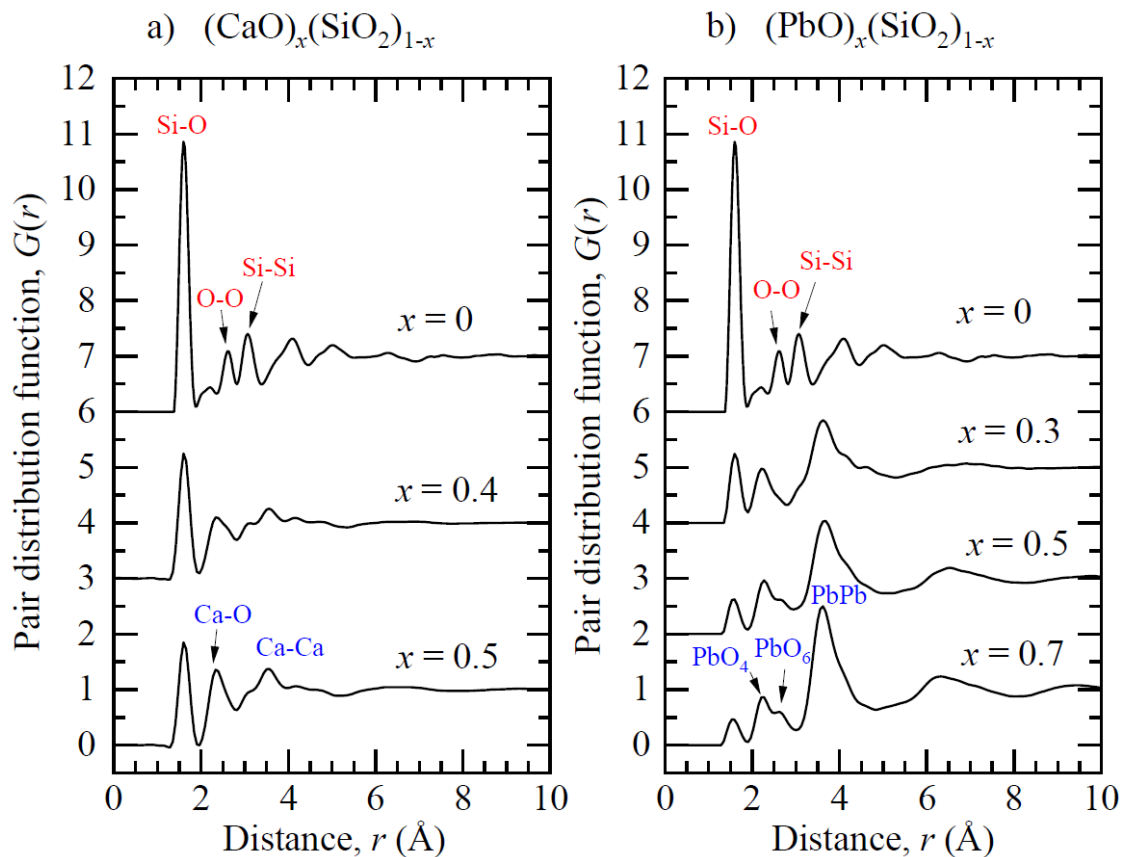


**Figure 6:** Total pair distribution functions  $G(r)$   $\text{SiO}_2$  and silicate glasses in the system  $(\text{MO})_x(\text{SiO}_2)_{1-x}$  for a)  $M = \text{Ca}$  and b)  $M = \text{Pb}$  (previously unpublished x-ray diffraction measurements made at beamline ID11 at the European Synchrotron Radiation Facility (ESRF), Grenoble, France).

### Diffraction measurements

First, we consider x-ray pair distribution functions  $G(r)$  measured for Ca- and Pb-silicate glasses shown in figure 6 which have features typical for all alkali, alkaline earth, and metal-oxide silicate glasses. The first peak between 1.6 and 1.7 Å arises from the nearest neighbour Si-O bond, with its intensity and variation dependent upon the nature of the  $M$  cation and the proportion of silica. The peak is relatively insensitive to the proportion of NBO as the difference in Si-BO or Si-NBO bond lengths is less than 0.05 Å (Cormack and Du 2001; Du and Cormack 2004). On addition of CaO we observe a peak at 2.3 Å arising from Ca-O bonds in Ca-centered polyhedra with an average 6-fold coordination by oxygen. New Ca-Ca correlations also give rise to a peak at ~ 3.5 Å. With increasing CaO fraction, both the Ca-O and Ca-Ca peaks become progressively more significant with a corresponding reduction in height of the Si-O peak. This is even more evident in the  $G(r)$  functions measured for Pb-silicate glasses, due to the high atomic number of Pb ( $Z=82$ ) compared to Si, O, or Ca, leading to a higher x-ray scattering cross-section. At high Pb concentrations ( $x > 0.5$ ) two clear Pb-O peaks at 2.2 Å and 2.6 Å are resolved, corresponding to Pb in 4- and 6-fold coordination, respectively.

NDIS is a powerful tool for isolating weaker, heavily overlapped pair correlations. Figure 7 shows the first order (Eckersley et al. 1988) and second order “double” (Gaskell et al. 1991) difference functions from  $^{44}\text{Ca}^{\text{nat}}\text{Ca}$  NDIS measurements of  $\text{CaSiO}_3$  (Ca50) glass (with 3 mol. %  $\text{Al}_2\text{O}_3$  added to prevent nucleation, Eckersley et al. 1989). The results reveal well

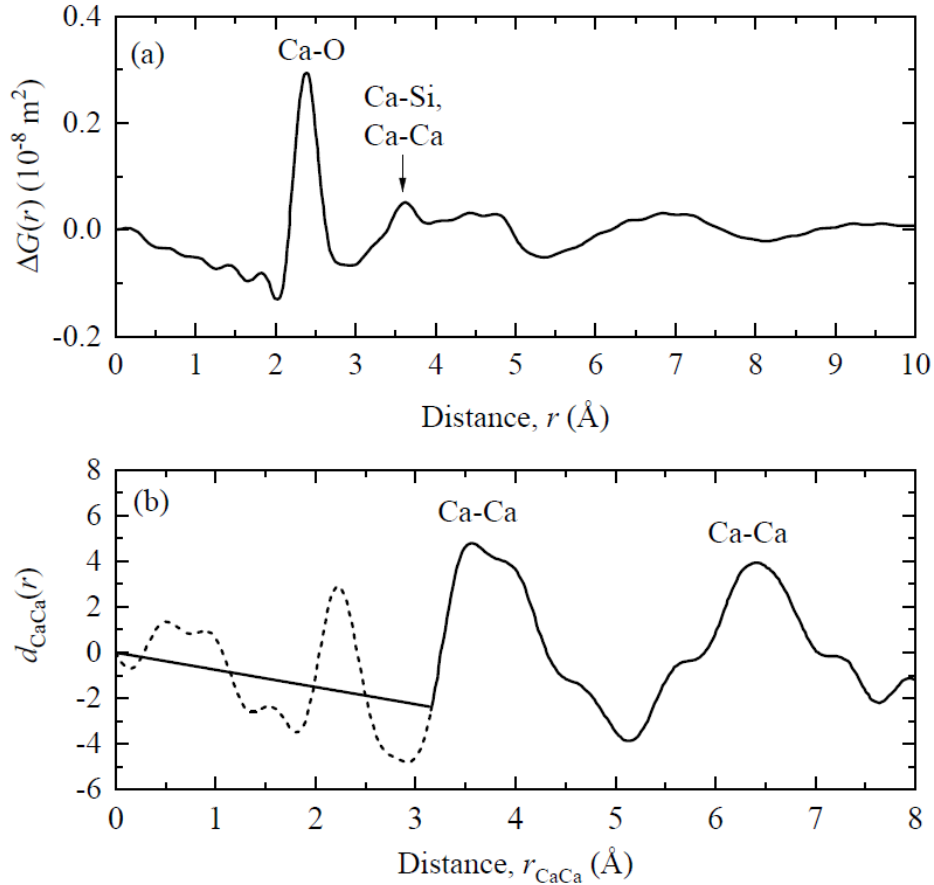


**Figure 7:** (a) First order difference function  $\Delta G(r)$  and (b) reduced partial pair distribution function  $d_{\text{CaCa}}(r) = 4\pi r \rho [g_{\text{CaCa}}(r) - 1]$  by double difference from the  $^{44}\text{Ca}/^{nat}\text{Ca}$  NDIS results reported in Eckersley et al. (1989) and Gaskell et al. (1991) for  $(\text{CaO})_{0.48}(\text{SiO}_2)_{0.49}(\text{Al}_2\text{O}_3)_{0.03}$  glass. The dashed curve in (b) below the first Ca-Ca interatomic distance arises in part from an incomplete subtraction of partials  $g_{\alpha\beta \neq \text{CaCa}}(r)$ .

defined Ca-O and Ca-Ca distances indicating ordering of the modifier  $\text{Ca}^{2+}$  cations up to  $10 \text{\AA}$ . Originally attributed by Gaskell et al. to sheets of edge shared  $\text{CaO}_6$  octahedra, subsequent MD simulations reveal this cationic ordering on medium range length scales arises from chainlike linkages or channels of Ca-centered polyhedra (Mead and Mountjoy 2006; Benmore et al. 2010; Skinner et al. 2012a; Cormier and Cuello 2013). A similar distribution of Mg-centered polyhedra contributing to MRO is observed from a  $^{25}\text{Mg}/^{nat}\text{Mg}$  NDIS study of  $\text{MgSiO}_3$  glass (Cormier and Cuello 2011). These inhomogeneous distributions of cation centered polyhedra pervading the silicate network appears to substantiate the Greaves MRN model (figure 1b). Further NDIS measurements of the development of cationic ordering on vitrification of oxide melts are discussed later in this chapter.

### ***Raman spectroscopy measurements***

We now consider unpolarized Raman spectra for full range of  $M$ -silicate compositions are shown in figure 8, for which distinct and progressive changes are observed with the type and proportion of  $M$  cation content. In the following, we discuss the structural information provided by these spectra with respect to the four key spectral regimes; the boson ( $20\text{-}200 \text{ cm}^{-1}$ ), low ( $200\text{-}600 \text{ cm}^{-1}$ ), intermediate ( $600\text{-}800 \text{ cm}^{-1}$ ), and high ( $800\text{-}1200 \text{ cm}^{-1}$ ) wavenumber regions.

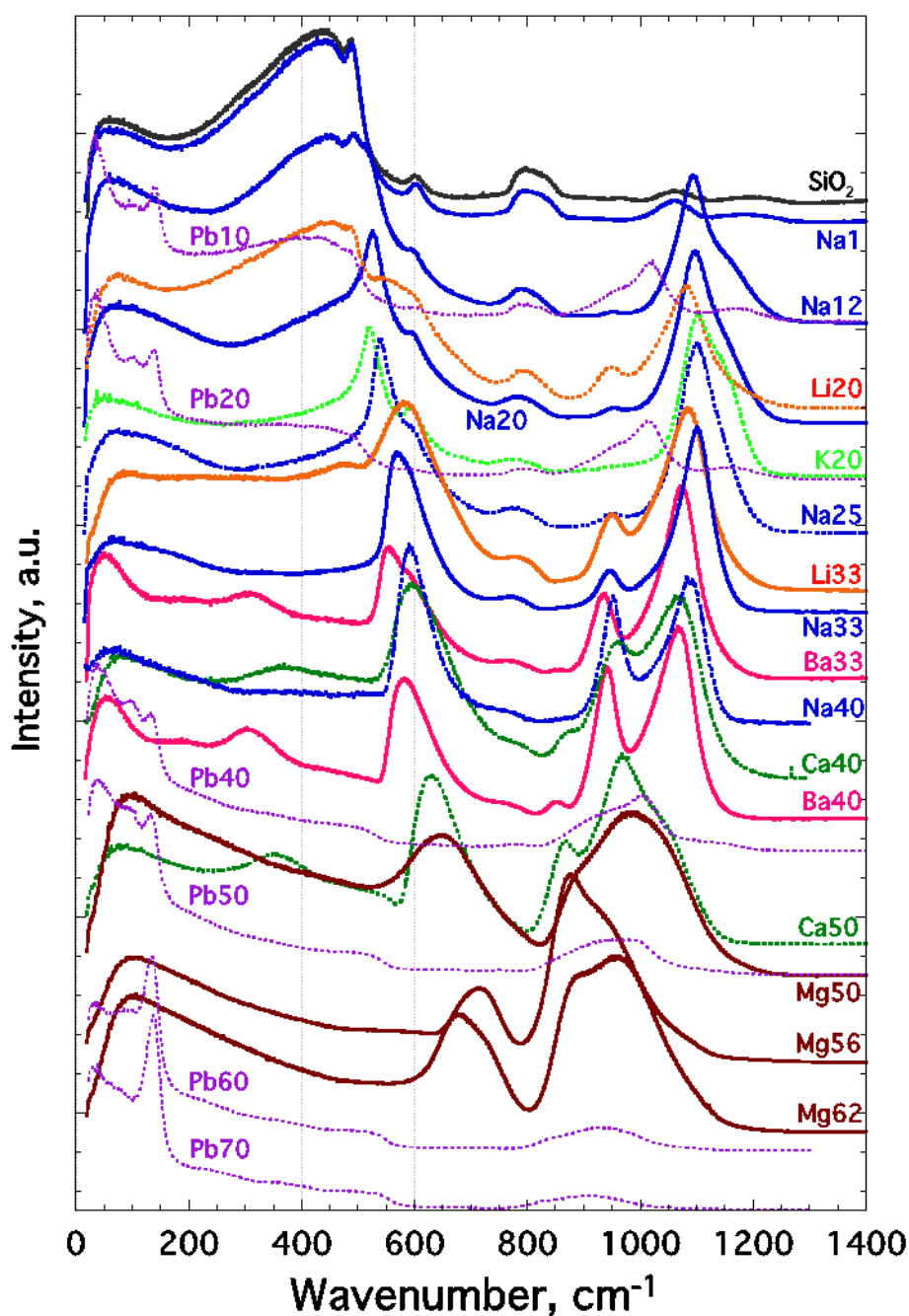


**Figure 8:** Unpolarized Raman spectra of  $\text{SiO}_2$  and silicate glasses in the system  $(\text{MO})_x(\text{SiO}_2)_{1-x}$  for  $M=\text{Li}_2, \text{Na}_2, \text{K}_2, \text{Mg}, \text{Ca}, \text{Ba}, \text{Pb}$ . The spectra are labelled  $\text{MX}$  for cation fraction  $X$  in mole %. Original data are in Neuville et al. (2014) and Ben Kacem et al., (2017).

*The Boson region:* At low wavenumbers, the BP generally experiences an increase in frequency with reducing  $\text{SiO}_2$  concentrations, indicating a correlation between the BP frequency and glass depolymerization (Neuville, 2006, 2014). The BP is also influenced by the introduction of different network modifiers, where at constant  $\text{SiO}_2$  concentration (hence constant polymerization) the BP shifts to higher frequency with the addition of small or medium ions and lower frequency with the introduction of larger heavier ions (Neuville 2005, 2006). These changes are accompanied by a narrowing of the BP width for glasses containing heavier-

elements (Ba, Pb) compared to lighter-elements (Na, Li, Mg, Ca), consistent with a very narrow boson peak observed in the Raman spectra of cesium silicate glasses (O'Shaughnessy et al. 2016). This appears to point towards a modification of MRO in the silicate glasses, and perhaps the development of ordering of the modifier cations. Changes in intensity and position of the BP may also be explained by distortion of the  $\text{SiO}_4$  tetrahedra (Hehlen et al. 2002).

*The low frequency region:* With the addition of modifier oxides, the  $R$ ,  $D_1$ , and  $D_2$  bands in the spectral domain between  $\sim 250$  and  $600 \text{ cm}^{-1}$  evolve into a broad peak in the region of the  $D_2$  vibration at  $\sim 580$  to  $680 \text{ cm}^{-1}$ , reflecting the breaking of Si-O-Si bonds and introduction of NBO leading to a reduction in the size of the ring structures formed from interconnected  $\text{SiO}_4$  tetrahedra. However, for lighter modifier elements (e.g. Li-silicate glass) the spectrum retains significant resemblance to the pure  $\text{SiO}_2$  glass spectrum indicating the presence of silica-rich regions in the glass (Matson et al. 1983). This has been interpreted as consistent with the MRN model, where Li atoms form MRO clusters within an underlying silicate network (Le Losq et al. 2019).

The  $R$ ,  $D_1$ , and  $D_2$  bands are highly polarized. Polarized Raman measurements of Na-silicate glasses, where spectra are recorded with parallel (VV) or perpendicular (VH) polarizations of incident and scattered light, reveal a strong reduction in intensity of the  $R$ -band in polarized (VV) spectra accompanied by the development of a strong narrow band between  $\sim 540$  to  $600 \text{ cm}^{-1}$  with increasing  $\text{Na}_2\text{O}$  fraction (Hehlen and Neuville 2015). This is consistent with a reduction in the Si-O-Si angle due to a reduction in ring size and increasing preponderance of  $D_2$  modes. The  $R$ ,  $D_1$ , and  $D_2$  bands are inactive in the depolarized (VH) spectra which instead reveal the development of a peak at  $\sim 350 \text{ cm}^{-1}$  and a lower frequency peak at  $\sim 175 \text{ cm}^{-1}$  with increasing cation concentration and are attributed to cation motions (Hehlen and Neuville 2015). This will be discussed in more detail in relation to the dual role of cations as network modifiers or compensators in aluminosilicate compositions.

*The intermediate frequency region:* The asymmetric band observed in silica and silica-rich glasses at around  $800 \text{ cm}^{-1}$  is attributed to bending vibrations in  $\text{SiO}_4$  tetrahedra (Sarnthein et al. 1997; Taraskin and Elliott 1997; Spiekermann et al. 2012). It is, however, interesting to note the presence of a high frequency shoulder in this peak for pure  $\text{SiO}_2$ . This asymmetry has been attributed to two different structures of  $\text{SiO}_4$  units with distinct inter-tetrahedral Si-O-Si angles coexisting in the glass (Seifert et al. 1982; Neuville and Mysen 1996; Kalampounias et al. 2006). However, direct structural studies have not observed a bimodal distribution of the Si-O-Si angle in  $\text{SiO}_4$  units and we note that different  $n$ -membered rings will have different Si-O-Si angles. As such the Si-O stretching frequency in tetrahedral units should vary as a function of ring size (Le Losq et al. 2019). This is supported by the loss of this high-frequency shoulder with the addition of modifier cations and hence reduction in the ring size and Si-O-Si distributions.

*The high frequency region:* The high frequency Raman bands for silicate glasses centered at  $\sim 1100 \text{ cm}^{-1}$  are associated with Si-O stretching vibrations in different  $Q^n$  tetrahedral units and typically interpreted by spectral deconvolution (Mysen et al. 1982a,b; McMillan 1984), as discussed in detail in chapter 2 (Henderson and Stebbins 2020, this volume). Here we provide additional details for selected glass compositions.

Spectral deconvolution of these high-frequency bands into their constituent components by Gaussian curve fitting is illustrated in figure 9 for Na40 and Ca40 glass spectra (Neuville 2006). Here the Gaussian bands at  $\sim 900 \text{ cm}^{-1}$ ,  $960 \text{ cm}^{-1}$ , and  $1080 \text{ cm}^{-1}$  can be attributed to the vibrations of  $Q^1$ ,  $Q^2$ , and  $Q^3$  species, respectively. To fully model the high-frequency region, it is necessary to include an additional band at  $1020 \text{ cm}^{-1}$  for Ca40 and  $1040 \text{ cm}^{-1}$  for Na40. This



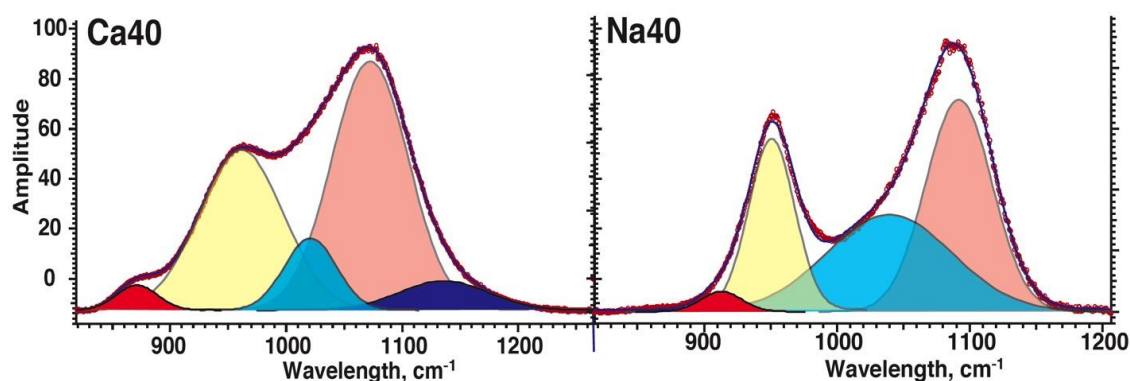


**Figure 9:** Decomposition of Raman spectra in Gaussian bands for Ca40 and Na40, redrafted from (Neuvill 2006), bands are from low to high frequency,  $Q^1$ ,  $Q^2$ ,  $T_{2s}$ ,  $Q^3$  and  $Q^4$ . No  $Q^4$  species are present in the Na40 glass.

contribution can be compared to the band observed at  $\sim 1070 \text{ cm}^{-1}$  in the pure  $\text{SiO}_2$  glass spectrum (figure 4). This band has been attributed to the  $T_2$  stretching mode of  $Q^4$  units (Neuvill et al. 2014a) although recent studies (Bancroft et al., 2018, O'Shaughnessy et al., 2020) assigned this band to  $Q^3$  tetrahedra close to alkali cations. The Raman spectrum of the Na1 glass (figure 8) shows that the addition of only 1 mol % of  $\text{Na}_2\text{O}$  in silica leads to a slight increase of the intensity of the peak at  $1070 \text{ cm}^{-1}$ . Further addition of modifier leads to a large increase of the intensity corresponding to the A1 mode (Bancroft et al. 2018; O'Shaughnessy et al. 2020). At low alkali oxide contents, the A1 mode is composed of 2 bands which merge into a single band after the addition of 20 mol% alkali oxide (O'Shaughnessy et al. 2020).

The band at  $1135 \text{ cm}^{-1}$  in the Ca40 spectrum is attributed to the  $A_1$  stretching mode of  $Q^4$  units. Substitution of Ca by Na reduces the network polymerization as evident by the complete absence of this  $Q^4$  band in the Na40 glass spectrum. With increasing modifier cation concentration, increasingly depolymerized species are present, including  $Q^0$  and  $Q^1$  species, leading to a significant shift in the intensity maximum of the Si-O stretching bands to lower frequencies (see e.g. the spectra for Mg62 and Mg56 and figure 12 of Neuvill et al. 2014a).

### Lead Silicate Glasses

The high-frequency domain,  $850\text{-}1300 \text{ cm}^{-1}$ , in the Raman spectra of lead silicate glasses appears less intense compared to other glass compositions. This is a result of the normalization process as Pb-silicate glasses exhibit the highest intensity peaks at low frequency. Two very intense low-frequency peaks at  $100 \text{ cm}^{-1}$  and  $141 \text{ cm}^{-1}$  are dominant features in Raman spectra of Pb-silicate glasses (Worrell and Henshall 1978; Furukawa et al. 1978; Ohno et al., 1991; Zahra et al. 1993; Feller et al. 2010, Ben Kacem et al. 2017). The peak at  $141 \text{ cm}^{-1}$  is attributed to covalent Pb-O-Pb bonding in interconnected tetrahedral  $\text{PbO}_4$  units (Furukawa et al. 1978; Worrell and Henshall (1978); Zahra et al. 1993) and correlates with NMR spectra which show the proportion of Pb-O-Pb linkages increases with PbO content (Lee and Kim 2015).

A variety of charge balancing models have been reported which predict MRO in the form of different extended networks of interconnected Pb-centered units in the glass, including dimeric zigzag chains of covalently bonded  $\text{PbO}_4$  tetrahedra (Morikawa et al. 1982), screw chains of  $\text{PbO}_n$  polyhedra ( $n = 3$  or  $4$ ) (Imaoka et al. 1986), Pb cations in predominantly edge-shared  $\text{PbO}_3$  trigonal pyramid arrangements (Takaishi et al. 2005), and pyramidal  $\text{PbO}_n$  units with a mix of corner and edge sharing with electron lone-pairs organizing to form voids in the glass (Alderman et al. 2013).

XRD reveals Pb can adopt both 4- and 6-fold coordinated sites in Pb-silicate glasses (figure 6b), where Pb in 4-fold coordination acts as a network former and Pb in 6-fold coordination



depolymerizes the glass via the generation of non-bridging oxygens. The Raman band at  $100\text{ cm}^{-1}$  has been attributed to ionic Pb-O bond, implying the presence of  $\text{Pb}^{2+}$  compensated by  $\text{O}^{2-}$  (Worrell and Henshall 1978; Ohno et al. 1991) which can be attributed to the two additional NBO atoms in the  $\text{PbO}_6$  unit. The attribution of this band can be confusing. Since this band remains constant along the PbO-SiO<sub>2</sub> join, while the intensity of the Pb-O-Pb band at  $141\text{ cm}^{-1}$  increases, this peak was previously attributed to “free oxygen” (oxygen atoms only bonded to Pb atoms) whose proportion increases above the orthosilicate composition (Bockris and Mellors 1956; Nesbitt and Fleet 1981; Hess, 1975).

To summarize, Pb in lead-silicate glasses adopts a dual role as network former and modifier in 4- and 6-fold coordination sites, respectively (Ben Kacem et al. 2017). Pb in 6-fold coordination plays similar role to alkali or alkaline-earth elements breaking up the silicate network polymerization by forming NBO's. Pb in 4-fold coordination is a “soft network former” that forms an interconnected sub-network or percolation channel, mixing mechanically with the SiO<sub>4</sub> tetrahedral network without chemical interaction. This is supported by the glass transition temperature for PbO-SiO<sub>2</sub> glasses which varies almost linearly between 30 and 90 mol. % of SiO<sub>2</sub> fraction (Ben Kacem et al. 2017) implying heterogenous mixing.

### **Aluminosilicate glasses**

Aluminosilicate glasses and their melts are of interest due to their relevance to natural magmas. Aluminium is classed as an intermediate glass former due to its ability to both compete with Si to form a 4-fold coordinated network structure or to behave as a network modifier assuming 5- or 6-fold coordination and reducing the glass network connectivity via the formation of non-bridging oxygens. This behaviour is particularly sensitive to the relative proportions of Al and other modifier cations. To form a perfectly connected network of AlO<sub>4</sub> tetrahedra the Al:O ratio needs to be precisely 1:2 such that any two Al atoms are connected by a single bridging oxygen. For the  $(\text{MO})_x(\text{Al}_2\text{O}_3)_{1-x}$  compositions this occurs at the ratio  $R = \text{MO}/\text{Al}_2\text{O}_3 = 1$  ( $x = 0.5$ ), where modifier cations, assuming a uniform distribution, will perfectly charge compensate AlO<sub>4</sub> units which have an overall charge of -1. Aluminosilicate compositions along this join are denoted tectosilicate or meta-aluminosilicate glasses. Peraluminous aluminosilicates, classified as glasses with the ratio  $R = \text{MO}/\text{Al}_2\text{O}_3 < 1$ , have an excess of Al and are unable to form an ideal charge compensated corner-sharing network of AlO<sub>4</sub> tetrahedra. This oxygen deficiency may be compensated for by the formation of highly coordinated AlO<sub>5</sub> and AlO<sub>6</sub> units and/or a change in network connectivity. In peralkaline glasses ( $R = \text{MO}/\text{Al}_2\text{O}_3 > 1$ ) there are excess modifier cations which will act to charge compensate AlO<sub>4</sub> tetrahedra and potentially depolymerize the network. There is, however, increasing evidence for deviations from this simple model, with significant proportions of 5-fold coordinated Al and even 5-fold Si observed in glasses that are sufficiently charge compensated by metal cations (Stebbins et al. 1997; Toplis et al. 2000; Stebbins et al. 1991). Significant fractions of AlO<sub>4</sub> have also been observed in the alumina-rich glasses (Mysen 2005), where charge neutrality is accomplished by the formation of O:Al<sub>3</sub> tri-clusters in which one O atom is shared by three AlO<sub>4</sub> tetrahedra (Lacy 1963).

### ***Diffraction and Raman measurements along the tectosilicate join***

The  $G(r)$  functions from neutron diffraction experiments and Raman spectra for MO-Al<sub>2</sub>O<sub>3</sub>-SiO<sub>2</sub> ( $M = \text{Ca, Sr}$ ) glasses along the tectosilicate join ( $R = \text{MO}/\text{Al}_2\text{O}_3 = 1$ ) are shown in figure 10. Compositions are denoted by concatenating the modifier element  $M$  with the mole fraction  $X$  of SiO<sub>2</sub> and  $Y$  of Al<sub>2</sub>O<sub>3</sub> in per cent ( $\text{MX.Y}$ ). With increasing substitution of Si by Al the nearest neighbour peak T-O in  $G(r)$  is broadened and shifts to higher distances from  $1.60\text{ \AA}$

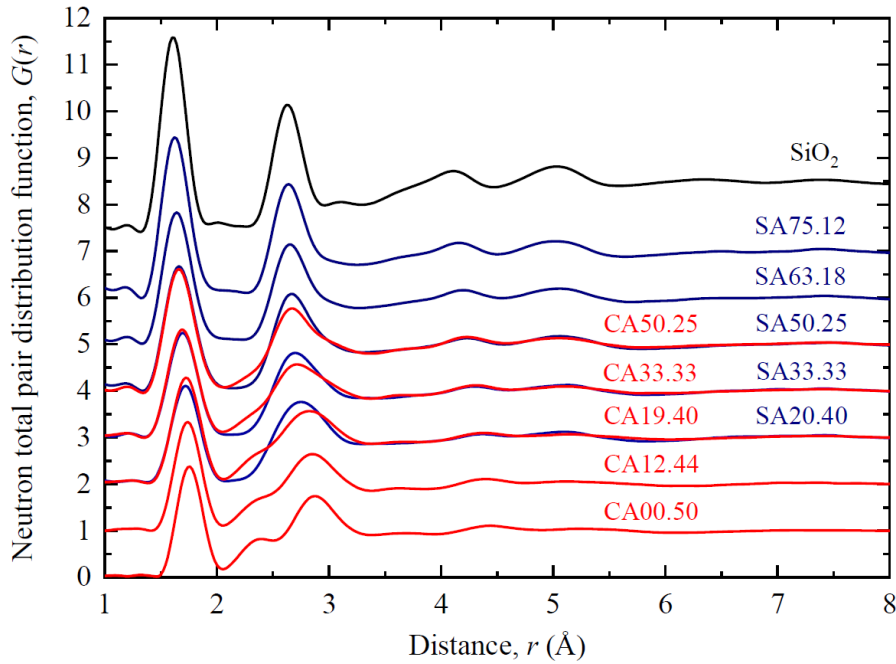


**Figure 10:** Neutron total pair distribution functions for  $M$ -aluminosilicate ( $M = \text{Ca}, \text{Sr}$ ) glasses along the tectosilicate ( $R = 1$ ) join (data from Bowron, 2008; Hennet et al, 2016; Florian et al, 2018; unpublished data). Compositions are denoted by  $MX.Y$  for mole per cent fraction  $X$  of  $\text{SiO}_2$  and  $Y$  of  $\text{Al}_2\text{O}_3$ , where the fraction  $MO = 100 - (X+Y)$ .

in pure  $\text{SiO}_2$  to  $1.76 \text{ \AA}$  in silica-free  $\text{Ca}0.50$  glass. This results from Al-O correlations with longer nearest neighbour lengths overlapping the shorter Si-O correlations (Cormier et al. 2000, 2003; Hennet et al. 2016). For the Ca-aluminosilicate glasses, the peak at  $\sim 2.30$  to  $2.35 \text{ \AA}$  is attributed to the first Ca-O bond and becomes increasingly conspicuous with reducing  $\text{SiO}_2$  concentration due to higher weighting on the  $g_{\text{CaO}}(r)$  partial pair distribution functions. It is difficult to precisely determine the Ca-O coordination environment using conventional x-ray or neutron diffraction due to considerable overlap by the  $g_{\text{OO}}(r)$  partial pair distribution functions (Hannon and Parker 2000; Benmore et al. 2003; Mei et al. 2008a, 2008b; Drewitt et al. 2011; Hennet et al. 2016). Direct measurements of the first Ca-O coordination shell in both calcium-silicate and -aluminate glasses by NDIS provide average Ca-O coordination numbers of  $\sim 6.2$  to  $6.5$  (Eckersley et al. 1988; Drewitt et al. 2012), with MD simulations revealing a broad distribution of Ca-O polyhedra centered  $\sim 6$  (Jakse et al. 2012; Drewitt et al. 2012).

Despite the larger neutron scattering length  $b_{\text{Sr}} = 0.702(2) \text{ fm}$ , compared to  $b_{\text{Ca}} = 0.470(2) \text{ fm}$  (Sears 1992), the nearest neighbour Sr-O correlations are not discernible in the  $G(r)$  functions for Sr-aluminosilicate glasses. This is due to the larger ionic radius of  $\text{Sr}^{2+}$  cf.  $\text{Ca}^{2+}$  (Shannon, 1976) due to both higher atomic number and larger Sr-O coordination number of  $\sim 8$  to  $9$  (Novikov et al. 2017; Charpentier et al. 2018). Furthermore, the O-O correlations associated with these highly coordinated Sr-centered polyhedra are shifted to lower distances compared to Ca-aluminosilicate measurements. As a result, the nearest neighbour peak in  $g_{\text{SrO}}(r)$  is completely overlapped by the  $g_{\text{OO}}(r)$  correlations (Florian et al. 2018).

Similar spectral features and vibrations are observed for Al as for Si, where Al can adopt  $Q^4$ ,  $Q^3$  and  $Q^2$  speciation depending on silica fraction (McMillan and Piriou 1983; Neuville et al. 2008ab, 2010; Licheron et al. 2011). The substitution of Al for Si in tetrahedral positions leads to detectable shifts in frequency, broadening, and reduction in spectral resolution of the Raman bands relative to the  $\text{SiO}_2$  glass spectrum (Mysen et al. 1981; Seifert et al. 1982; McMillan et

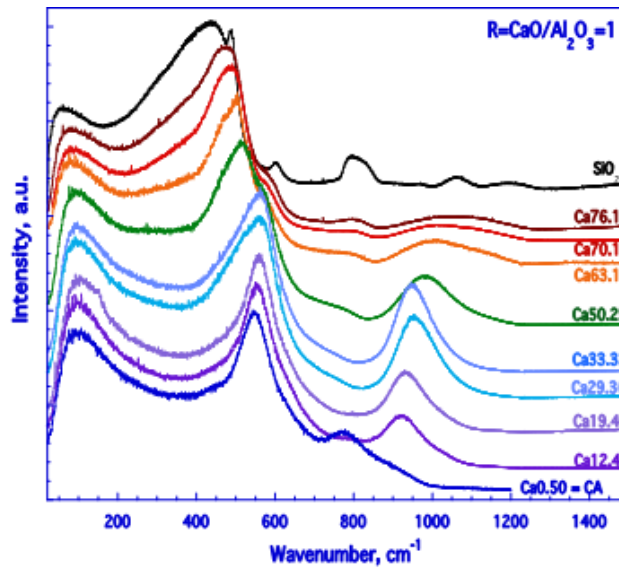


**Figure 11:** Raman spectra for calcium aluminosilicate glasses along the tectosilicate ( $R = 1$ ) join (data from REFERENCE). Compositions are denoted by the notation  $\text{Ca}X.Y$  for mole per cent fraction  $X$  of  $\text{SiO}_2$  and  $Y$  of  $\text{Al}_2\text{O}_3$ , where the fraction  $\text{CaO} = 100 - (X+Y)$ .

al 1982; McMillan and Piriou 1982, 1983; McMillan 1984; Neuville and Mysen 1996; Neuville et al. 2004, 2006, 2008a,b; Le Losq and Neuville, 2013; Le Losq et al. 2017). In particular, the  $T$ - $O$  stretching vibrations shift to lower wavenumber, with a corresponding increase in position of  $T$ - $O$ - $T$  bending modes, as a result of a reduction in the  $(\text{Si,Al})$ - $\text{O}$  force constant and/or  $\text{Si,Al}$  coupling (Rossano and Mysen, 2012). These changes are illustrated for calcium aluminosilicate glasses in Figure 11 showing the Raman spectra along the tectosilicate join. Along this join, glasses are fully polymerized and  $\text{Al}^{3+}$  substitutes for  $\text{Si}^{4+}$  in  $Q^4$  tetrahedral sites regardless of the modifier element (Neuville and Mysen 1996; Neuville et al. 2004, 2006, 2008; Novikov et al. 2017; Le Losq and Neuville 2013; Le Losq et al. 2017, Ben Kacem, 2017). This is illustrated in figure 12a, where the  $Q^{4I}$ ,  $Q^{4II}$  and  $T_{2s}$  vibrational modes determined by Gaussian deconvolution, experience a linear shift to lower wavenumbers with increasing substitution of

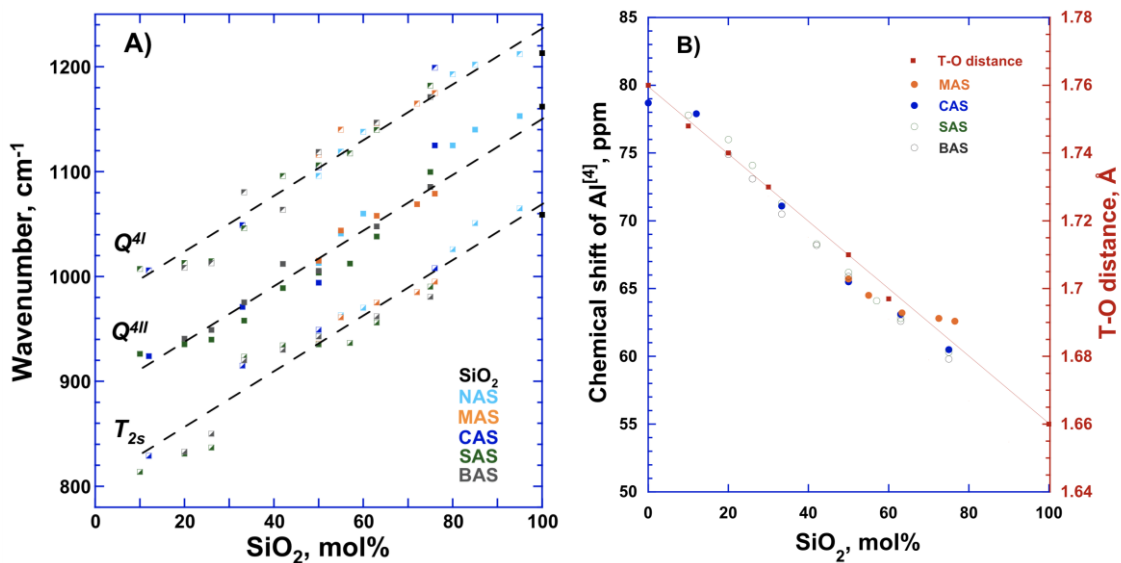


**Figure 12:** a) Wavenumber of the 3 Gaussian bands as a function of  $\text{SiO}_2$  for NAS, MAS, CAS, SAS and BAS tectosilicate glasses (Neuville and Mysen 1996, Neuville et al. 2004, 2006, 2008; Novikov et al. 2017) and b)  $^{27}\text{Al}$  NMR chemical shift,  $\delta_{\text{iso}}$  and  $T$ - $O$  distance obtained from the  $G(r)$  as a function of  $\text{SiO}_2$  for CAS glass system (Figure 10).

Si for Al associated with a continuous shift from the Si-O-Si vibration to pure Al-O-Al vibrations in the CA50.00 glass (McMillan and Piriou 1983; Neuville and Mysen, 1996; Neuville et al., 2004, 2006, 2008, 2010; Licheron et al. 2011; Novikov et al., 2017). This variation correlates well with  $^{27}\text{Al}$  NMR chemical shift for Al in four-fold coordination and the T-O bond length measured by diffraction (Figure 12b), which both increase linearly with increasing Al fraction (Neuville et al., 2004, 2006, 2008).

Along the tectosilicate join,  $M$  acts as a charge compensator and does not disturb the network structure significantly. However, some differences are apparent in the Raman  $R$ ,  $D_1$  and  $D_2$  bands associated with ring arrangements, particularly with the incorporation of large cations. For example, in the  $\text{K}_2\text{O}-\text{Al}_2\text{O}_3-\text{SiO}_2$  system, the frequency of the  $Q^{4I}$ ,  $Q^{4II}$  and  $T_{2s}$  bands and the chemical shift of the 4-fold coordinated Al from  $^{27}\text{Al}$  NMR follow a similar trend as for the other aluminosilicate systems. Furthermore, percolation channels have been suggested to occur in these glasses (Le Losq et al., 2017), with their presence indicated by an increase of the  $D_1$  and  $D_2$  peak intensity.

### *Charge compensator versus network modifier*

As noted above the substitution of an alkali or alkaline-earth element by Al has a significant influence on the Raman spectra of aluminosilicate glasses. Some of the changes are related to whether the added alkali or alkaline-earth cations behave as charge compensators or network modifiers. The dual role of the cations can be explored through analysis of the depolarized (VH) component of polarized Raman spectra. (Neuville et al. 2014a; Hehlen and Neuville, 2015).

The VH Raman spectra of calcium aluminosilicate glasses along the 50%  $\text{SiO}_2$  join are shown in figure 13. A strong band is apparent in near  $350\text{cm}^{-1}$  for the alumina-free calcium silicate glass (Ca50.00) which is not visible in unpolarized Raman spectra of the Ca50.X series (figure 8). The intensity of this peak reduces with decreasing  $\text{CaO}/\text{Al}_2\text{O}_3$  ratio and its position

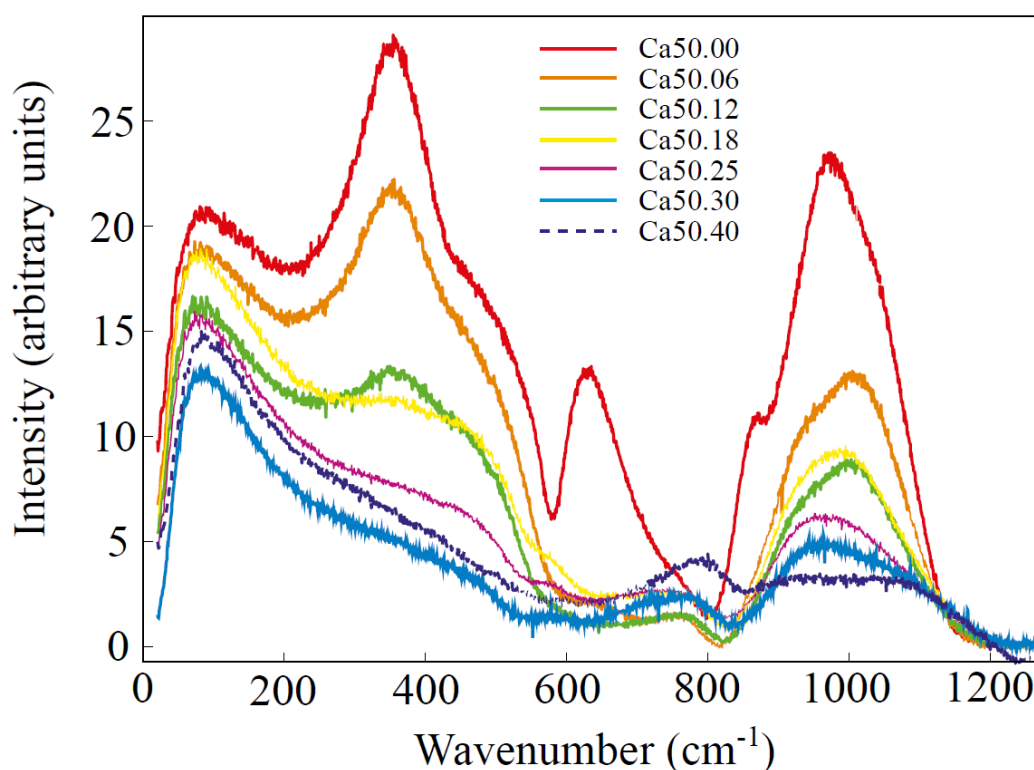


**Figure 13:** VH Raman spectra of calcium aluminosilicate glasses along the 50%  $\text{SiO}_2$  join (redrafted from Hehlen and Neuville, 2015).

is sensitive to the mass of the cation (Na: 350 cm<sup>-1</sup>, Mg: 360 cm<sup>-1</sup>, Ca: 352 cm<sup>-1</sup>, Sr: 334 cm<sup>-1</sup>, Ba: 310 cm<sup>-1</sup>, Hehlen and Neuville 2015, 2020). This low frequency vibration is attributed to cations acting as network modifiers. When cations adopt a charge compensation role for the AlO<sub>4</sub><sup>-</sup> tetrahedra this vibration disappears.

This variable role of modifier cations is supported by the change of the pre-edge observed in x-ray absorption near edge structure (XANES) measurements at the Ca K-edge of Ca-aluminosilicate glasses from Ca50 to Ca50.25 compositions (Cicconi et al. 2016). Similar changes are also observed in <sup>23</sup>Na NMR spectra of Na-aluminosilicate glasses, which exhibit a shift from -2 to -18 ppm when Na switches roles from a network modifier to a charge compensator. This also appears to correlate with the disappearance of the peak at 350cm<sup>-1</sup> observed in the VH Raman spectra between sodium silicate and sodium tectosilicate glasses (Hehlen and Neuville, 2015). Being able to determine the behaviour of alkali and alkaline-earth cations as compensators or formers is very useful. Clearly, there is potential in examining the VH spectra and more work needs to be done.

## GLASSES AND MELTS UNDER EXTREME CONDITIONS

Despite decades of research focused on aluminosilicate glasses, much less direct information is available on the structure of magmas in their high temperature liquid state or under the high *p* conditions of deep planetary interiors. This is due to the challenges associated with making measurements above the high melting temperatures of aluminosilicates (> 1500 K), where conventional furnaces present a high risk of chemical reaction with a sample, spectroscopy measurements are inhibited by thermal radiation, and the thermal motions and structural disorder lead to weaker signals compared to the solid glass. Measurements at high-*p* and/or -*T* are doubly challenging, requiring specialized instrumentation to generate these extreme conditions while simultaneously allowing good accessibility to the sample and minimizing unwanted contributions from the sample environment. As a result, quenched glasses have long been used as analogues for the study of melts (Henderson 2005). However, while important, information obtained on glass structure is not always representative of melts in their natural liquid state (Wilding et al. 2010; Drewitt et al. 2012). This is particularly apparent for so-called *fragile* liquids such as depolymerized silicate melts (Giordano and Dingwell 2003) in which dynamical properties such as viscosity exhibit a marked deviation from Arrhenius behaviour, compared to more traditional *strong* glass forming liquids such as pure silica (Angell 1995). Glasses and melts also experience significant reorganization in SRO and MRO under compression such that measurements made at high-*p* conditions are necessary to understand the full nature of magmas at depth.

### High temperature containerless processing

In recent years, containerless techniques such as aerodynamic-levitation with laser-heating have enabled *in situ* diffraction and spectroscopy measurements of the structure of liquid oxides (Price 2010; Hennet et al. 2011a; Benmore and Weber 2017). Levitating liquids on a stream of inert gas eliminates the possibility of chemical reaction with containment material and experiments provide clean data sets of the liquid sample enabling advanced techniques such as NDIS to be applied (Drewitt et al. 2012; Skinner et al. 2012a; Drewitt et al. 2017; Drewitt et al. 2019). The high flux of synchrotron sources means that XRD measurements using ultra-fast millisecond acquisition times are possible with large area detectors. This enables diffraction patterns to be measured as an oxide liquid is supercooled into the solid glass state (Hennet et al. 2007; Hennet et al. 2011b; Skinner et al. 2013a; Drewitt et al. 2019). Another key advantage of levitation is the absence of a container suppresses heterogenous nucleating to promote deep

supercooling which combined with rapid quenching facilitates the formation of glass compositions such as peridotite (Auzende et al. 2011) or pure aluminates (Drewitt et al. 2019) that cannot ordinarily be formed using conventional methods.

### *Aluminate melts*

Pure liquid alumina has a poor glass forming ability and cannot be quenched to a glass (Skinner et al. 2013b; Shi et al. 2019). However, the glass forming ability of aluminate compositions is significantly enhanced by the addition of alkali, alkaline earth, or metal oxides. Extensive experimental and simulation studies have been made to understand the structure of silica-free calcium aluminate glasses and their melts typically by using containerless processing techniques (McMillan and Piriou 1983; Morikawa et al. 1983; Poe et al. 1993; Poe et al. 1994; Massiot et al. 1995; McMillan et al. 1996; Daniel et al. 1996; Hannon and Parker 2000; Weber et al. 2003; Benmore et al. 2003; Iuga et al., 2005; Kang et al., 2006; Thomas et al., 2006; Hennet et al. 2007; Mei et al., 2008a,b; Cristiglio et al. 2010; Neuville et al. 2010; Mountjoy et al. 2011; Licheron et al. 2011; Drewitt et al. 2011, 2012, 2017, 2019; Liu et al. 2020). Other compositions have also been investigated, including barium (Licheron et al. 2011; Skinner et al. 2012b), strontium (Weber et al. 2003; Licheron et al. 2011; Novikov et al. 2017), lead (Barney et al. 2007), and rare-earth aluminates (Wilding et al. 2002; Weber et al. 2004a; Du and Corrales, 2007; Barnes 2015). A liquid-liquid phase transition (LLPT) has been proposed in the yttria-aluminate system, inferred from the observation of coexisting low-density and high-density phases in the supercooled melts (Aasland and McMillan 1994). However, although further studies purportedly support this finding (Wilding et al. 2002; Weber et al. 2004a,b; Wilson and McMillan 2004; Wilding et al. 2005; Greaves et al. 2008; Wilding et al. 2015), the result is disputed by subsequent measurements that find no structural or thermal signatures consistent with a LLPT (Barnes et al. 2009) with the observations attributed to nanocrystalline inclusions forming within the glassy material (Nagashio and Kuribayashi 2002; Tangeman et al. 2004; Skinner et al. 2008; Barnes et al. 2009).

Molten calcium aluminates are very *fragile* refractory liquids. Fragile liquids tend to exhibit greater variation in SRO and MRO compared to *strong* glass forming liquids and encounter high potential energy barriers during supercooling such that they become trapped in deep local energy minima on approach to the glass transition (Drewitt et al. 2019). The comprehensive range of techniques that have been brought to bear on the calcium aluminate system reveal significant transformations in SRO and MRO structure take place in these liquids during glass formation.

Neutron and XRD  $G(r)$  functions for  $(\text{CaO})_x(\text{Al}_2\text{O}_3)_{1-x}$  glasses and melts with  $x = 0.5$  ( $\text{CaAl}_2\text{O}_4$ , CA) and  $x = 0.75$  ( $\text{Ca}_3\text{Al}_2\text{O}_6$ , C3A) are shown in figure 14 (Drewitt et al. 2011, 2012, 2017, 2019). The results of MD simulations made using aspherical ion model (AIM) potentials, which consider polarization effects up to the quadrupolar level (see Jahn 2020, this volume), are also shown (Drewitt et al. 2011; Drewitt et al. 2012; Drewitt et al. 2019). The first peak in  $G(r)$  for the melts at  $\sim 1.78 \text{ \AA}$  is attributed to the nearest neighbour Al-O bond, with a second peak at  $\sim 2.3 \text{ \AA}$  arises from Ca-O correlations (Drewitt et al. 2011). On vitrification, the intensity and resolution of the Al-O and Ca-O peaks is significantly enhanced, reflecting the thermal motions and higher overall structural disorder in the liquid state. The Al-O and Ca-O peak positions experience shifts to  $\sim 1.75 \text{ \AA}$  and  $\sim 2.35 \text{ \AA}$ , consistent with a reduction and increase in Al-O and Ca-O coordination numbers, respectively. However, accurate quantification of these coordination numbers is hindered by the penetration of Ca-O correlations into the first Al-O coordination shell and considerable overlap with other atom-atom interactions at higher bond lengths. This is particularly acute for the liquids, but also



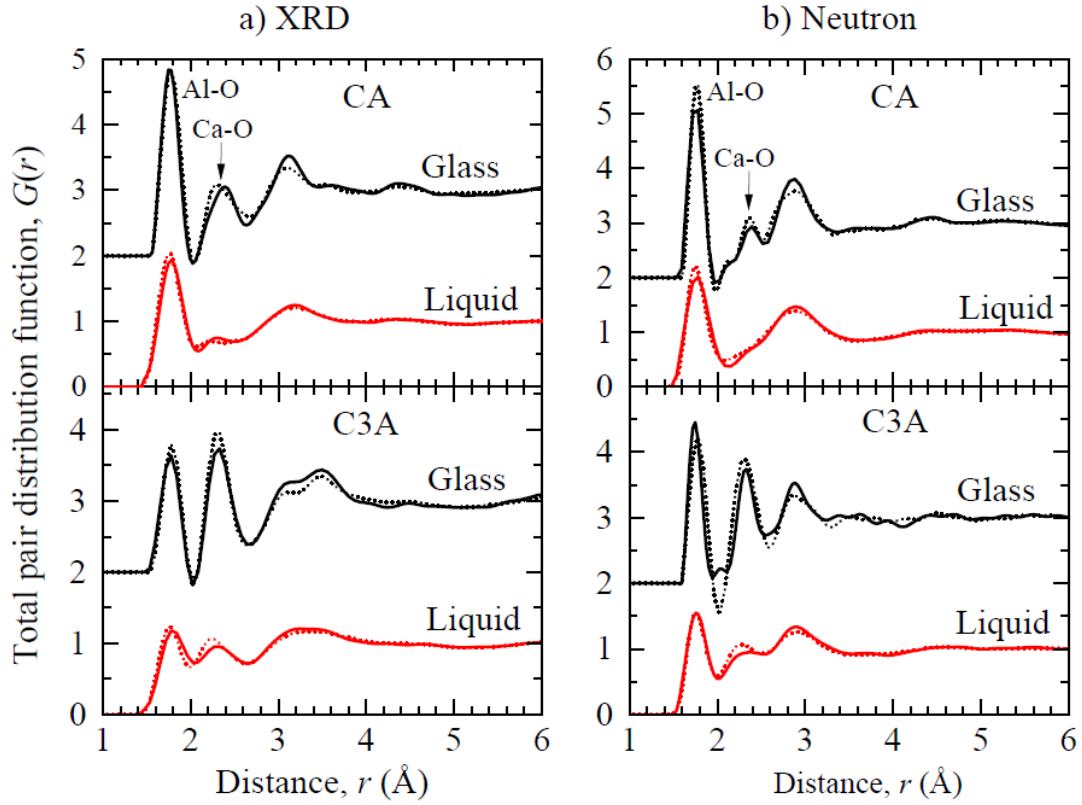


**Figure 14:** Total pair distribution functions  $G(r)$  from a) x-ray and b) neutron diffraction of CA and C3A glasses (solid black curves) and liquids (solid red curves) together with the corresponding functions computed directly from MD simulations (dotted curves) (data from Drewitt et al. 2011, 2012, 2017, 2019).

affects the glass measurements (Hannon and Parker 2000; Mei et al. 2008a,b; Drewitt et al. 2011). Element selective techniques are, therefore, required to isolate the Al and Ca coordination environments. This represents a significant challenge at high temperatures:  $^{27}\text{Al}$  NMR spectroscopy measurements observe the fast exchange limit such that individual coordination populations cannot be resolved in the high temperature melts (Coté et al. 1992; Poe et al. 1993; Poe et al. 1994; Massiot et al. 1995; Florian et al. 2018),  $^{43}\text{Ca}$  NMR is limited by low sensitivity and natural abundance (Dupree et al. 1997), x-ray absorption measurements of high temperature levitated melts are difficult to perform, and NDIS is limited by the sample size and neutron flux.

Drewitt et al. have successfully applied NDIS to precisely measure the Al-O and Ca-O coordination environments in levitated liquid CA and C3A (Drewitt et al. 2012, 2017), despite the small size ( $\sim 2\text{-}3$  mm diameter) of the levitated droplets. The pseudo-binary pair distribution functions  $g_{\mu\mu}(r)$  and  $g_{\text{Ca}\mu}(r)$  for the CA and C3A melts and the quenched CA glass are shown in figure 15. In  $g_{\mu\mu}(r)$  all interactions involving Ca are eliminated and the function contains contributions from  $\mu\text{-}\mu$  ( $\mu = \text{Al}, \text{O}$ ) pair correlations only, showing well resolved peaks corresponding to Al-O nearest neighbours and O-O bonds. In contrast,  $g_{\text{Ca}\mu}(r)$  is comprised solely from Ca- $\mu$  pair correlations and the main peak corresponds to the Ca-O nearest neighbours. The NDIS experiments for liquid C3A and CA glass go one step further to provide direct measurement of the  $g_{\text{CaCa}}(r)$  partial pair distribution function, as shown in figure 16.

Overall, the AIM-MD model is in excellent agreement with the NDIS and XRD measurements. The CA composition has an Al:O ratio of 1:2 such that it is feasible to form a fully polymerized network of  $Q^4$  in which any two Al atoms are connected by a single bridging



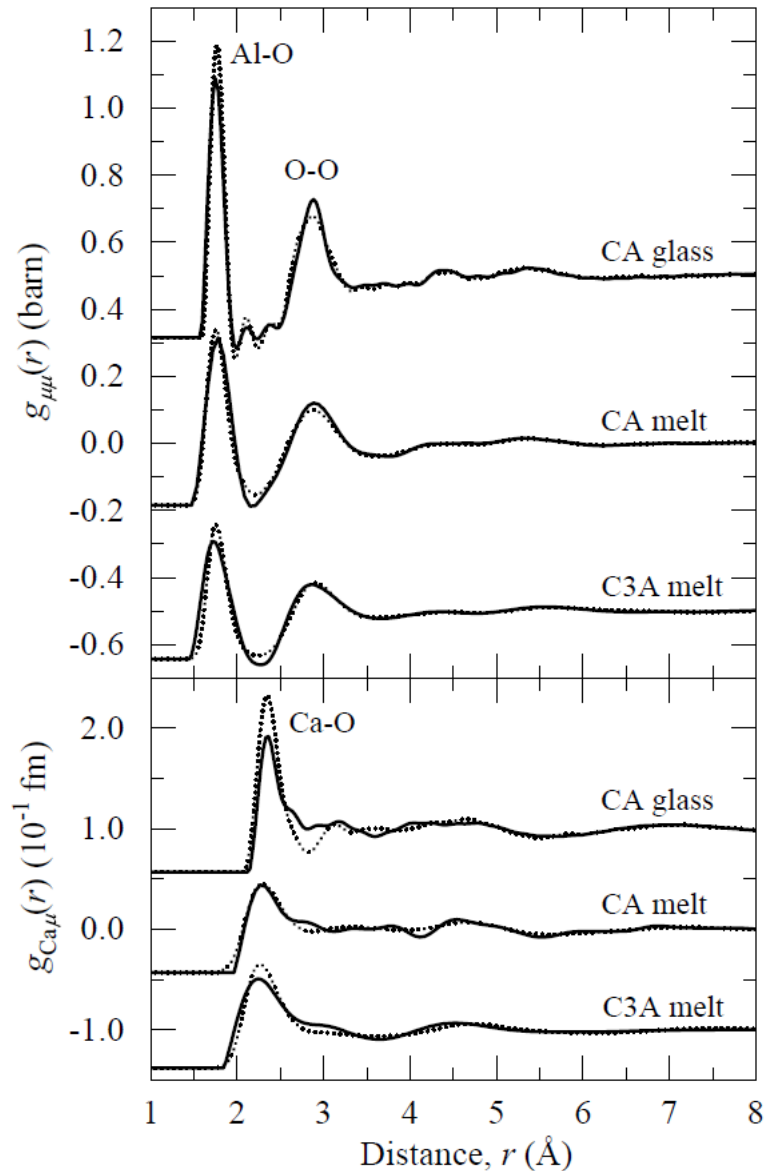


**Figure 15:** The real-space pseudo-binary pair distribution functions  $g_{\mu\mu}(r)$  and  $g_{Ca,\mu}(r)$  for the CA (Drewitt et al. 2012) and C3A (Drewitt et al. 2017) melts from NDIS measurements (solid curves) and AIM-MD simulations (Drewitt et al. 2011; Drewitt et al. 2012). (Reprinted from Drewitt et al. 2019 doi:[10.1088/1742-5468/ab47fc](https://doi.org/10.1088/1742-5468/ab47fc) © SISSA Medialab Srl. Reproduced by permission of IOP Publishing. All rights reserved).

oxygen. The C3A composition on the other hand is significantly depolymerized with a theoretical mean number of 2 bridging oxygens per Al atom. The combined NDIS, XRD, and AIM-MD results reveal that the structure of liquid CA deviates from this simple network model containing 83 %  $\text{AlO}_4$  tetrahedra with 12 % non-bridging oxygens and 15 %  $\text{AlO}_5$  units, many of which share edges (Drewitt et al. 2012). Considering all Al-O pairs, 18 % oxygen atoms have a coordination  $> 2$ , with 7 % formal triclusters in which one oxygen is connected to three  $\text{AlO}_4$  tetrahedra. Liquid C3A is composed of a higher fraction of  $\text{AlO}_4$  tetrahedra (93 %) with 60 % non-bridging oxygen and 36 % bridging oxygen atoms (Drewitt et al. 2017), where the latter is slightly higher than expected from the O:Al ratio (Skinner et al. 2012b). This is accounted for by the presence of 3 to 4 % “free oxygen” ions, which do not participate in Al-O bonding, and  $\sim 1$  % oxygen triclusters. While the majority of  $\text{AlO}_4$  tetrahedra in C3A melt belong to a single

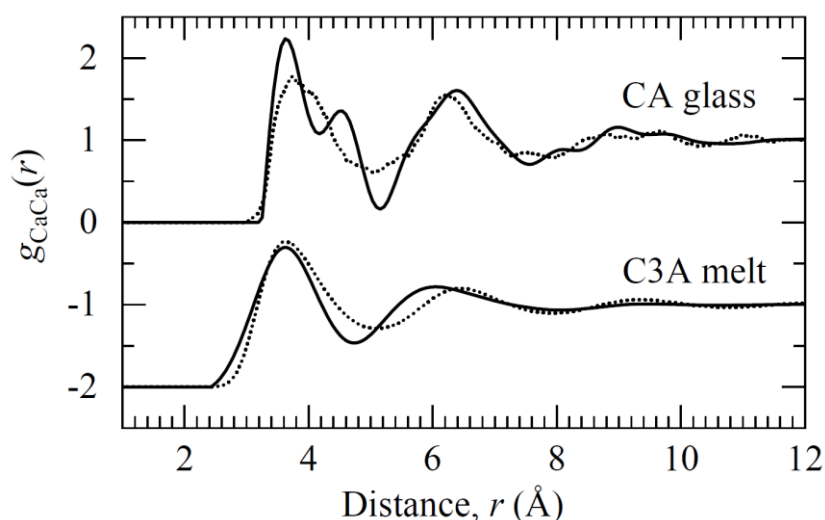


**Figure 16:** The partial pair distribution function  $g_{\text{CaCa}}(r)$  for CA glass (Drewitt et al. 2012) and C3A melt (Drewitt et al. 2017) determined directly from NDIS experiments (solid curves) and generated from the AIM-MD simulations (Drewitt et al. 2011; Drewitt et al. 2012). (Reprinted from Drewitt et al. 2019 doi:[10.1088/1742-5468/ab47fc](https://doi.org/10.1088/1742-5468/ab47fc) © SISSA Medialab Srl. Reproduced by permission of IOP Publishing. All rights reserved).

infinitely connected network, 15 to 20 % belong to smaller clusters with ~ 10 % forming  $\text{Al}_2\text{O}_7$  dimers or isolated  $\text{AlO}_4$  tetrahedra.

On vitrification, the over coordinated CA glass structure reorganizes to form a predominantly corner shared network of  $\text{AlO}_4$  tetrahedra. The C3A glass is also characterised by a preponderance (99 %) of aluminium in  $\text{AlO}_4$  tetrahedra with 85% belonging to a single infinite network. This is consistent with  $^{27}\text{Al}$  NMR (Neuville et al. 2006, 2007) and XANES spectroscopy at the L and K-edges (Neuville et al. 2008b, 2010) which show Al is predominantly four-fold coordinated by oxygen in glasses with compositions  $x = 0.5$  to 0.75. There is, however, a residual 3.5 % Al in  $\text{AlO}_5$  units remaining in CA glass (Neuville et al. 2006) and the AIM-MD results indicate the presence of ~ 4% residual  $\text{AlO}_5$  units in CA glass, accompanied by 7 % non-bridging oxygens and 5 % formal oxygen triclusters (Drewitt et al. 2012). This latter result is consistent with 5 % oxygen triclusters detected in the glass by heteronuclear correlation NMR spectroscopy (Iuga et al. 2005).

Differences in network connectivity are apparent from the Raman spectra of CA, C12A7 ( $x = 0.632$ ,  $\text{Ca}_{12}\text{Al}_{14}\text{O}_{33}$ ) and C3A glasses shown in figure 17. All spectra exhibit a Boson peak at ~ 90  $\text{cm}^{-1}$ , a strong band at ~ 560  $\text{cm}^{-1}$  with significant asymmetry at higher wavenumbers, and another strong band at ~ 780  $\text{cm}^{-1}$ , which increases in intensity relative to the 560  $\text{cm}^{-1}$  band with increasing CaO content. The 560  $\text{cm}^{-1}$  band is attributed to transverse motions of bridging oxygens in Al-O-Al linkages, with the high frequency asymmetry caused by Al-O stretching vibrations of the fully polymerized tetrahedral aluminate groups (McMillan and Piriou 1983). This band experiences a shift to higher frequencies and reduction in intensity with increasing CaO content associated with changes in the polarizability of the Al-O-Al vibrations resulting from an increase in the Al-O force constant as  $Q^2$  species are introduced into the glass network. This is consistent with a shift to lower energies of the  $L_{2,3}$ -edge in Al XANES spectroscopy measurements attributed to the presence of  $Q^2$  species and associated stronger hybridization of non-bridging oxygens (Neuville et al. 2010). The weak band in the CA glass spectrum at 780  $\text{cm}^{-1}$ , and shoulder at 910  $\text{cm}^{-1}$ , are attributed to Al-O stretching vibrations of  $Q^4$  Al species. The increase in intensity and shift to lower frequencies of the 780  $\text{cm}^{-1}$  band with increasing CaO content is attributed to increasing fractions of non-bridging oxygens giving rise to more intense vibrations compared to bridging oxygens (McMillan and Piriou 1983). This is consistent

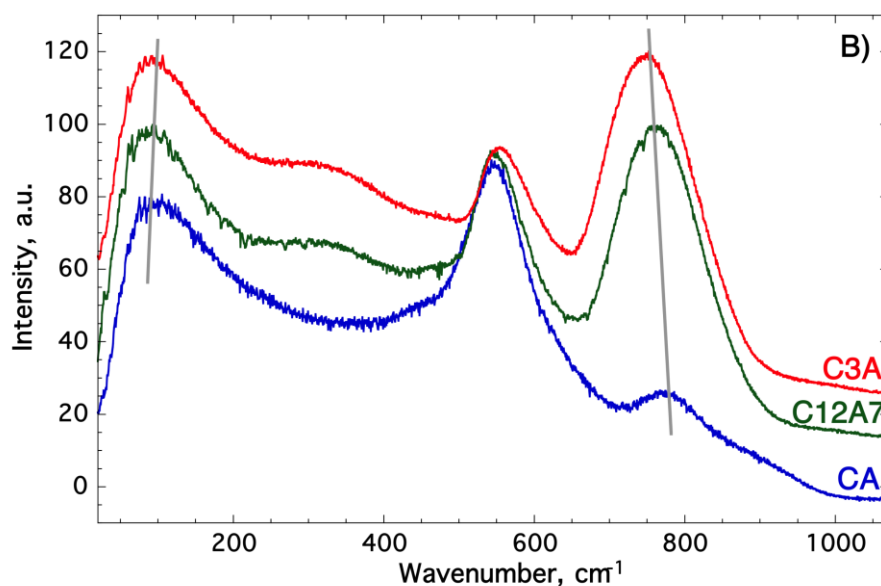


**Figure 17:** Raman spectra of CA, C12A7, C3A glasses (data from Neuville et al. 2006; Neuville et al. 2010; Licheron et al. 2011).

with  $^{27}\text{Al}$  NMR (Neuville et al. 2006) and Al K-edge XANES results (Neuville et al. 2008a,b), which suggest Al units predominantly in  $Q^2$  and  $Q^3$  speciation in C3A glass. It also implies that the C12A7 glass contains a significant fraction of non-bridging oxygens.

Calcium has a broad distribution of 4- to 9-fold Ca-O coordination sites, with average Ca-O coordination numbers of 6.2 in CA (Drewitt et al. 2012) and 5.6 in C3A (Drewitt et al. 2017) melts. In CA melt, edge- and face-sharing Ca-centered polyhedra form small clusters. In C3A melt all Ca-centered units are connected by corners to a single network with 90 % edge- and face-sharing. The direct measurement of  $g_{\text{CaCa}}(r)$  by NDIS (figure 16) gives an average Ca-Ca coordination number of  $\sim 8$  ( $\sim 8.5$  from AIM-MD) compared to a value  $\sim 5$  determined in CA melt, reflecting the greater fraction of Ca in the C3A composition and hence greater

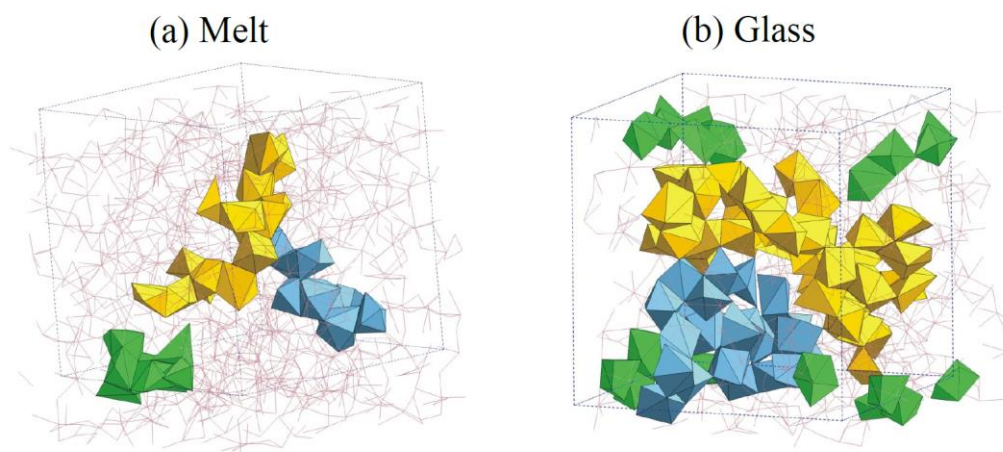


**Figure 18:** Snapshots illustrating the largest clusters of edge-sharing Ca-centered polyhedra in the AIM-MD simulations of  $\text{CaAl}_2\text{O}_4$  from Drewitt et al. (2012) for (a) the melt 2500 K and (b) the glass at 350 K. The clusters are represented by the light (yellow), dark (blue), and medium (green) shaded units which involve 16, 9, and 8 Ca atoms in the liquid or 44, 24, and 19 Ca atoms in the glass, respectively. Reprinted figure with permission from Drewitt et al. Physical Review Letters 109:235501 (2012) doi:[10.1088/0953-8984/24/9/099501](https://doi.org/10.1088/0953-8984/24/9/099501). Copyright (2012) by the American Physical society.

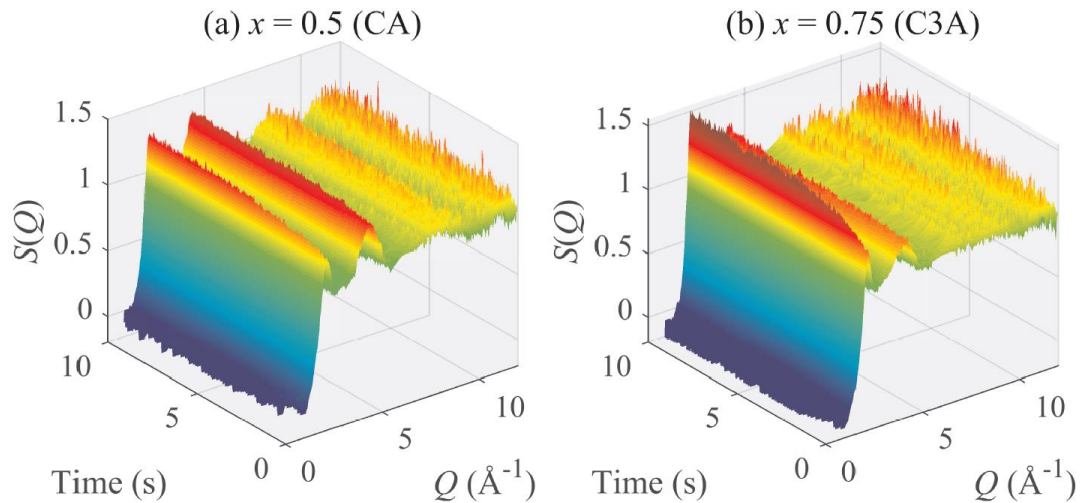



**Figure 19:** Time resolved x-ray diffraction measurements of the structure factors  $S(Q)$  of aerodynamically levitated liquid (a) CA and (b) C3A during glass formation with 30 ms acquisition times. (Reprinted from Drewitt et al. 2019 doi:[10.1088/1742-5468/ab47fc](https://doi.org/10.1088/1742-5468/ab47fc) © SISSA Medialab Srl. Reproduced by permission of IOP Publishing. All rights reserved).

tendency towards clustering. However, on vitrification, the CA glass experiences a remarkable development of cationic MRO with edge- and face-sharing Ca-O polyhedra with an average coordination of 6.4 which form large branched chains that weave through the glass network (figure 18).

To summarize, at the  $\text{Al}_2\text{O}_3$ -rich limit of the glass forming region of calcium aluminate melts up to 20 % of the Al reside in  $\text{AlO}_5$  coordination sites (Drewitt et al. 2011), increasing to over 30 % in pure alumina (Skinner et al. 2013b). These highly coordinated Al units are incompatible with glass formation. However, although the equimolar (CA) melt contains 15 %  $\text{AlO}_5$  polyhedra (Drewitt et al. 2011), these highly coordinated units and oxygen triclusters breakdown on vitrification and the supercooled melt structure reorganizes to form a predominantly corner-shared  $\text{AlO}_4$  tetrahedral glass network (Drewitt et al. 2012). This is accompanied by the development of cationic ordering associated with the formation of long chains of edge- and face-sharing Ca-centered polyhedra (figure 18). While significantly depolymerized, the structure of C3A melt remains largely composed of  $\text{AlO}_4$  tetrahedra (Drewitt et al. 2011). Although many of these tetrahedra belong to a single infinite network, ~ 20 % aluminium in in C3A melt belong to smaller clusters with ~ 10% unconnected  $\text{Al}_2\text{O}_7$  dimers and  $\text{AlO}_4$  monomers (Drewitt et al. 2017). On vitrification, C3A glass is characterized by a tetrahedral aluminium network structure, where 85 % of  $\text{AlO}_4$  units belong to a single infinite structure with only 5 % isolated tetrahedra or dimers (Drewitt et al. 2019). Beyond the CaO-rich limit of the glass forming region, the number of isolated  $\text{AlO}_4$  units is expected to increase such that the glass can no longer support the formation of an infinitely connected network of  $\text{AlO}_4$  units (Drewitt et al. 2017).

The significant structural transformations that take place during glass formation in the calcium aluminate glasses are captured by time-resolved measurements of aerodynamically levitated liquid calcium aluminates recorded during solidification of the high temperature melts through their glass transition (Hennet et al. 2007; Drewitt et al. 2019). In particular, the changes in MRO associated with the development of cationic ordering is indicated by the evolution of the FSDP in  $S(q)$  attributed to cation-cation correlations (figure 19). The work reviewed here for a representative fragile glass-forming system demonstrates that caution is required when considering glasses as proxies for geological melts. Similar differences in the local structural environment has been observed in fragile  $\text{MgO-SiO}_2$  liquids (Wilding et al. 2010). Natural

silicate melts in the CaO-MgO-Al<sub>2</sub>O<sub>3</sub>-SiO<sub>2</sub> (CMAS) system encompass a range of kinetic fragilities (Giordano and Dingwell 2003; Giordano and Russell 2007; Giordano et al. 2008). As such measurements made on glasses cannot be assumed to be representative of melts in their natural liquid state and models should be based, where possible, on liquid-state measurements. 

### *Aluminosilicate melts*

As for aluminates, aluminosilicate melts have high melting points and only a few diffraction studies have been reported, mainly using laser heating with aerodynamic levitation at neutron sources (Jakse et al 2012, Hennet et al 2016, Florian et al 2018) or levitation inside the bore of a NMR spectrometer (Poe et al. 1992; Florian 2018). Alternatively, wire furnace methods, in which a small quantity of sample is placed in a small hole (~ 500 μm diameter) in a Pt-Ir wire and melted by resistive heating (Mysen and Frantz, 1992; Richet et al. 1993; Neuville et al. 2014), has been adopted for XAS (Neuville et al, 2008b), Raman spectroscopy (Neuville and Mysen 1996; Daniel et al. 1995), and x-ray diffraction (Neuville et al. 2014b) of aluminosilicate melts.

In contrast to aluminate melts, which can be stably levitated for days without significant mass loss (Drewitt et al. 2012; Drewitt et al. 2017), aerodynamically levitated laser heated silicate melts experience significant sample vaporization at high SiO<sub>2</sub> fractions. This leads to significant changes in composition, as experienced by *in situ* XRD measurements of liquid SiO<sub>2</sub> (Mei et al. 2007; Skinner et al. 2013a) and NDIS measurements of CaSiO<sub>3</sub> melt (Skinner et al. 2012a) for which sample mass loss is particularly detrimental due to the requirement for the different isotopically enriched samples to have identical composition. Thus, neutron diffraction experiments of aluminosilicate melts, which require counting times of several hours, have been limited to compositions up to about 33% of silica in melts containing CaO (Hennet et al. 2016) and 42% in melts containing SrO (Florian et al. 2018).

Figure 20a shows a comparison of the neutron structure factors measured for a range of calcium aluminosilicates melts along the charge compensator line together with the corresponding glass. On melting, the FSDP becomes less distinct with lower intensity and increased broadening, which is indicative of increased disorder in the organization of polyhedra at intermediate distances. This augmentation of disorder is also evident in the broadening and reduction in structure of the peaks over the full  $q$ -range. Similar changes are observed for other CaO/Al<sub>2</sub>O<sub>3</sub> ratios (Hennet et al. 2016). Along the join  $R=1$ , this disorder is mainly related to an increase of the proportion of AlO<sub>5</sub>, which is apparent from the asymmetric high- $r$  broadening of the first peak in  $G(r)$  (figure 20b), related to a slight increase of the Al-O distance (Drewitt et al. 2012). As previously observed for glasses, the CaO correlation, which was largely overlapped with the O-O correlations coming from the SiO<sub>4</sub> tetrahedra, is now fully overlapped at high temperature making the interpretation difficult. Thus, molecular dynamics simulations have been employed to provide more insight on the liquid structure revealing the AlO<sub>5</sub> units are accompanied by increased proportions of NBO and oxygen triclusters (Jakse, 2012).

The MD simulations reveal that the addition of silica to aluminate compositions reduces the quantity of AlO<sub>5</sub> present from ~ 18% in Ca<sub>0.50</sub> to ~ 10% in Ca<sub>12.44</sub> and Ca<sub>19.40</sub> melts. These melts contain ~ 14% OAl<sub>3</sub> triclusters and ~ 12% NBO. The simulations reveal a continuous development in the AlO<sub>4</sub> network and corresponding reduction in AlO<sub>5</sub> units, oxygen triclusters, and NBOs during supercooling to a glass. Calcium occupies a distribution of coordination sites ranging from 4 to 8 with an average Ca-O coordination number of ~ 6. This structural environment describes relatively well the dynamical behavior of these melts (Bouhadja et al, 2013).



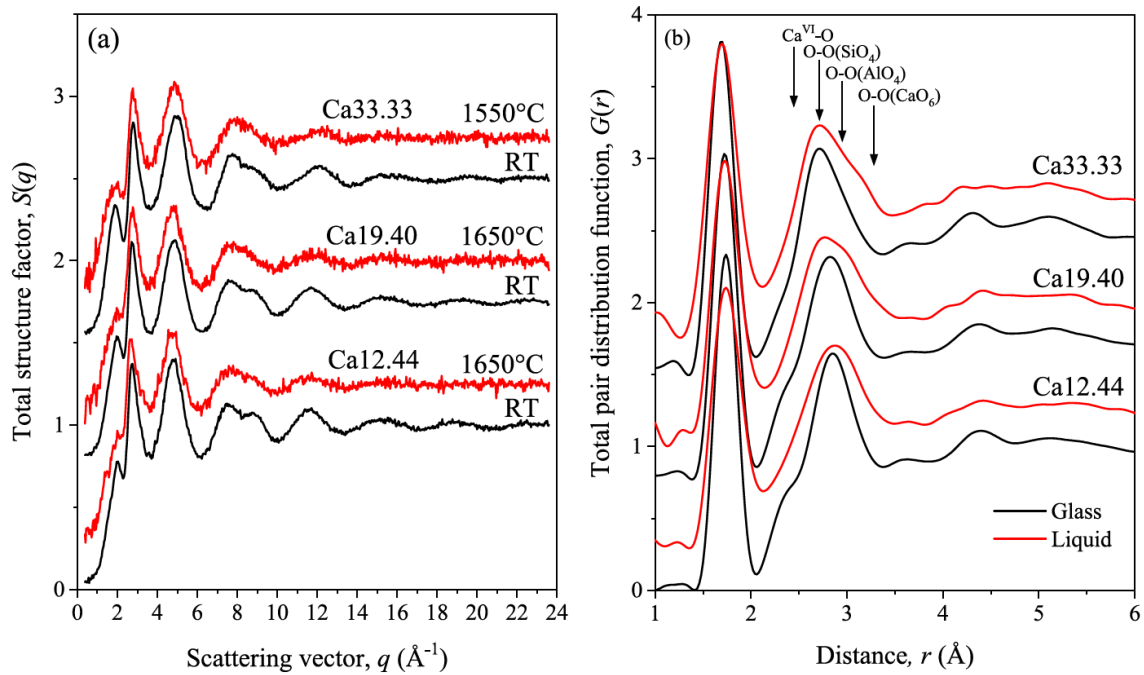


**Figure 20:** Total structure factors  $S(q)$  of some CAS glasses measured using neutron scattering (a) and corresponding total pair distribution functions (b). The liquid temperatures are reported in the figure. (Data from Hennet et al. 2016).

Neutron diffraction measurements of  $\text{SrO-Al}_2\text{O}_3\text{-SiO}_2$  melts reveal similar SRO associated with the Al and Si atoms as for calcium aluminates with an increase in the fraction of  $\text{AlO}_5$  units in the melts estimated at 5-6% (Florian et al 2018). As for the glasses, it is difficult to extract information from the SrO contribution, which is overlapped by O-O correlations arising from Si-O and Al-O tetrahedra and highly coordinated Sr-O polyhedra (cf. figure 10). By looking at the possible O-O correlations coming from these Sr-O polyhedra, the Sr-O coordination number was estimated to be  $\sim 8$  for the join  $R = 3$  and somewhat less for  $R = 1$  (Florian et al. 2018).

The *in situ* high temperature NMR experiments (Florian et al. 2018) give more information about the network structure. Along the  $R=1$  join, Al is gradually replaced by Si with increasing Si content. The same behavior is found along the join  $R=3$  for Si content  $\equiv$  as  $\text{Si}/(\text{Al}+\text{Si}) > 0.7$ . Below this composition, NBOs are found on the  $\text{AlO}_4$  units, breaking the aluminosilicate network. Consequently, for a given silica content, the addition of SrO reduces the medium range order (smaller ring sizes for  $R=3$  than for  $R=1$ ). For per-aluminous compositions, large amounts of 5- and 6-fold coordinated aluminium are found in in the melts. Different mechanisms that those observed along the joins  $R = 1$  and 3, especially at low silica content could also suggest the presence of oxygen triclusters.

### *Iron silicate melts and glasses*

As the fourth most abundant element in the Earth's crust, iron plays an important role due to its high mass having a strong influence on the density and viscosity of natural volcanic magmas. Iron adopts a dual character as both a network former and modifier in silicate glasses, typically used as proxies for melts. This behaviour is modulated by the coexistence of ferrous ( $\text{Fe}^{2+}$ ) and ferric ( $\text{Fe}^{3+}$ ) iron cations which adopt different structural roles. The redox ratio  $\text{Fe}^{3+}/\sum\text{Fe}$  is strongly influenced by chemical composition, temperature, and oxygen fugacity

(Wilke 2005). This mixed valency complicates the interpretation of the local coordination environment in structural measurements. In general,  $\text{Fe}^{3+}$  in silicate glasses is predominantly a network former in 4-fold coordination (Burkhard 2000), although this is highly dependent on composition and oxidation state with  $\text{Fe}^{3+}$  potentially occupying higher coordination sites when excess  $\text{Fe}^{3+}$  is added to charge-balanced glasses (Kim and Lee 2020). In traditional models of iron silicate glasses,  $\text{Fe}^{2+}$  is assumed to occupy 6-fold coordinated sites (Mysen and Richet, 2005). However, a wide distribution of 4-, 5-, and 6-fold coordination with oxygen has been reported in synthetic and natural iron silicate glasses by using x-ray, Mössbauer and optical absorption spectroscopies (Calas and Petiau 1983; Virgo and Mysen 1985; Binsted et al. 1986; Iwamoto et al. 1987; Dingwell and Virgo 1988; Hannoyer et al. 1992; Keppler 1992; Wang et al. 1993; Rossano et al. 1999; Wu et al. 1999; Rossano et al. 1999, 2000a,b; Galois et al. 2001; Giuli et al. 2002; Farges et al. 2004; Wilke et al. 2004; Jackson et al. 2005; Mysen 2006; Wilke et al. 2007; Bingham et al. 2007; Giuli et al. 2011; Giuli et al. 2012; Nyrow et al. 2014; Zhang et al. 2016; Alderman et al. 2017a; Nayak et al. 2019) and x-ray and neutron diffraction (Johnson et al. 1999; Holland et al. 1999; Weigel et al. 2006; Wiegel et al. 2008a,b; Drewitt et al. 2013; Wright et al. 2014).

More limited direct information is available on the local coordination environment of iron in silicate melts by comparison with the quenched glass. Using a conventional XRD source,

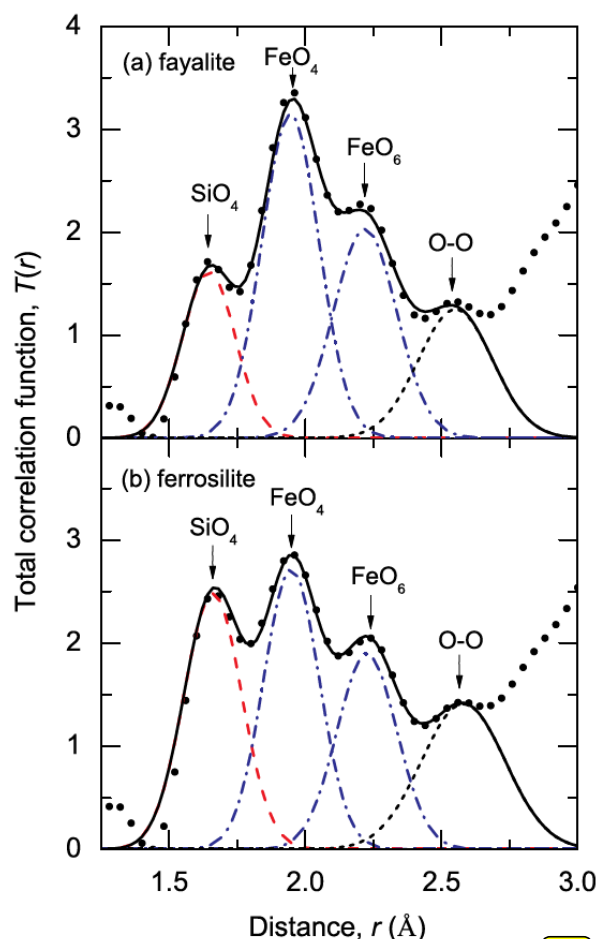


**Figure 21:** Gaussian fits to the main peaks in  $T(r) = 4\pi r \rho G(r)$  from synchrotron XRD measurements by Drewitt et al. (2013) for (a) liquid fayalite ( $\text{Fe}_2\text{SiO}_4$ ) and (b) liquid ferrosilite ( $\text{FeSiO}_3$ ). The black circles are the measured data and the solid black curves are the superposition of the fitted Gaussian functions. Reprinted figure with permission from Drewitt et al. Physical Review B 87:224201 (2013) doi:[10.1103/PhysRevB.87.224201](https://doi.org/10.1103/PhysRevB.87.224201) Copyright (2013) by the American Physical society.



Waseda et al. were the first to report the structure of iron silicate melts suggesting a reduction in Fe-O coordination from 6- to 4-fold with increasing SiO<sub>2</sub> fraction (Waseda and Toguri 1978; Waseda et al. 1980). However, serious inconsistencies have been found in this data including the assignment of unrealistically small Fe-Si bond distance and Fe-O-Si bond angle (Jackson et al. 1993; Drewitt et al. 2013). High temperature x-ray absorption spectroscopy (XAS) measurements alkali silicate (Waychunas et al. 1988) melts indicated Fe<sup>2+</sup> residing solely in 4-fold sites, and a complete conversion from 6-fold Fe<sup>2+</sup> sites in crystalline fayalite (Fe<sub>2</sub>SiO<sub>4</sub>) to 4-fold in the melt (Jackson et al. 1993). A subsequent XAS study found only slightly higher quantities of low coordinated Fe<sup>2+</sup> in reduced silicate melts (Wilke et al. 2007). This is confirmed by *in situ* synchrotron XRD measurements of laser heated silicate liquids, including Fe<sub>2</sub>SiO<sub>4</sub> and FeSiO<sub>3</sub>, levitated on an Ar gas stream in air (Drewitt et al. 2013). Here, two distinct Fe-O peaks are resolved (figure 21) with bond lengths 1.93 and 2.20 Å corresponding to FeO<sub>4</sub> and FeO<sub>6</sub> units, respectively, with average Fe-O coordination numbers of 4.8 (Fe<sub>2</sub>SiO<sub>4</sub>) and 5.1 (FeSiO<sub>3</sub>). Both Fe-O peaks are also apparent in the measurements of a basalt glass and melt. Although only two Fe-O peaks are apparent, the results do not exclude the presence of up to ~ 10-25 % FeO<sub>5</sub> units in the iron silicate melts and glasses studied (Drewitt et al. 2013). The coexistence of 4-, 5-, and 6-fold coordinated iron in silicate melts has important implications for the partitioning behaviour of iron in natural melts or transport properties of magmas. The ratio of these different units is affected by oxygen fugacity, with *in situ* Fe K-edge XANES and synchrotron XRD measurements of levitated fayalitic melts revealing average Fe-O coordination numbers increasing from 4.4 in the reduced melt to 4.7 at higher Fe<sup>3+</sup>/ΣFe (Alderman et al. 2017b).

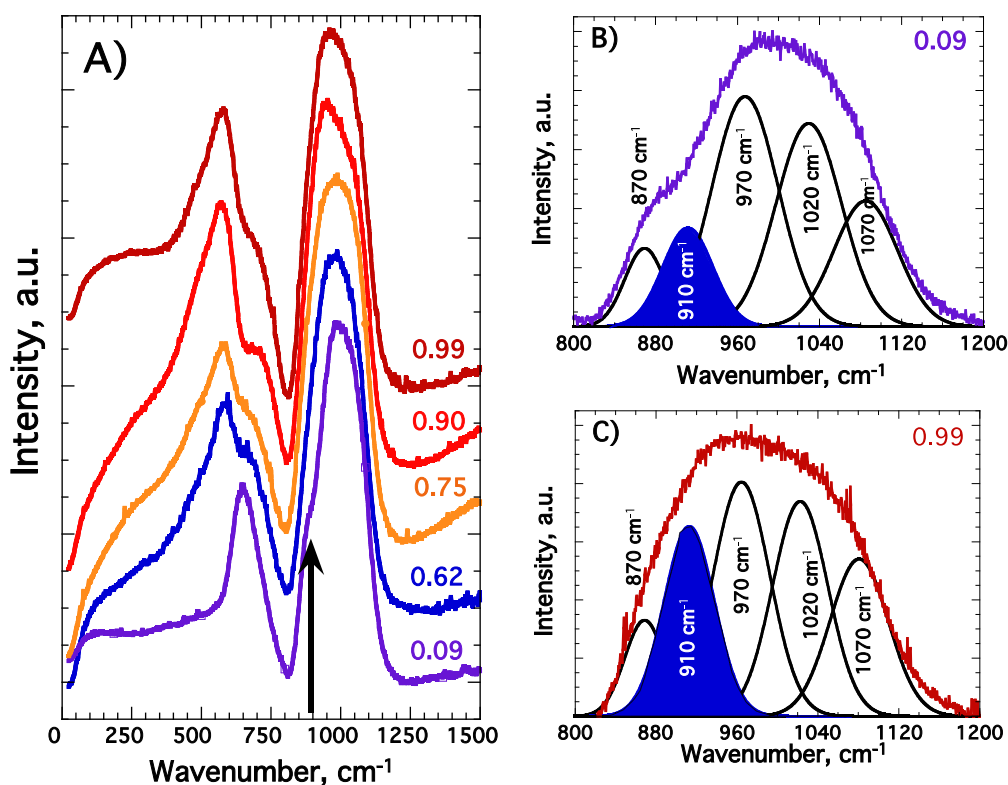


**Figure 22:** a) Raman spectra at room temperature for a series of iron-pyroxene glasses (redrafted from Magnien et al. 2006). The Fe<sup>3+</sup>/ΣFe redox ratio is indicated and the spectra are displaced vertically for clarity. The spectra were normalized to the maximum intensity of the spectra corrected from the excitation lines (see Neuville et al., 2014). b) Deconvolution of Raman spectrum of pyroxene glass with redox ratio Fe<sup>3+</sup>/ΣFe = 0.09, and c) Fe<sup>3+</sup>/ΣFe = 0.99.

Raman spectroscopy has also been used to interpret the structural role of iron in silicate glasses and melts and link the redox equilibrium to the silicate structure (Mysen et al. 1980, Fox et al. 1982, Mysen et al. 1984, 1985; Wang et al. 1993, 1995), and more recently to quantify the Fe redox ratio (Magnien et al. 2006, 2008; Roskosz et al. 2008; Di Muro et al. 2009; Cochain et al. 2012; Di Genova et al. 2015, 2016, 2017; Le Losq et al. 2019). Raman spectra of iron silicate glasses and melts vary systematically with varying  $\text{Fe}^{3+}/\Sigma\text{Fe}$  ratio due to the different roles of  $\text{Fe}^{2+}$  and  $\text{Fe}^{3+}$  influencing the network structure and  $Q^n$  speciation in different ways (LeLosq et al. 2019). Samples with high  $\text{Fe}^{3+}/\Sigma\text{Fe}$  ratio have characteristically strong intensity at  $\sim 900\text{cm}^{-1}$  assigned to  $\text{Fe}^{3+}\text{-O}$  stretching vibrations (Wang et al. 1995; Magnien et al. 2004, 2006, 2008; Di Muro et al. 2009; Cochain et al. 2012; Le Losq et al. 2019). This is illustrated in figure 22 for an iron-pyroxene glass composition with variation of the redox state  $\text{Fe}^{3+}/\Sigma\text{Fe}$  from 0.09 to 0.97. Here the intensity of the  $\text{Fe}^{3+}\text{-O}$  stretching band at  $910\text{cm}^{-1}$  increases significantly with increasing  $\text{Fe}^{3+}$  fraction. This peak correlates perfectly with the Fe pre-edge peak of XANES spectra at the K-edge attributable to 4-fold coordinated  $\text{Fe}^{3+}$  (Wilke et al. 2001), and its frequency is dependent upon the glass or melt silica fraction (Mysen et al. 1980; Wang et al. 1995).

### Glasses and melts at high pressure

Pressure can lead to considerable reorganization of SRO and MRO in glasses and melts. The structural response of melts at high  $p$  determines the density and dynamical properties of natural magmas in deep planetary interiors. Understanding the link between structure and properties of melts at high- $p$  is integral to understanding a range of problems including the distribution and causes of chemical alteration (metasomatism) of the mantle due to upward or lateral migration of melts, large scale differentiation from an early magma ocean, and mantle melting at mid-ocean ridges and subduction zones. Gravity driven melt transportation is proportional to melt mobility, which is dependent upon the viscosity of the melt and the density contrast between the melt and solid mantle. Early equation of state data for melts indicated that basaltic magmas are more compressible than mantle minerals leading to the possible existence of a melt-crystal density crossover at depth (Stolper et al. 1981; Rigden et al. 1984; Agee and Walker 1988).

To some extent, glass structure can exhibit irreversible behaviour on recovery from cold (i.e. room temperature) compression (Bridgman and Šimon 1953; Grimsditch 1984; Polian and Grimsditch 1990; Susman et al. 1991; Ishihara et al. 1999; Inamura et al. 2001; Trachenko and Dove 2002; Sampath et al. 2003; Champagnon et al. 2008; Rouxel et al. 2008). Further permanent densification may be promoted by heat treatment during compression (Polian and Grimsditch 1990; Ishihara et al. 1999; Trachenko and Dove 2002; Inamura et al. 2004). Notably, glasses synthesized from temperature quenched high- $p$  melts can preserve the equilibrium structure of the high- $p$  liquid-state for subsequent examination under ambient conditions (Li et al. 1995; Yarger et al. 1995; Ohtani et al. 1985; Xue et al. 1989; Stebbins and Poe 1999). However, to fully capture the evolution in SRO and MRO in glasses and melts at high  $p$ , *in situ* measurements are required and are clearly essential for melts which do not quench to a glass.

Recent advances in experimental and analytical techniques now allow for the measurement of the structure and properties of glasses and melts to be measured *in situ* at high- $p$ . Pressure cells used for high- $p$  research can be classified into two main types: large volume devices, such as a piston cylinder devices or multi anvil (MA) apparatus (Ito 2007), or the diamond anvil cell (DAC) (Mao and Mao 2007).

Large volume devices are typically used for *ex situ* phase equilibrium experiments under simultaneous high- $p$ - $T$  conditions using resistive heating. Piston cylinder devices can achieve moderate  $p$  up to 5-6 GPa and  $1800\text{ }^\circ\text{C}$  (Holloway and Wood 1988), corresponding to upper

mantle or lunar core conditions. As the name suggests, the MA apparatus utilizes multiple anvils to compress a sample from four or more directions to generate conditions of up to 30 GPa and 3000 °C (Holloway and Wood 1988), corresponding to mid to lower mantle conditions. Use of sintered diamond MA cubes, in place of standard tungsten carbide cubes, allows  $p$  as high as 90 GPa to be generated (Zhai and Ito 2011), providing access to deep lower mantle conditions. MA devices with x-ray transparent apertures are now commonplace at most third-generation synchrotron radiation sources (Liebermann 2011) and have been exploited for *in situ* high- $p$  measurements of the structure and properties of silicate glass melts (Funamori et al. 2004; Ohtani et al. 2005). However, MA devices are expensive to build and operate and sample accessibility is limited by their large-scale bulky nature of the apparatus. The Paris-Edinburgh (PE) cell is a large volume press specifically designed to optimize sample accessibility for *in situ* powder neutron diffraction experiments at  $p$  up to  $\sim 25$  GPa (Besson et al. 1992; Klotz et al. 1995). The PE cell has been adapted for simultaneous high- $p$ - $T$  synchrotron x-ray diffraction experiments (Besson et al. 1996; Mezouar et al. 1999; Crichton and Mezouar 2005) and used for *in situ* x-ray scattering measurements of silicate melts (Yamada et al. 2011; Sakamaki et al. 2012; Kono et al. 2014). Recently, a double-stage large volume cell was developed by incorporating a pair of secondary diamond anvils into a primary-stage PE cell to generate pressures in the megabar (1 Mbar = 100 GPa) regime (Kono et al. 2019) and has been used for measuring structure of different glasses at ultrahigh pressure (Kono et al. 2016; Kono et al. 2018; Ohira et al. 2019; Shibazaki et al. 2019; Wilding et al. 2019).

The DAC generates extremely high static pressures by compressing a sample between two opposing single crystal diamond anvils (Bassett 2009). High- $p$  experiments up to  $\sim 1$  megabar (1 Mbar = 100 GPa) are routine in the DAC (Li et al. 2018), with multimegabar pressures feasible by employing beveled (Bell et al. 1984) or toroidal (Dewaele et al. 2018) anvils to provide access to static  $p$  corresponding to Earth's core and beyond, with  $p$  in the Terapascal (1000 GPa) regime achievable using secondary micro-ball nanocrystalline diamond anvils (Dubrovinsky et al. 2012; Dubrovinskaia et al. 2016). The DAC is an extremely versatile and highly portable device which is relatively inexpensive to manufacture, and the transparency of diamonds across the electromagnetic spectrum offers a key advantage over other high- $p$  methods. Thus, the sample can be observed *in situ* under compression using optical microscopy, spectroscopy, and x-ray scattering techniques. This also enables laser heating techniques to heat the sample at high- $p$  at temperatures up to  $\sim 5000$  K and dedicated laser heated diamond anvil cell (LHDAC) setups for *in situ* high- $p$ - $T$  structure measurements are now widely available at synchrotron sources around the world (Watanuki et al. 2001; Shen et al. 2001; Meng et al. 2006; Caldwell et al. 2007; Liermann et al. 2010; Petitgirard et al. 2014). The LHDAC method combined with synchrotron XRD has been exploited in the Earth Sciences to study metallic (Shen et al. 2004; Morard et al. 2013; Morard et al. 2017) and silicate (Sanloup et al. 2013b; Drewitt et al. 2015) melt structure under deep mantle and core conditions. Simultaneous high- $p$ - $T$  conditions may also be achieved in a resistively heated (RH) DAC. Although the maximum attainable temperature is lower than for the LHDAC, the RHDAC has the distinct advantage of providing homogeneous heating over the whole sample allowing the measurement of larger wholly molten samples without contamination from thermal insulation media or laser coupling material (de Grouchy et al. 2017; Louvel et al. 2020; Drewitt et al. 2020).

Regardless of whether large volume or DAC apparatus are used, measuring glass or melt structure *in situ* at high- $p$  requires accurate characterization of the  $p$ -dependent background scattering from the cell to extract a precise measurement of the diffuse glass or melt signal (Shen et al. 2003; Drewitt et al. 2010). This background scattering can be reduced using spatial collimation (Mezouar et al. 2002) or by reducing the fraction of non-sample components within the path of the incident beam: e.g. much of the x-ray Compton scattering from DAC anvils can be eliminated by using perforated diamonds (Soignard et al. 2010).

## Pressure induced modifications in MRO and SRO in SiO<sub>2</sub> and GeO<sub>2</sub> glass

*In situ* high- $p$  spectroscopy (Grimsditch 1984; Hemley et al. 1986; Williams and Jeanloz 1988; Zha et al. 1994; Polsky et al. 1999; Lin et al. 2007; Champagnon et al. 2008; Murakami and Bass 2010), and x-ray (Meade et al. 1992; Inamura et al. 2004; Sato and Funamori 2008; Sato and Funamori 2010; Benmore et al. 2010; Shen et al. 2011; Prescher et al. 2017) and neutron (Zeidler et al. 2014) diffraction have been used extensively to determine the  $p$ -induced structural modifications of pure SiO<sub>2</sub> glass. Extensive spectroscopy (Itié et al. 1989; Durben and Wolf 1991; Polsky et al. 1999; Hong et al. 2007; Vaccari et al. 2009; Baldini et al. 2010; Dong et al. 2017; Spiekermann et al. 2019), and x-ray (Guthrie et al. 2004; Hong et al. 2007; Mei et al. 2010; Hong et al. 2014; Kono et al. 2016) and neutron (Guthrie et al. 2004; Drewitt et al. 2010; Salmon et al. 2012; Wezka et al. 2012) diffraction measurements reveal GeO<sub>2</sub> glass undergoes analogous  $p$ -induced transformations to SiO<sub>2</sub> but over a much lower- $p$  regime.

There is firm consensus from these studies for the operation of two key densification mechanisms in pure SiO<sub>2</sub> and GeO<sub>2</sub> glass starting with a steady collapse in MRO associated with the closure of open ring structures which is accompanied at higher pressures by a continuous transformation from a tetrahedral to octahedral glass network. The changes in MRO are evident in the reciprocal space diffraction patterns from a shift in position of the FSDP at 1.55 Å<sup>-1</sup> at ambient- $p$  to higher  $q$  values with increasing  $p$  (figure 23). This change is accompanied by the development of a second peak at ~3 Å<sup>-1</sup>. The emergence of a new peak observed at ~3 Å<sup>-1</sup> in  $S(q)$  for SiO<sub>2</sub> and GeO<sub>2</sub> glass at high- $p$  is observed for many other types of oxide glasses and melts including calcium aluminate (CaAl<sub>2</sub>O<sub>4</sub>) and anorthite (CaAl<sub>2</sub>Si<sub>2</sub>O<sub>8</sub>) (Drewitt et al. 2015), forsterite (Mg<sub>2</sub>SiO<sub>4</sub>) (Benmore et al. 2011; Adjaoud et al. 2008), and jadeite (NaAlSi<sub>2</sub>O<sub>6</sub>), albite (NaAlSi<sub>2</sub>O<sub>6</sub>) and diopside (CaMgSi<sub>2</sub>O<sub>6</sub>) (Sakamaki et al. 2014a,b). For SiO<sub>2</sub> glass, this peak was originally associated with the breakdown of MRO and emergence of SiO<sub>6</sub> octahedra (Meade et al. 1992; Benmore et al. 2010). More generally, this peak is consistent with the development of short-range topological ordering arising from a more densely packed structure (Elliot 1995; Salmon et al. 2005,2006; Sakamaki et al. 2014b; Drewitt

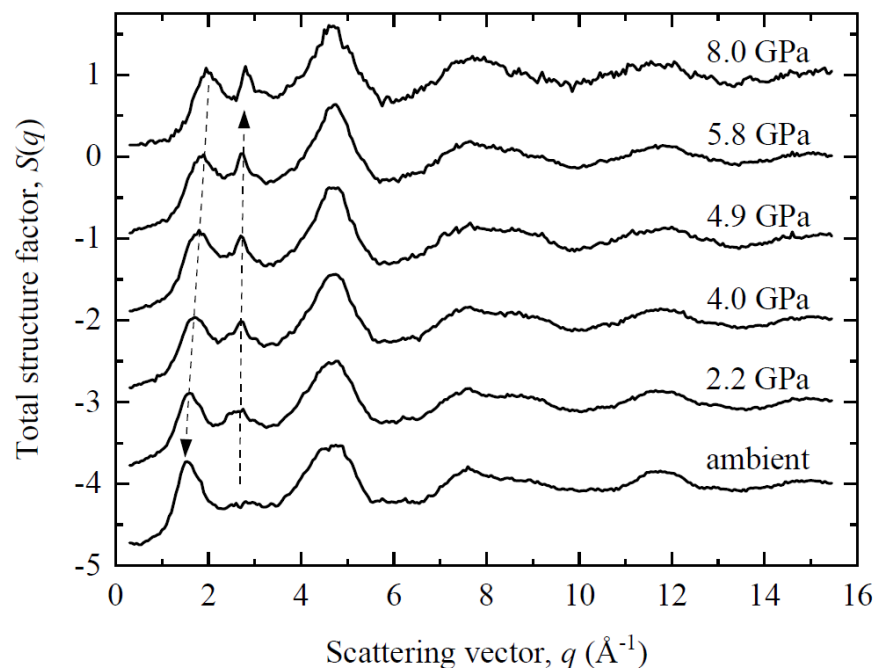


**Figure 23:** Total structure factors  $S(q)$  for GeO<sub>2</sub> glass as measured by *in situ* neutron diffraction at high pressure in the PE cell from ambient to 8.0 GPa. The changes in intensity and position of the FSDP and principal peak are indicated by the arrows. (Data from Drewitt et al. 2010).

et al. 2015). Advances made in neutron diffraction methodologies for high precision *in situ* measurements of glasses at high  $p$  (Drewitt et al. 2010) have enabled NDIS measurements of GeO<sub>2</sub> glass to resolve the individual Ge and O environments (Wezka et al. 2012). From these measurements, the  $p$ -dependence of the mean Ge-O-Ge bond angle was found, which reduces with increasing  $p$  consistent with compaction of the open corner shared tetrahedral network structure.

The transformation in SRO from a tetrahedral to octahedral glass network occurs over the  $p$  range of  $\sim 10$  to  $\sim 40$  GPa (SiO<sub>2</sub>) and  $\sim 5$  to 30 GPa (GeO<sub>2</sub>). The onset of coordination change in network forming structural motifs for a wide range of oxide glasses can be rationalised in terms of the oxygen packing fraction (Wang et al. 2014; Zeidler et al. 2014; Zeidler and Salmon 2016). The upper limit of stability for tetrahedral motifs in both SiO<sub>2</sub> and GeO<sub>2</sub> glass occurs at the same oxygen packing fraction of  $\sim 0.58$  consistent with random loose packing of hard spheres. The conversion to an octahedral network is largely completed at an oxygen packing fraction of  $\sim 0.64$  consistent with random close packing of hard spheres (Zeidler et al. 2014). Molecular dynamics simulations reveal that GeO<sub>5</sub> and SiO<sub>5</sub> units act as important intermediaries on transformation towards an octahedral glass, where the coordination changes primarily from  $4 \rightarrow 5$  and  $5 \rightarrow 6$  (Wezka et al. 2012; Zeidler et al. 2014). This is supported by the measured mean O-Ge-O bond angle from NDIS (Wezka et al. 2012) and can be understood in terms of a ‘zipper’ mechanism for ring closure developed for SiO<sub>2</sub> glass in which a tetrahedral SiO<sub>4</sub> unit belonging to a ring structure forms a new bond with a bridging oxygen within the ring, leading to the formation of distorted square pyramidal SiO<sub>5</sub> units and threefold coordinated oxygen atoms (Wezka et al. 2012; Zeidler et al. 2014). This demonstrates a striking interrelation between the changes experienced in SRO and MRO which is underscored by a correlation between the position of the FSDP in  $S(q)$ , relative to its position at ambient- $p$ , and the onset of coordination change (Zeidler and Salmon 2016).

Some studies using *in situ* XRD (Sato and Funamori 2010), Brillouin spectroscopy (Murakami and Bass 2010) and  $K\beta''$  x-ray emission spectroscopy (Spiekermann et al. 2019) suggest a plateau in octahedral coordination persisting in SiO<sub>2</sub> and GeO<sub>2</sub> glass beyond 100 GPa. However, molecular dynamics simulations of both SiO<sub>2</sub> and GeO<sub>2</sub> glass (Brazhkin et al. 2011) and SiO<sub>2</sub> melt (Karki et al. 2007) indicate a continuous increase in coordination number  $> 6$  at 100 GPa. Recent *in situ* XRD measurements for SiO<sub>2</sub> glass in a DAC up to 172 GPa (Prescher et al. 2017) and GeO<sub>2</sub> glass in a double stage large-volume cell up to 91.7 GPa (Kono 2016) appear to confirm this, indicating that after the initial continuous  $4 \rightarrow 5 \rightarrow 6$  transition at lower  $p$  **there** follows a gradual increase in coordination number approaching 7-8 in the megabar regime.

### ***Silicate melt structure at high pressure***

*In situ* diffraction measurements of the structure of silicate melts have advanced significantly in the last decade. Exploratory *in situ* diffraction study of molten silicates were first reported for CaSiO<sub>3</sub> and MgSiO<sub>3</sub> melts up to 6 GPa using a cubic multi-anvil device with synchrotron XRD (Funamori et al. 2004). In the last decade, the structure of a range of silicate melts have been measured by diffraction using large volume pressure cells at pressures up to  $\sim 10$  GPa including forsterite-enstatite (Mg<sub>2</sub>SiO<sub>4</sub>-MgSiO<sub>3</sub>) (Yamada et al. 2007; Yamada et al. 2011), albite (NaAlSi<sub>3</sub>O<sub>8</sub>) (Yamada et al. 2011), jadeite (NaAlSi<sub>2</sub>O<sub>6</sub>) (Sakamaki 2012, 2014a; Wang et al. 2014), fayalite (Fe<sub>2</sub>SiO<sub>4</sub>) (Sanloup 2013a), diopside (CaMgSi<sub>2</sub>O<sub>6</sub>) (Wang et al. 2014), and basaltic melts (Sakamaki et al. 2013; Crépeau et al. 2014).

A compilation of structure, density, and viscosity data of silicate melts under pressure reveals a reduction in isothermal viscosity of polymerized melts up to  $\sim 3$ -5 GPa where it encounters a turnover to a normal (positive)  $p$ -dependence (Wang et al. 2014). This viscosity



turnover is attributed to the tetrahedral packing limit, below which the structural transformations are dominated by changes in network connectivity and the collapse of MRO resulting in a reduction in inter-tetrahedral bond angle which leads to high compressibility. Above the viscosity turnover, the structural response is dominated by the increase in coordination of Si and Al atoms (Wang et al. 2014). The structural measurements for molten fayalite reveal an increase in average Fe-O coordination from 4.8 GPa at ambient-*p* (Drewitt et al. 2013) to 7.2 at 7.5 GPa (Sanloup et al. 2013a). It is suggested that this rapid increase in Fe coordination is responsible for the higher compressibility of fayalite melt compared with molten Mg-rich San Carlos olivine (Guillot and Sator 2007, Sanloup et al. 2013a).

To date, only two studies have been reported for the *in situ* structure of silicate melts beyond 10 GPa. Both studies utilise the LHDAC combined with synchrotron XRD, with molten basalt reported to lower mantle conditions up to 60 GPa using Yb-fibre laser heating (Sanloup et al. 2013b) and liquid anorthite reported to 32.5 GPa using CO<sub>2</sub> laser heating (Drewitt et al. 2015). The measurements of molten basalt reveal an increase in Si-O coordination change from 4 at ambient-*p* (Drewitt et al. 2013) to six at 35 GPa, consistent with the results for pure SiO<sub>2</sub> glass discussed above. By normalising the x-ray intensities using an iterative procedure that minimises the unphysical low-*r* oscillations below the first interatomic bond distance (Eggert et al. 2002) a converged solution for melt density was determined directly from the liquid diffraction measurements. The results reveal that molten basalt experiences a density crossover with the solid mantle and may be gravitationally stable in the deep lower mantle (Sanloup et al. 2013b). This supports the Labrosse layered model of a crystallising magma ocean, where a crystalline layer separates an upper and lower magma ocean (Labrosse et al. 2007).

### ***Al coordination change at high pressure***

NMR and x-ray spectroscopy measurements of permanently densified aluminosilicate glasses, synthesised from high-*p* melts (up to 12 GPa) in multi anvil apparatus and recovered to ambient conditions, revealed the development of highly coordinated AlO<sub>5</sub> and AlO<sub>6</sub> populations occur at far lower pressures than changes observed for Si-O coordination and as such has a greater influence on controlling magma mobility in the shallow upper mantle (Li et al. 1995; Yarger et al. 1995; Allwardt et al. 2005a,b; Kelsey et al. 2009). Direct *in situ* synchrotron XRD measurements of Al coordination change in CaAl<sub>2</sub>O<sub>4</sub> and CaAl<sub>2</sub>Si<sub>2</sub>O<sub>6</sub> (anorthite) glasses to 30 GPa reveal a continuous increase in Al-O coordination reaching an average value of ~6 by 25 GPa (Drewitt et al. 2015). The only reported *in situ* measurements of Al-O coordination change in a melt at high-*p*, made for liquid CaAl<sub>2</sub>Si<sub>2</sub>O<sub>6</sub> to 32.4 GPa using synchrotron XRD in a DAC with CO<sub>2</sub> laser heating, reveals a the change in local Al structure is comparable to the glass with average Al-O coordination of 5 by ~ 10 GPa and 6 by ~ 30 GPa (Drewitt et al. 2015).

The increase in Al-O coordination from 4-, to 5-, to 6-fold up to 30 GPa measured for molten anorthite is consistent with the results of MD simulations (de Koker 2010; Drewitt et al. 2015). At ambient pressure, chemical ordering dominates in the form of AlO<sub>4</sub> and SiO<sub>4</sub> tetrahedra. On initial pressurization, the relatively open network structure is compressed and destroyed (Drewitt et al. 2015). This is supported by *in situ* Raman measurements of the glass which reveal a rapid reduction in the inter-tetrahedral bond angle below 2 GPa (Moulton et al. 2019). The increase in Al-O coordination number increases almost immediately on compression with the formation of AlO<sub>5</sub> motifs and increasing fractions of AlO<sub>6</sub> units after ~ 5 GPa (Drewitt et al. 2015). At 10-15 GPa, the fraction of AlO<sub>5</sub> units reaches a maximum fraction of ~ 50% and are increasingly replaced by AlO<sub>6</sub> units to become the dominant feature at ≥ 30 GPa (figure 24a). These changes in coordination are accompanied by a reduction in NBO fraction to only a few per cent by 10-15 GPa (Drewitt et al. 2015), consistent with Raman spectroscopy

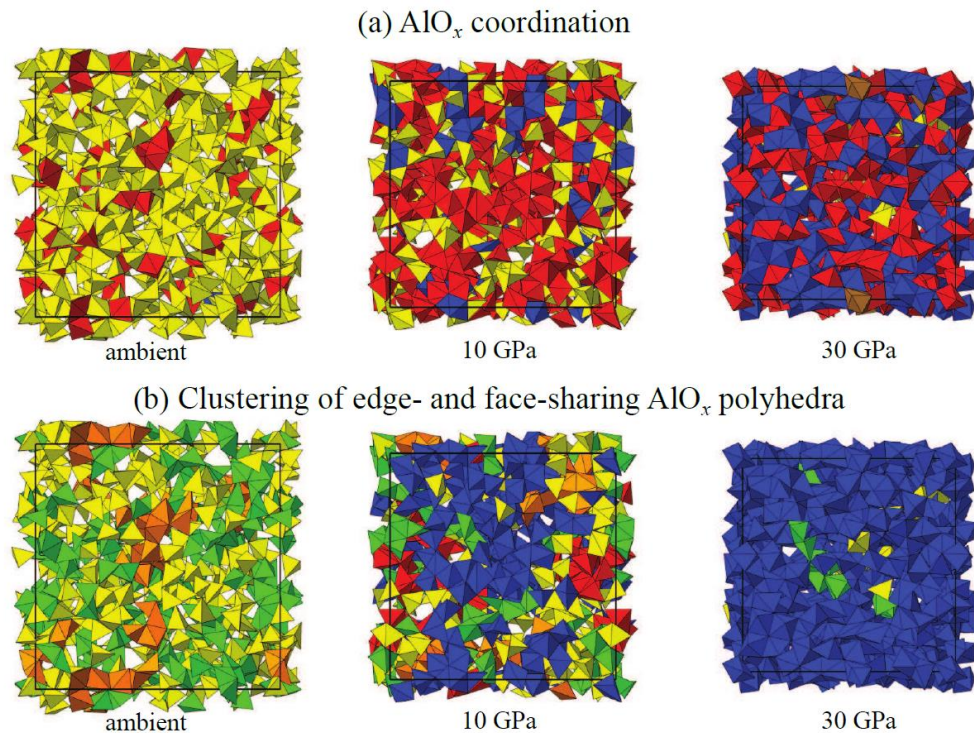


**Figure 24:** Snapshots from MD simulations of liquid  $\text{CaAl}_2\text{O}_4$  at 2500 K at ambient, 10 GPa, and 30 GPa. (a)  $\text{AlO}_x$  coordination with  $x = 4$  (yellow), 5 (red), 6 (blue), and 7 (brown). (b) clusters of  $> 100$  (blue), 10-100 (red), 5-9 (orange), 2-4 (green), and 1 (yellow) of edge- and face-sharing  $\text{AlO}_x$  polyhedra. Reprinted figure with permission from Drewitt et al. *Journal of Physics: Condensed Matter* 27:105103 (2015) doi:[10.1088/0953-8984/27/10/105103](https://doi.org/10.1088/0953-8984/27/10/105103) Copyright (2015) by the Institute of Physics.

measurements which indicate that depolymerized  $Q^2$  and  $Q^3$   $\text{AlO}_4$  units are the first to transform to higher coordination (Muniz et al. 2016). The Si-O coordination number follows a similar behaviour as for pure  $\text{SiO}_2$  glass. The Ca-O coordination begins to increase immediately on compression, rising continuously to an average value of  $\sim 10$  at 30 GPa. The increase in highly coordinated Al and Ca units is accompanied by a development in polyhedral connectivity. At 10 GPa,  $\sim 95\%$  Ca and  $50\%$  Al atoms belong to single large clusters, increasing to  $100\%$  Ca and  $90\%$  Al atoms by 30 GPa (figure 24b).

At higher pressures, recent *in situ* synchrotron XRD measurements of an aluminosilicate glass using a double-stage PE cell suggest the Al-O coordination number remains constant at  $\sim 6$  up to 110 GPa (Ohira et al. 2019). However, molecular dynamics simulations indicate a continuous increase in Al-O coordination number in aluminosilicate glasses and melts, approaching values of  $\sim 7$  at 100 GPa (de Koker 2010; Bajgain et al. 2015; Ghosh and Karki 2018). We note that it is not possible to separate the Si-O and Al-O nearest neighbour contributions in the total pair distribution functions of aluminosilicate glass measured by Ohira et al. (2019). This contrasts with the measurements reported by Drewitt et al. (2015) in the Al-O coordination environment was unambiguously quantified directly from the measurement of silica-free  $\text{CaAl}_2\text{O}_4$  glass.



## REFERENCES

- Aasland S and McMillan PF (1994) Density-driven liquid–liquid phase separation in the system  $\text{Al}_2\text{O}_3\text{--Y}_2\text{O}_3$ . *Nature* 369:633-636 doi:[10.1038/369633a0](https://doi.org/10.1038/369633a0)
- Adjaoud O, Steinle-Neumann G, Jahn S (2008)  $\text{Mg}_2\text{SiO}_4$  liquid under high pressure from molecular dynamics. *Chem Geol* 256:185-192 doi:[10.1016/j.chemgeo.2008.06.031](https://doi.org/10.1016/j.chemgeo.2008.06.031)
- Alderman OLG, Hannon AC, Holland D, Feller S, Lehr G, Vitale AJ, Hoppe U, Zimmerman M, Watenphul A (2013) Lone-pair distribution and plumbite network formation in high lead silicate glass,  $80\text{PbO}\cdot 20\text{SiO}_2$  *Phys Chem Chem Phys* 15:8506-8519 doi:[10.1039/C3CP51348C](https://doi.org/10.1039/C3CP51348C)
- Alderman OLG, Wilding MC, Tamalonis A, Sendelbach S, Heald SM, Benmore CJ, Johnson JA, Hah H-Y, Weber JKR (2017a) Iron K-edge x-ray absorption near-edge structure spectroscopy of aerodynamically levitated silicate melts and glasses. *Chem Geol* 453:169-185 doi:[10.1016/j.chemgeo.2017.01.020](https://doi.org/10.1016/j.chemgeo.2017.01.020)
- Alderman OLG, Lazareva L, Wilding MC, Benmore CJ, Heald SM, Johnson CE, Johnson JA, Hah H-Y, Sendelbach S, Tamalonis A, Skinner LB, Parise JB, Weber JKR (2017) Local structural variation with oxygen fugacity in  $\text{Fe}_2\text{SiO}_{4+x}$  fayalitic iron silicate melts. *Geochim Cosmochim Acta* 203:15-36 doi:[10.1016/j.gca.2016.12.038](https://doi.org/10.1016/j.gca.2016.12.038)
- Allwardt JR, Stebbins JF, Schmidt BC, Frost DJ, Withers AC, Hirschmann MM (2005) Aluminum coordination and the densification of high-pressure aluminosilicate glasses. *Am Mineral* 90:1218-1222 doi:[10.2138/am.2005.1836](https://doi.org/10.2138/am.2005.1836)
- Allwardt JR, Poe BT, Stebbins JF (2005) The effect of fictive temperature on Al coordination in high-pressure (10 GPa) sodium aluminosilicate glasses. *Am Mineral* 90:1453-1457 doi:[10.2138/am.2005.1736](https://doi.org/10.2138/am.2005.1736)
- Agee CB, Walker D (1988) Static Compression and Olivine Flotation in Ultrabasic Silicate Liquid. *J Geophys Res* 93:3437-3449 doi:[10.1029/JB093iB04p03437](https://doi.org/10.1029/JB093iB04p03437)
- Angell CA (1995) Formation of Glasses from Liquids and Biopolymers. *Science* 267:1924-1935 doi:[10.1126/science.267.5206.1924](https://doi.org/10.1126/science.267.5206.1924)
- Auzende A-L, Gillot J, Coquet A, Hennet L, Ona-Nguema G, Bonnin D, Esteve I, Roskosz M, Fiquet G (2011) Synthesis of amorphous MgO-rich peridotitic starting material for laser-heated diamond anvil cell experiments – application to iron partitioning in the mantle. *High Press Res* 31:199-213 doi:[10.1080/08957959.2011.556631](https://doi.org/10.1080/08957959.2011.556631)
- Bajgain S, Ghosh DB, Karki BB (2015) Structure and density of basaltic melts at mantle conditions from first-principles simulations. *Nature Commun* 6:8578 doi:[10.1038/ncomms9578](https://doi.org/10.1038/ncomms9578)
- Baldini M, Aquilanti G, Mao H-k, Yang W, Shen G, Pascarelli S, Mao WL (2010) High-pressure EXAFS study of vitreous  $\text{GeO}_2$  up to 44 GPa. 81:024201 doi:[10.1103/PhysRevB.81.024201](https://doi.org/10.1103/PhysRevB.81.024201)
- Baggioli M, Zaccone A (2019) Universal Origin of Boson Peak Vibrational Anomalies in Ordered Crystals and in Amorphous Materials. *Phys Rev Lett* 122:145501-145507 doi:[10.1103/PhysRevLett.122.145501](https://doi.org/10.1103/PhysRevLett.122.145501)
- Bancroft M, Nesbitt HW, Henderson GS, O'Shaughnessy C, Withers AC, Neuville DR (2018) Lorentzian dominated lineshapes and linewidths for Raman symmetric stretch peaks ( $800\text{--}1200\text{ cm}^{-1}$ ) in  $Q_n$  ( $n=1\text{--}3$ ) species of alkali silicate glasses/melts. *J Non-Cryst Solids* 484:72-83 doi:[10.1016/j.jnoncrysol.2018.01.018](https://doi.org/10.1016/j.jnoncrysol.2018.01.018)
- Barnes AC (2015) A comparison of structural models of  $\text{Tb}_3\text{Al}_5\text{O}_{12}$  and  $\text{Nd}_3\text{Al}_5\text{O}_{12}$  glasses obtained when using x-ray data alone and when x-ray and neutron data are combined. *Z Phys Chem* 230:387-415 doi:[10.1515/zpch-2015-0668](https://doi.org/10.1515/zpch-2015-0668)
- Barnes AC, Skinner LB, Salmon PS, Bytchkov A, Pozdnyakova I, Farmer TO, Fischer HE (2009) Liquid-Liquid Phase Transition in Supercooled Yttria-Alumina. *Phys Rev Lett* 103:225702 doi:[10.1103/PhysRevLett.103.225702](https://doi.org/10.1103/PhysRevLett.103.225702)
- Barney ER, Hannon AC, Holland D, Winslow D, Rijal B, Affatigato M, Feller SA (2007) Structural studies of lead aluminate glasses. *J Non-Cryst Solids* 353:1741-1747 doi:[10.1016/j.jnoncrysol.2007.02.007](https://doi.org/10.1016/j.jnoncrysol.2007.02.007)
- Barrio RA, Galeener FL, Martínez E, Elliot RJ (1993) Regular ring dynamics in  $\text{AX}_2$  tetrahedral glasses. *Phys Rev B* 48:15672-15689 doi:[10.1103/PhysRevB.48.15672](https://doi.org/10.1103/PhysRevB.48.15672)
- Bassett WA (2009) Diamond anvil cell, 50<sup>th</sup> birthday. *High Press Res* 29:163-186 doi:[10.1080/08957950802597239](https://doi.org/10.1080/08957950802597239)

- Bell PM, Mao H-k, Goettel K (1984) Ultrahigh Pressure: Beyond 2 Megabars and the Ruby Fluorescence Scale. *Science* 226:542-544 doi:[10.1126/science.226.4674.542](https://doi.org/10.1126/science.226.4674.542)
- Ben Kacem I, Gautron L, Coillot D, Neuville DR (2017) Structure and properties of lead silicate glasses and melts. *Chem Geol* 461:104-114 doi:[10.1016/j.chemgeo.2017.03.030](https://doi.org/10.1016/j.chemgeo.2017.03.030)
- Benmore CJ, Weber JKR, Sampath S, Siewenie J, Urquidí J, Tangeman JA (2003) A neutron and x-ray diffraction study of calcium aluminate glasses. *J Phys: Condens Matter* 15:S2413-S2423 doi:[10.1088/0953-8984/15/31/316](https://doi.org/10.1088/0953-8984/15/31/316)
- Benmore CJ, Weber JKR, Wilding MC, Du J, Parise JB (2010) Temperature-dependent structural heterogeneity in calcium silicate liquids. *Phys Rev B* 82:224202 doi:[10.1103/PhysRevB.82.224202](https://doi.org/10.1103/PhysRevB.82.224202)
- Benmore CJ, Soignard E, Amin SA, Guthrie M, Shastri SD, Lee PL, Yarger JL (2010) Structural and topological changes in silica glass at pressure. *Phys Rev B* 81:054105 doi:[10.1103/PhysRevB.81.054105](https://doi.org/10.1103/PhysRevB.81.054105)
- Benmore CJ, Soignard E, Guthrie M, Amin SA, Weber JKR, McKiernan K, Wilding MC, Yarger JL (2011) High pressure x-ray diffraction measurements on Mg<sub>2</sub>SiO<sub>4</sub> glass. *J Non-Cryst Solids* 357:2632-2636 doi:[10.1016/j.jnoncrystol.2010.12.064](https://doi.org/10.1016/j.jnoncrystol.2010.12.064)
- Benmore CJ (2015) X-ray diffraction from glass. In: *Modern Glass Characterisation*, Affatigato M (Ed), John Wiley and Sons, USA, p 241-270 doi:[10.1002/9781119051862.ch6](https://doi.org/10.1002/9781119051862.ch6)
- Benmore CJ and Weber JKR (2017) Aerodynamic levitation, supercooled liquids and glass formation. *Adv Phys X* 2:717-736 doi:[10.1080/23746149.2017.1357498](https://doi.org/10.1080/23746149.2017.1357498)
- Besson JM, Nelmes RJ, Hamel G, Loveday JS, Weill G, Hull S (1992) Neutron powder diffraction above 10 GPa. *Physica B* 180-181:907-910 doi:[10.1016/0921-4526\(92\)90505-M](https://doi.org/10.1016/0921-4526(92)90505-M)
- Besson JM, Grima P, Gauthier M, Itié JP, Mézouar M, Häusermann D, Hanfland M (1996) Pretransitional Behavior in Zinblendes HgTe under High Pressure and Temperature. *Phys Stat Sol* 198:419-425 doi:[10.1002/pssb.2221980154](https://doi.org/10.1002/pssb.2221980154)
- Binsted N, Greaves GN, Henderson CMB (1986) Fe K-edge x-ray absorption spectroscopy of silicate minerals and glasses. *J Phys Colloques* 47:C8-837-C8-840 doi:[10.1051/jphyscol:19868160](https://doi.org/10.1051/jphyscol:19868160)
- Bingham PA, Parker JM, Searle TM, Smith I (2007) Local structure and medium range ordering of tetrahedrally coordinated Fe<sup>3+</sup> ions in alkali-alkaline earth-silica glasses. *J Non-Cryst Solids* 353:2479-2494 doi:[10.1016/j.jnoncrystol.2007.03.017](https://doi.org/10.1016/j.jnoncrystol.2007.03.017)
- Brink T, Koch L, Able K (2016) Structural origins of the boson peak in metals: From high-entropy alloys to metallic glasses. *Phys. Rev. B* 94:224203 doi:[10.1103/PhysRevB.94.224203](https://doi.org/10.1103/PhysRevB.94.224203)
- Bockris JO, Mellors GW, (1956) Electric transport in liquid lead silicates and borates. *J Phys Chem* 60:1321-1328 doi:[10.1021/j150543a040](https://doi.org/10.1021/j150543a040)
- Börjesson L, Hassan AK, Swenson J, Torell LM, Fontana A (1993) Is There a Correlation between the First Sharp Diffraction Peak and the Low Frequency Vibrational Behavior of Glasses? *Phys Rev Lett* 70:1275-1278 doi:[10.1103/PhysRevLett.70.1275](https://doi.org/10.1103/PhysRevLett.70.1275)
- Bowron DT, (2008) An experimentally consistent atomistic structural model of silica glass. *Mater Sci Eng B* 149:166-170 doi: [10.1016/j.mseb.2007.11.030](https://doi.org/10.1016/j.mseb.2007.11.030)
- Bridgman PW, Šimon I (1953) Effects of Very High Pressures on Glass. *J Appl Phys* 24:405-413 doi:[10.1063/1.1721294](https://doi.org/10.1063/1.1721294)
- Bucheneau U, Prager M, Nucker N, Dianoux AJ, Ahmad N, Phillips WA (1986) Low-frequency modes in vitreous silica. *Phys Rev B* 34:5665-5673 doi:[10.1103/PhysRevB.34.5665](https://doi.org/10.1103/PhysRevB.34.5665)
- Bucheneau U, Galperin YM, Gurevich VL, and Schober HR (1991) Anharmonic potentials and vibrational localization in glasses. *Phys Rev B* 43:5039 doi:[10.1103/PhysRevB.43.5039](https://doi.org/10.1103/PhysRevB.43.5039)
- Bucheneau U, Galperin YM, Gurevich VL, Parshin DA, Ramos MA, Schober HR (1992) Interaction of soft modes and sound waves in glasses *Phys Rev B* 46:2798-2808 doi:[10.1103/PhysRevB.46.2798](https://doi.org/10.1103/PhysRevB.46.2798)
- Burkhard DJM (2000) Iron-bearing silicate glasses at ambient conditions. *J Non-Cryst Solids* 275:175-188 doi:[10.1016/S0022-3093\(00\)00252-0](https://doi.org/10.1016/S0022-3093(00)00252-0)
- Calas G, Petiau J (1983) Coordination of iron in oxide glasses through high-resolution K-edge spectra: Information from the pre-edge. *Solid State Commun* 48:625-629 doi:[10.1016/0038-1098\(83\)90530-6](https://doi.org/10.1016/0038-1098(83)90530-6)
- Caldwell WA, Kunz M, Celestre RS, Domning EE, Walter MJ, Walker D, Glossinger J, MacDowell AA, Padmore HA, Jeanloz R, Clark SM (2007) Laser-heated diamond anvil cell at the advanced light source beamline 12.2.2. *Nucl Instr Meth Phys Res A* 582:221-225 doi:[10.1016/j.nima.2007.08.113](https://doi.org/10.1016/j.nima.2007.08.113)

- Champagnon B, Martinet C, Boudeulle M, Vouagner D, Coussa C, Deschamps T, Grosvalet (2008) High pressure elastic and plastic deformations of silica: In situ diamond anvil cell Raman experiments. *J Non-Cryst Solids* 354:569-573 doi:[10.1016/j.jnoncrysol.2007.07.079](https://doi.org/10.1016/j.jnoncrysol.2007.07.079)
- Charpentier T, Okhotnikov K, Novikov AN, Hennet L, Fischer HE, Neuville DR, Florian P (2018) Structure of Strontium Aluminosilicate Glasses from Molecular Dynamics Simulation, Neutron Diffraction, and Nuclear Magnetic Resonance Studies. *J Phys Chem B* 122:9567-9583 doi:[10.1021/acs.jpcc.8b05721](https://doi.org/10.1021/acs.jpcc.8b05721)
- Crichton WA, Mezouar M (2005) Methods and application of the Paris-Edinburgh Press to X-ray diffraction structure solution with large-volume samples at high pressures and temperatures. *In: Advances in High-Pressure Technology for Geophysical Applications*, Chen J, Wang Y, Duffy TS, Shen G, Dobrzhinetskaya LF (eds) Elsevier, Holland, Chapter 17, 353-369 doi:[10.1016/B978-044451979-5.50019-3](https://doi.org/10.1016/B978-044451979-5.50019-3)
- Chumakov AI, Monaco G, Monaco A, Crichton WA, Bosak A, Rüffer R, Meyer A, Kargl F, Comez L, Fioretto D, Giefers H, Roitsch S, Wortmann G, Manghnani MH, Hushur A, Williams Q, Balogh J, Parliński K, Jochym P, Piekarczyk P (2011) Equivalence of the Boson Peak in Glasses to the Transverse Acoustic van Hove Singularity in Crystals. *Phys Rev Lett* 106: 225501-225512. doi:[10.1103/PhysRevLett.106.225501](https://doi.org/10.1103/PhysRevLett.106.225501)
- Cicchini MR, de Ligny D, Gallo TM, Neuville DR (2016) Ca Neighbors from XANES spectroscopy: a tool to investigate structure, redox and nucleation processes in silicate glasses, melts and crystals. *Am Mineral* 101:1232-1236 doi:[10.2138/am-2016-5663](https://doi.org/10.2138/am-2016-5663)
- Cochain B, Neuville DR, Henderson GS, McCammon C, Pinet O, Richet P (2012) Iron content, redox state and structure of sodium borosilicate glasses: A Raman, Mössbauer and boron K-edge XANES spectroscopy study. *J Am Ceram Soc* 94:1-12 doi:[10.1111/j.1551-2916.2011.05020.x](https://doi.org/10.1111/j.1551-2916.2011.05020.x)
- Cormack AN, Du J (2001) Molecular dynamics simulations of soda-lime silicate glasses. *J Non-Cryst Solids* 293-295:283-289 doi:[10.1016/S0022-3093\(01\)00831-6](https://doi.org/10.1016/S0022-3093(01)00831-6)
- Cormier L, Neuville DR, Calas G (2000) Structure and properties of low-silica calcium aluminosilicate glasses. *J Non-Cryst Solids* 274:110-114 doi:[10.1016/S0022-3093\(00\)00209-X](https://doi.org/10.1016/S0022-3093(00)00209-X)
- Cormier L, Ghaleb D, Neuville DR, Delaye JM, Calas G (2003) Chemical dependence of network topology of calcium aluminosilicate glasses: a computer simulation study. *J. Non-Cryst Solids* 332:255-270 doi:[10.1016/j.jnoncrysol.2003.09.012](https://doi.org/10.1016/j.jnoncrysol.2003.09.012)
- Cormier L and Cuello GJ (2011) Mg coordination in a MgSiO<sub>3</sub> glass using neutron diffraction coupled with isotopic substitution. *Phys Rev B* 83:224204 doi:[10.1103/PhysRevB.83.224204](https://doi.org/10.1103/PhysRevB.83.224204)
- Cormier L and Cuello GJ (2013) Structural investigation of glasses along the MgSiO<sub>3</sub>-CaSiO<sub>3</sub> join: Diffraction studies. *Geochim Cosmochim Acta* 122:498-510 doi: [10.1016/j.gca.2013.04.026](https://doi.org/10.1016/j.gca.2013.04.026)
- Cormier L (2019) Neutron and X-ray Diffraction of Glass. *In: Handbook of Glass*, Musgraves JD, Hu J, Calvez L (eds) Springer Nature, Switzerland pp 1045-1092 doi:[10.1007/978-3-319-93728-1](https://doi.org/10.1007/978-3-319-93728-1)
- Coté B, Massiot D, Taulelle F, Coutures J-P (1992) <sup>27</sup>Al NMR spectroscopy of aluminosilicate melts and glasses. *Chem Geol* 96:367-370 doi:[10.1016/0009-2541\(92\)90065-D](https://doi.org/10.1016/0009-2541(92)90065-D)
- Crépeau C, Morard G, Bureau H, Prouteau G, Morizet Y, Petitgirard S, Sanloup C (2014) Magmas trapped at the continental lithosphere-asthenosphere boundary. *Earth Planet Sci Lett* 393:105-112 doi:[10.1016/j.epsl.2014.02.048](https://doi.org/10.1016/j.epsl.2014.02.048)
- Cristiglio V, Cuello GJ, Hennet L, Pozdnyakova I, Leydier M, Kozaily J, Fischer HE, Johnson MR, Price DL (2010) Neutron diffraction study of molten calcium aluminates. *J Non-Cryst Solids* 356:2492-2496 doi:[10.1016/j.jnoncrysol.2010.03.027](https://doi.org/10.1016/j.jnoncrysol.2010.03.027)
- Daniel I, Gillet P, Ghose F (1995) An *in situ* high-temperature structural study of stable and metastable CaAl<sub>2</sub>Si<sub>2</sub>O<sub>8</sub> polymorphs. *Mineral Mag* 59:25-33 doi [10.1180/minmag.1995.59.394.03](https://doi.org/10.1180/minmag.1995.59.394.03)
- Daniel I, McMillan PF, Gillet P, Poe BT (1996) Raman spectroscopic study of structural changes in calcium aluminate (CaAl<sub>2</sub>O<sub>4</sub>) glass at high pressure and high temperature. *Chem Geol* 128:5-15 doi:[10.1016/0009-2541\(95\)00159-X](https://doi.org/10.1016/0009-2541(95)00159-X)
- de Grouchy CJL, Sanloup C, Cochain B, Drewitt JWE, Kono Y, Crépeau C (2017) Lutetium incorporation in magmas at depth: Changes in melt local environment and the influence on partitioning behaviour. *Earth Planet Sci Lett* 464:155-165 doi:[10.1016/j.epsl.2017.02.017](https://doi.org/10.1016/j.epsl.2017.02.017)
- de Koker N (2010) Structure, thermodynamics, and diffusion in CaAl<sub>2</sub>Si<sub>2</sub>O<sub>8</sub> liquid from first-principles molecular dynamics. *Geochim Cosmochim Acta* 74:5657-5671 doi:[10.1016/j.gca.2010.02.024](https://doi.org/10.1016/j.gca.2010.02.024)

- Di Genova D, Morgavi D, Hess K-U, Neuville DR, Borovkov N, Perugini D, Dingwell DB (2015) Approximate chemical analysis of volcanic glasses using Raman spectroscopy. *J Raman Spectr* 46:1235-1244 doi:[10.1002/jrs.4751](https://doi.org/10.1002/jrs.4751)
- Di Genova D., Kolzenburg S, Vona A, Chevrel MO, Hess K-U, Neuville DR, Ertel-Ingrisch W, Romano C, Dingwell DB (2016) Raman spectra of Martian glass analogues: A tool to approximate their chemical composition. *J Geophys Res Planets* 121:740–752 doi:[10.1002/2016JE005010](https://doi.org/10.1002/2016JE005010)
- Di Genova D, Vasseur J, Hess K-U, Neuville DR, Dingwell DB (2017) Effect of oxygen fugacity on the glass transition, viscosity and structure of silica- and iron-rich magmatic melts. *J Non-Cryst Solids* 470:78-85 doi:[10.1016/j.jnoncrsol.2017.05.013](https://doi.org/10.1016/j.jnoncrsol.2017.05.013)
- Di Muro A, Métrich N, Mercier M, Giordano D, Massare D, Montagnac G (2009) *Chem Geol* 259:78-88 doi:[10.1016/j.chemgeo.2008.08.013](https://doi.org/10.1016/j.chemgeo.2008.08.013)
- Dingwell DB, Virgo D (1988) Viscosities of melts in the Na<sub>2</sub>O-FeO-Fe<sub>2</sub>O<sub>3</sub>-SiO<sub>2</sub> system and factors controlling relative viscosities of fully polymerized silicate melts. *Geochim Cosmochim Acta* 52:395-403 doi:[10.1016/0016-7037\(88\)90095-6](https://doi.org/10.1016/0016-7037(88)90095-6)
- Dong J, Yao H, Guo Z, Jia Q, Wang Y, An P, Gong Y, Liang Y, Chen D (2017) Revisiting local structural changes in GeO<sub>2</sub> glass at high pressure. *J Phys Condens Matter* 29:465401 doi:[10.1088/1361-648X/aa8d50](https://doi.org/10.1088/1361-648X/aa8d50)
- Drewitt JWE, Salmon PS, Barnes AC, Klotz S, Fischer HE, Crichton WA (2010) Structure of GeO<sub>2</sub> glass at pressures up to 8.6 GPa. *Phys Rev B* 81: 014202 doi:[10.1103/PhysRevB.81.014202](https://doi.org/10.1103/PhysRevB.81.014202)
- Drewitt JWE, Jahn S, Cristiglio V, Bytchkov A, Leydier M, Brassamin S, Fischer HE, Hennet L (2011) The structure of liquid calcium aluminates as investigated using neutron and high energy x-ray diffraction in combination with molecular dynamics simulation methods. *Journal of Physics: Condensed Matter* 23, 155101 doi:[10.1088/0953-8984/24/9/099501](https://doi.org/10.1088/0953-8984/24/9/099501)
- Drewitt JWE, Hennet L, Zeidler A, Jahn S, Salmon PS, Neuville DR, Fischer HE (2012) Structural transformations on vitrification in the fragile glass-forming system CaAl<sub>2</sub>O<sub>4</sub>. *Phys Rev Lett* 109:235501 doi:[10.1103/PhysRevLett.109.235501](https://doi.org/10.1103/PhysRevLett.109.235501)
- Drewitt JWE, Sanloup C, Bytchkov A, Brassamin S, Hennet L (2013) Structure of (Fe<sub>x</sub>Ca<sub>1-x</sub>O)<sub>y</sub>(SiO<sub>2</sub>)<sub>1-y</sub> liquids and glasses from high-energy x-ray diffraction: Implications for the structure of natural basaltic magmas. *Phys Rev B* 87:224201 doi:[10.1103/PhysRevB.87.224201](https://doi.org/10.1103/PhysRevB.87.224201)
- Drewitt JWE, Jahn S, Sanloup C, de Grouchy C, Garbarino G, Hennet L (2015) Development of chemical and topological structure in aluminosilicate liquids and glasses at high pressure. *J Phys: Condens Matter* 27:105103 doi:[10.1088/0953-8984/27/10/105103](https://doi.org/10.1088/0953-8984/27/10/105103)
- Drewitt JWE, Barnes AC, Jahn S, Kohn SC, Walter MJ, Novikov A, Neuville DR, Fischer HE, Hennet L (2017) Structure of liquid tri-calcium aluminate. *Phys Rev B* 95:064203-064214 doi:<https://doi.org/10.1103/PhysRevB.95.064203>
- Drewitt JWE, Jahn S, Hennet L (2019) Configurational constraints on glass formation in the liquid calcium aluminate system. *J Stat Mech* 104012 doi:[10.1088/1742-5468/ab47fc](https://doi.org/10.1088/1742-5468/ab47fc)
- Drewitt JWE, Turci F, Heinen BJ, Macleod SG, Qin F, Kleppe AK, Lord OT (2020) Structural Ordering in Liquid Gallium under Extreme Conditions. *Phys Rev Lett* 124:145501 doi:[10.1103/PhysRevLett.124.145501](https://doi.org/10.1103/PhysRevLett.124.145501)
- Du J, and Cormack AN (2001) The medium range structure of sodium silicate glasses: a molecular dynamics simulation. *J Non-Cryst Solids* 349:66-79 doi:[10.1016/j.jnoncrsol.2004.08.264](https://doi.org/10.1016/j.jnoncrsol.2004.08.264)
- Du J, Corrales R (2007) Understanding lanthanum aluminate glass structure by correlating molecular dynamics simulation results with neutron and x-ray scattering data. *J Non-Cryst Solids* 353:210-214 doi:[10.1016/j.jnoncrsol.2006.06.025](https://doi.org/10.1016/j.jnoncrsol.2006.06.025)
- Dubrovinskaia N, Dubrovinsky L, Solopova NA, Abakumov A, Turner S, Hanfland M, Bykova E, Bykov M, Prescher C, Prakapenka VB, Petitgirard S, Chuvashova I, Gasharova B, Mathis Y-L, Ershov P, Snigireva I, Snigirev A (2016) Terapascal static pressure generation with ultrahigh yield strength nanodiamond. *Science Adv* 2:e1600341 doi:[10.1126/sciadv.1600341](https://doi.org/10.1126/sciadv.1600341)
- Dubrovinsky L, Dubrovinskaia N, Prakapenka VB, Abakumov AM (2012) Implementation of micro-ball nanodiamond anvils for high-pressure studies above 6 Mbar. *Nat Commun* 3:1163 doi:[10.1038/ncomms2160](https://doi.org/10.1038/ncomms2160)
- Dupree R, Howes AP, Kohn S (1997) Natural abundance solid state <sup>43</sup>Ca NMR. *Chem Phys Lett* 276:399-404 doi:[10.1016/S0009-2614\(97\)00863-4](https://doi.org/10.1016/S0009-2614(97)00863-4)
- Durben DJ, Wolf GH (1991) Raman spectroscopic study of the pressure-induced coordination change in GeO<sub>2</sub> glass. *Phys Rev B* 43:2355 doi:[10.1103/PhysRevB.43.2355](https://doi.org/10.1103/PhysRevB.43.2355)

- Duval E, Boukenter A, Champagnon B (1986) Vibration Eigenmodes and Size of Microcrystallites in Glass: Observation by Very-Low-Frequency Raman Scattering. *Phys Rev Lett* 56:2052-2055 doi:[10.1103/PhysRevLett.56.2052](https://doi.org/10.1103/PhysRevLett.56.2052)
- Eckersley MC, Gaskell PH, Barnes AC, Chieux P (1988) Structural ordering in a calcium silicate glass. *Nature* 335:525-527 doi:[10.1038/335525a0](https://doi.org/10.1038/335525a0)
- Eggert JH, Weck G, Loubeyre P, Mezouar M (2002) Quantitative structure factor and density measurements of high-pressure fluids in diamond anvil cells by x-ray diffraction: Argon and water. *Phys Rev B* 65:174105 doi:[10.1103/PhysRevB.65.174105](https://doi.org/10.1103/PhysRevB.65.174105)
- Elliot S (1991) Medium-range structural order in covalent amorphous solids. *Nature* 354:445–452 doi:[10.1038/354445a0](https://doi.org/10.1038/354445a0)
- Elliot S (1992) A Unified Model for the Low-Energy Vibrational Behaviour of Amorphous Solids. *Europhys Lett* 19:201-206 doi:[10.1209/0295-5075/19/3/009](https://doi.org/10.1209/0295-5075/19/3/009)
- Elliot SR (1995) Second sharp diffraction peak in the structure factor of binary covalent network glasses. *Phys Rev B* 51:8599-8601 doi:[10.1103/PhysRevB.51.8599](https://doi.org/10.1103/PhysRevB.51.8599)
- Faber TE, Ziman J.M. (1965) A theory of the electrical properties of liquid metals: III. the resistivity of binary alloys. *Philosophical Magazine*, 11: 153-173 doi: [10.1080/14786436508211931](https://doi.org/10.1080/14786436508211931)
- Farges F, Lefrère Y, Rossano S, Berthereau A, Calas G, Brown Jr GE (2004) The effect of redox state on the local structural environment of iron in silicate glasses: a combined XAFS spectroscopy, molecular dynamics, and bond valence study. *J Non-Cryst Solids* 344:176-188 doi:[10.1016/j.jnoncrysol.2004.07.050](https://doi.org/10.1016/j.jnoncrysol.2004.07.050)
- Feller S, Lodden G, Riley A, Edwards T, Croskrey J, Schue A, Liss D, Stentz D, Blair S, Kelley M, Smith G, Singleton S, Affatigato M, Holland D, Smith ME, Kamitsos EI, Varsamis CPE, Loannou E (2010) A multispectroscopic structural study of lead silicate glasses over an extended range of compositions. *J Non-Cryst Solids* 356:304–313 doi:[10.1016/j.jnoncrysol.2009.12.003](https://doi.org/10.1016/j.jnoncrysol.2009.12.003)
- Fischer HE, Barnes AC, Salmon PS (2006) Neutron and x-ray diffraction studies of liquids and glasses. *Rep Prog Phys* 69: 233–299 doi:[10.1088/0034-4885/69/1/R05](https://doi.org/10.1088/0034-4885/69/1/R05)
- Florian P, Novikov A, Drewitt JWE, Hennem L, Sarou-Kanian V, Massiot D, Fischer HE, Neuville DR (2018) Structure and dynamics of high-temperature strontium aluminosilicate melts. *Phys Chem Chem Phys* 20:27865-27877 doi:[10.1039/C8CP04908D](https://doi.org/10.1039/C8CP04908D)
- Fox KE, Furukawa Y, White WB (1982) Transition metal ions in silicate melts. Part 2. Iron in sodium silicate glasses. *Phys Chem Glasses* 23:169-178
- Funamori N, Yamamoto S, Yagi T, Kikegawa (2004) Exploratory studies of silicate melt structure at high pressures and temperatures by in situ X-ray diffraction. *J Geophys Res* 109:B03203 doi:[10.1029/2003JB002650](https://doi.org/10.1029/2003JB002650)
- Furukawa T, Brawer SA, White WB, (1978) The structure of lead silicate glasses determined by vibrational spectroscopy. *J Mater Sci* 13:268–282 doi: <https://doi.org/10.1007/BF00647770>
- Galeener FL (1982a) Planar rings in vitreous silica. *J Non-Cryst Solids* 49:53-62 doi:[10.1016/0022-3093\(82\)90108-9](https://doi.org/10.1016/0022-3093(82)90108-9)
- Galeener FL (1982b) Planar rings in glasses. *Solid State Commun* 44:1037–1040 doi:[10.1016/0038-1098\(82\)90329-5](https://doi.org/10.1016/0038-1098(82)90329-5)
- Galeener FL, Leadbetter AJ, Stringfellow MW (1983) Comparison of the neutron, Raman, and infrared vibrational spectra of vitreous SiO<sub>2</sub>, GeO<sub>2</sub>, and BeF<sub>2</sub>. *Phys Rev B* 27:1052-1078 doi:[10.1103/PhysRevB.27.1052](https://doi.org/10.1103/PhysRevB.27.1052)
- Galoisy L, Calas G, Arrio MA (2001) High-resolution XANES spectra of iron in minerals and glasses: structural information from the pre-edge region. *Chem Geol* 174:307-319 doi:[10.1016/S0009-2541\(00\)00322-3](https://doi.org/10.1016/S0009-2541(00)00322-3)
- Gaskell PH, Eckersley MC, Barnes AC, Chieux P (1991) Medium-range order in the cation distribution of a calcium silicate glass. *Nature* 350:675-677 doi:[10.1038/350675a0](https://doi.org/10.1038/350675a0)
- Geissberger AE and Galeener FL (1983) Raman studies of vitreous SiO<sub>2</sub> versus fictive temperature. *Phys Rev B* 28:3266-3271 doi:[10.1103/PhysRevB.28.3266](https://doi.org/10.1103/PhysRevB.28.3266)
- Ghosh DB and Karki BB (2018) First-principles molecular dynamics simulations of anorthite (CaAl<sub>2</sub>Si<sub>2</sub>O<sub>8</sub>) glass at high pressure. *Phys Chem Mater* 45:575-587 doi:[10.1007/s00269-018-0943-4](https://doi.org/10.1007/s00269-018-0943-4)
- Giordano D, Dingwell DB (2003) The kinetic fragility of natural silicate melts. *J Phys: Condens Matter* 15:S945 doi:[10.1088/0953-8984/15/11/318](https://doi.org/10.1088/0953-8984/15/11/318)
- Giordano D, Russell JK (2007) A rheological model for glassforming silicate melts in the systems CAS, MAS, MCAS. *J Phys: Condens Matter* 19:205148 doi:[10.1088/0953-8984/19/20/205148](https://doi.org/10.1088/0953-8984/19/20/205148)



- Giordano D, Russell JK, Dingwell DB (2008) Viscosity of magmatic liquids: A model. *Earth Planet. Sci. Lett.* 271:123-134 doi:[10.1016/j.epsl.2008.03.038](https://doi.org/10.1016/j.epsl.2008.03.038)
- Giuli G, Pratesi G, Cipriani C, Paris E (2002) Iron local structure in tektites and impact glasses by extended x-ray absorption fine structure and high-resolution x-ray absorption near-edge structure spectroscopy. *Geochim Cosmochim Acta* 66:4347-4353 doi:[10.1016/S0016-7037\(02\)01030-X](https://doi.org/10.1016/S0016-7037(02)01030-X)
- Giuli G, Paris E, Hess K-U, Dingwell DB, Cicconi MR, Eeckhout SG, Fehr KT, Valenti P (2011) XAS determination of the Fe local environment and oxidation state in phonolite glasses. *Am Mineral* 96:631-636 doi:[10.2138/am.2011.3464](https://doi.org/10.2138/am.2011.3464)
- Giuli G, Alonso-Mori R, Cicconi MR, Paris E, Glatzel P, Eeckhout SG, Scaillet B (2012) Effect of alkalis on the Fe oxidation state and local environment in peralkaline rhyolitic glasses. *Am Mineral* 97:468-475 doi:[10.2138/am.2012.3888](https://doi.org/10.2138/am.2012.3888)
- Goldstein M (1969) Viscous Liquids and the Glass Transition: A Potential Energy Barrier Picture. *J Chem Phys* 51:3728-3739 doi:[10.1063/1.1672587](https://doi.org/10.1063/1.1672587)
- Greaves GN (1985) EXAFS and the structure of glass. *J Non-Cryst Solids* 71:203-217 doi:[10.1016/0022-3093\(85\)90289-3](https://doi.org/10.1016/0022-3093(85)90289-3)
- Greaves GN and Sen S (2007) Inorganic glasses, glass-forming liquids and amorphizing solids *Advances in Physics* 56: 1-166 doi:[10.1080/00018730601147426](https://doi.org/10.1080/00018730601147426)
- Greaves GN, Wilding MC, Fearn S, Langstaff D, Kargl F, Cox S, Van QV, Majérus O, Benmore CJ, Weber R, Martin CM, Hennem L (2008) *Science* 322:566-570 doi:[10.1126/science.1160766](https://doi.org/10.1126/science.1160766)
- Grigera TS, Martin-Mayer V, Parisi G, Verrocchio P (2003)
- Grimsditch M (1984) Polymorphism in Amorphous SiO<sub>2</sub>. *Phys Rev Lett* 52:2379-2381 doi:[10.1103/PhysRevLett.52.2379](https://doi.org/10.1103/PhysRevLett.52.2379)
- Gross von E, Romanova M (1929) Über die Lichtstreuung in Quarz und festen amorphen Stoffen, welche die Gruppe SiO<sub>2</sub> enthalten. *Zeitschrift für Physik* 55:744-752 doi:[10.1007/BF01330754](https://doi.org/10.1007/BF01330754)
- Guillot B, Sator N (2007) A computer simulation study of natural silicate melts. Part II: High pressure properties. *Geochim Cosmochim Acta* 71:4538-4556 doi:[10.1016/j.gca.2007.05.029](https://doi.org/10.1016/j.gca.2007.05.029)
- Gurevich VL, Parshin DA, Pelous J, Schober HR (1993) Theory of low-energy Raman scattering in glasses. *Phys Rev B* 48:16318-16331 doi:[10.1103/PhysRevB.48.16318](https://doi.org/10.1103/PhysRevB.48.16318)
- Guthrie M, Tulk CA, Benmore CJ, Xu J, Yarger JL, Klug DD, Tse JS, Mao H-k, Hemley RJ (2004) Formation and Structure of a Dense Octahedral Glass. *Phys Rev Lett* 93:115502 doi:[10.1103/PhysRevLett.93.115502](https://doi.org/10.1103/PhysRevLett.93.115502)
- Hannon AC and Parker JM (2000) The structure of aluminate glasses by neutron diffraction. *J Non-Cryst Solids* 274:102-109 doi:[10.1016/S0022-3093\(00\)00208-8](https://doi.org/10.1016/S0022-3093(00)00208-8)
- Hannon AC (2015) Neutron diffraction techniques for structural studies of glasses. *In: Modern Glass Characterisation*, Affatigato M (Ed), John Wiley and Sons, USA, p 158–240 doi:[10.1002/9781119051862.ch5](https://doi.org/10.1002/9781119051862.ch5)
- Hannoyer B, Lenglet M, Dürr J, Cortes R (1992) Spectroscopic evidence of octahedral iron (III) in soda-lime silicate glasses. *J Non-Cryst Solids* 151:209-216 doi:[10.1016/0022-3093\(92\)90031-E](https://doi.org/10.1016/0022-3093(92)90031-E)
- Hehlen B, Courtens E, Vacher R, Yamanaka A, Kataoka M, Inoue K (2000) Hyper-Raman scattering observation of the Boson peak in vitreous silica. *Phys Rev Lett* 84:5355-5358 doi:[10.1103/PhysRevLett.84.5355](https://doi.org/10.1103/PhysRevLett.84.5355)
- Hehlen B, Courtens E, Yamanaka A, Inoue K (2002) Nature of the Boson peak of silica glasses from hyper-Raman scattering. *J Non-Cryst Solids* 307-310:87-91 doi:[10.1016/S0022-3093\(02\)01444-8](https://doi.org/10.1016/S0022-3093(02)01444-8)
- Hehlen B, Neuville DR (2015) Raman response of network modifier cations in alumino-silicate glasses. *J Phys Chem B* 119:4093–4098 doi:[10.1021/jp5116299](https://doi.org/10.1021/jp5116299)
- Hehlen B and Neuville DR (2020) Non network-former cations in oxide glasses spotted by Raman scattering. *J Phys Chem B* doi:[10.1039/d0cp00630k](https://doi.org/10.1039/d0cp00630k)
- Hemley RJ, Mao HK, Bell PM, Mysen BO (1986) Raman Spectroscopy of SiO<sub>2</sub> Glass at High Pressure. *57:747-750* doi:[10.1103/PhysRevLett.57.747](https://doi.org/10.1103/PhysRevLett.57.747)
- Henderson GS (2005) The Structure of Silicate Melts: A Glass Perspective. *Can Mineral* 43:1921-1958 doi:[10.2113/gscanmin.43.6.1921](https://doi.org/10.2113/gscanmin.43.6.1921)
- Henderson GS, Stebbins (2020) The Short-Range Order (SRO) and Structure. *Rev Mineral Geochem* XX:XX-XX**
- Hennem L, Pozdnyakova I, Bytchkov A, Price DL, Greaves GN, Wilding M, Fearn S, Martin CM, Thiaudière D, Bézar J-F, Boudet N, Saboungi M-L (2007) Development of structural order during supercooling of a fragile oxide melt. *J Chem Phys* 126:074906 doi:[10.1063/1.2646812](https://doi.org/10.1063/1.2646812)



- Hennet L, Cristiglio V, Kozaily J, Pozdnyakova I, Fischer HE, Bytchkov A, Drewitt JWE, Leydier M, Thiaudière D, Gruner S, Brassamin S, Zanghi D, Cuello GJ, Koza M, Magazù S, Greaves GN, Price DL (2011a) Aerodynamic levitation and laser heating: Applications at synchrotron and neutron sources. *Eur Phys J* 196:151-165 doi:[10.1140/epjst/e2011-01425-0](https://doi.org/10.1140/epjst/e2011-01425-0)
- Hennet L, Pozdnyakova I, Bytchkov A, Drewitt JWE, Kozaily J, Leydier M, Brassamin S, Zanghi D, Fischer HE, Greaves GN, Price DL (2011b) Application of time resolved x-ray diffraction to study the solidification of glass-forming melts. *High Temp High Press* 40: 263-270
- Hennet L, Drewitt JWE, Neuville DR, Cristiglio V, Kozaily J, Brassamin S, Zanghi D, Fischer HE (2016) Neutron diffraction of calcium aluminosilicate glasses and melts. *J Non-Cryst Solids* 451:89-93 doi:[10.1016/j.jnoncrysol.2016.05.018](https://doi.org/10.1016/j.jnoncrysol.2016.05.018)
- Hess PC (1975) PbO-SiO<sub>2</sub> melts: structure and thermodynamics of mixing. *Geochim Cosmochim Acta* 39:671-687 doi:[10.1016/0016-7037\(75\)90010-1](https://doi.org/10.1016/0016-7037(75)90010-1)
- Hiraoka Y, Nakamura T, Hirata A, Escolar EG, Matsue K, Nishiura Y (2016) Hierarchical structures of amorphous solids characterized by persistent homology. *Proc Nat Acad Sci* 113:7035-7040 doi:[10.1073/pnas.1520877113](https://doi.org/10.1073/pnas.1520877113)
- Holland D, Mekki A, Gee IA, McConville CF, Johnson JA, Johnson CE, Appleyard P, Thomas M (1999) The structure of sodium iron silicate glass - a multi-technique approach. *J Non-Cryst Solids* 253:192-202 doi:[10.1016/S0022-3093\(99\)00353-1](https://doi.org/10.1016/S0022-3093(99)00353-1)
- Holloway JR, Wood BJ (1988) *Simulating the Earth: Experimental Geochemistry*. Boston: Unwin Hyman. doi:[10.1007/978-94-011-8028-3](https://doi.org/10.1007/978-94-011-8028-3)
- Hong X, Shen G, Prakapenka VB, Newville M, Rivers ML, Sutton SR (2007) Intermediate states of GeO<sub>2</sub> glass under pressures up to 35GPa. *Phys Rev B* 75:104201 doi:[10.1103/PhysRevB.75.104201](https://doi.org/10.1103/PhysRevB.75.104201)
- Hong X, Ehm L, Duffy TS (2014) Polyhedral units and network connectivity in GeO<sub>2</sub> glass at high pressure: An X-ray total scattering investigation. *Appl Phys Lett* 105:081904 doi:[10.1063/1.4894103](https://doi.org/10.1063/1.4894103)
- Hosokawa S, Bézar J-F, Boudet N, Pilgrim W-C, Pusztai L, Hiroi S, Maruyama K, Kohara S, Kato H, Fischer HE, Zeidler A (2019) Partial structure investigation of the traditional bulk metallic glass Pd<sub>40</sub>Ni<sub>40</sub>P<sub>20</sub>. *Phys Rev B* 100:054204 doi:[10.1103/PhysRevB.100.054204](https://doi.org/10.1103/PhysRevB.100.054204)
- Imaoka M, Hasegawa H, Yasui I (1986) X-ray diffraction analysis on the structure of the glasses in the system PbO-SiO<sub>2</sub>. *J Non-Cryst Solids* 85:393-412 doi:[10.1016/0022-3093\(86\)90011-6](https://doi.org/10.1016/0022-3093(86)90011-6)
- Itié JPP, Calas G, Petiau J, Fontaine A, Tolentino H (1989) Pressure-induced coordination changes in crystalline and vitreous GeO<sub>2</sub>. *Phys Rev Lett* 63:398 doi:[10.1103/PhysRevLett.63.398](https://doi.org/10.1103/PhysRevLett.63.398)
- Inamura Y, Arai M, Nakamura M, Otomo T, Kitamura N, Bennington SM, Hannon AC, Buchenau U (2001) Intermediate range structure and low-energy dynamics of densified vitreous silica. *J Non-Cryst Solids* 293-295:389-393 doi:[10.1016/S0022-3093\(01\)00824-9](https://doi.org/10.1016/S0022-3093(01)00824-9)
- Inamura Y, Katayama Y, Utsumi W, Funakoshi (2004) Transformations in the Intermediate-Range Structure of SiO<sub>2</sub> Glass under High Pressure and Temperature. 93:015501 doi:[10.1103/PhysRevLett.93.015501](https://doi.org/10.1103/PhysRevLett.93.015501)
- Ishihara T, Shirakawa Y, Iida T, Kitamura N, Matsukawa M, Ohtori N, Umesaki N (1999) Brillouin Scattering in Densified GeO<sub>2</sub> Glasses. *Jpn J Appl Phys* 38:3062-3065 doi:[10.1143/JJAP.38.3062](https://doi.org/10.1143/JJAP.38.3062)
- Ito E (2007) Multianvil cells and high-pressure experimental methods. *In: Treatise on Geophysics: Theory and Practice* (second edition), Elsevier, Holland 2:197-230 doi:[10.1016/B978-044452748-6.00036-5](https://doi.org/10.1016/B978-044452748-6.00036-5)
- Iuga D, Morais C, Gan Z, Neuville DR, Cormier L, Massiot D (2005) NMR Heteronuclear Correlation between Quadrupolar Nuclei in Solids. *J Am Chem Soc* 127:11540-11541 doi:[10.1021/ja052452n](https://doi.org/10.1021/ja052452n)
- Iwamoto N, Umesaki N, Atsumi T (1987) EXAFS and x-ray diffraction studies of iron ions in a 0.2(Fe<sub>2</sub>O<sub>3</sub>) · 0.8(Na<sub>2</sub>O · 2SiO<sub>2</sub>) glass. *J Mater Sci Lett* 6:271-273 doi:[10.1007/BF01729322](https://doi.org/10.1007/BF01729322)
- Jackson WE, Mustre de Leon J, Brown Jr GE, Waychunas GA, Conradson SD, Combes J-M (1993) High-Temperature XAS Study of Fe<sub>2</sub>SiO<sub>4</sub> Liquid: Reduced Coordination of Ferrous Iron. *Science* 262:229-233 doi:[10.1126/science.262.5131.229](https://doi.org/10.1126/science.262.5131.229)
- Jackson WE, Farges F, Yeager M, Mabrouk PA, Rossano S, Waychunas GA, Solomon EI, Brown Jr GE (2005) Multi-spectroscopic study of Fe(II) in silicate glasses: Implications for the coordination environment of Fe(II) in silicate melts. *Geochim Cosmochim Acta* 69:4315-4332 doi:[10.1016/j.gca.2005.01.008](https://doi.org/10.1016/j.gca.2005.01.008)
- Jakse N, Bouhadja M, Kozaily J, Drewitt JWE, Hennet L, Neuville DR, Fischer HE, Cristiglio V, Pasturel A (2012) Interplay between non-bridging oxygen, triclusters, and fivefold Al coordination in low silica content calcium aluminosilicate melts. *Appl Phys Lett* 101:201903 doi:[10.1063/1.4766920](https://doi.org/10.1063/1.4766920)
- Jahn S (2020) Molecular simulations of oxide and silicate melts and glasses. *Rev Mineral Geochem* XX:XX-XX

- Johnson JA, Johnson CE, Holland D, Mekki A, Appleyard P, Thomas MF (1999) Transition metal ions in ternary sodium silicate glasses: a Mössbauer and neutron study. *J Non-Cryst Solids* 246:104-114 doi:[10.1016/S0022-3093\(99\)00069-1](https://doi.org/10.1016/S0022-3093(99)00069-1)
- Kalampounias AG, Yannopoulos SN, Papatheodorou GN (2006) Temperature-induced structural changes in glassy, supercooled, and molten silica from 77 to 2150 K. *J Chem Phys* 124:014504 doi:[10.1063/1.2136878](https://doi.org/10.1063/1.2136878)
- Kang E-T, Lee S-J, Hannon AC (2006) Molecular dynamics simulations of calcium aluminate glasses. *J Non-Cryst Solids* 352:725-736 doi:[10.1016/j.jnoncrysol.2006.02.013](https://doi.org/10.1016/j.jnoncrysol.2006.02.013)
- Kelsey KE, Stebbins JF, Mosenfelder JL, Asimow PD (2009) Simultaneous aluminum, silicon, and sodium coordination changes in 6 GPa sodium aluminosilicate glasses. *Am Mineral* 94:1205-1215 doi: [10.2138/am.2009.3177](https://doi.org/10.2138/am.2009.3177)
- Keppler H (1992) Crystal field spectra and geochemistry of transition metal ions in silicate melts and glasses. *Am Mineral* 77:62-75
- Kim H, Lee SK (2020) Extent of disorder in iron-bearing albite and anorthite melts: Insights from multi-nuclear ( $^{29}\text{Si}$ ,  $^{27}\text{Al}$ , and  $^{17}\text{O}$ ) solid-state NMR study of iron-bearing  $\text{NaAlSi}_3\text{O}_8$  and  $\text{CaAl}_2\text{Si}_2\text{O}_8$  glasses. *Chem Geol* 538:119498 doi:[10.1016/j.chemgeo.2020.119498](https://doi.org/10.1016/j.chemgeo.2020.119498)
- Kohara S, Suzuya K (2005) Intermediate-range order in vitreous  $\text{SiO}_2$  and  $\text{GeO}_2$ . *J Phys: Condens Matter* 17:S77-S86 doi:[10.1088/0953-8984/17/5/009](https://doi.org/10.1088/0953-8984/17/5/009)
- Kono Y, Park C, Kenney-Benson C, Shen G, Wang Y (2014) Toward comprehensive studies of liquids at high pressures and high temperatures: Combined structure, elastic wave velocity, and viscosity measurements in the Paris–Edinburgh cell. *Phys Earth Planet Inter* 228:269-280 doi:[10.1016/j.pepi.2013.09.006](https://doi.org/10.1016/j.pepi.2013.09.006)
- Kono Y, Kenney-Benson C, Ikuta D, Shibazaki Y, Wang Y, Shen G (2016) Ultrahigh-pressure polyamorphism in  $\text{GeO}_2$  glass with coordination number > 6. *Proc Nat Acad Sci* 113:3436-3441 doi:[10.1073/pnas.1524304113](https://doi.org/10.1073/pnas.1524304113)
- Kono Y, Shibazaki Y, Kenney-Benson C, Wang Y, Shen G (2018) Pressure-induced structural change in  $\text{MgSiO}_3$  glass at pressures near the Earth's core–mantle boundary. *Proc Nat Acad Sci* 115:1742-1747 doi:[10.1073/pnas.1716748115](https://doi.org/10.1073/pnas.1716748115)
- Kono Y, Kenney-Benson C, Shen G (2019) Opposed type double stage cell for Mbar pressure experiment with large sample volume. *High Press Res* doi: <https://doi.org/10.1080/08957959.2019.1710744>
- Klinger MI (2010) Soft atomic motion modes in glasses: Their role in anomalous properties. *Phys Rep* 492:111-180 doi:[10.1016/j.physrep.2010.03.004](https://doi.org/10.1016/j.physrep.2010.03.004)
- Klotz S, Besson JM, Hamel G, Nelmes RJ, Loveday JS, Marshall WG, Wilson RM (1995) Neutron Powder Diffraction at Pressures Beyond. *Appl Phys Lett* 66:1735-1737 doi:[10.1063/1.113350](https://doi.org/10.1063/1.113350)
- Labrosse S, Hernlund JW, Coltice N (2007) A crystallizing dense magma ocean at the base of the Earth's mantle. *Nature* 450:866-869 doi:[10.1038/nature06355](https://doi.org/10.1038/nature06355)
- Lacy ED (1963) Aluminium in glasses and melts. *Phys Chem Glasses* 4:234-238
- Laird BB, Schober HR (1991) Localized Low-Frequency Modes in a Simple Model Glass. *Phys Rev Lett* 66:636-639 doi:[10.1103/PhysRevLett.66.636](https://doi.org/10.1103/PhysRevLett.66.636)
- Le Losq C, Neuville DR (2013) Effect of K/Na mixing on the structure and rheology of tectosilicate silica-rich melts. *Chem Geol* 346:57-71 doi:[10.1016/j.chemgeo.2012.09.009](https://doi.org/10.1016/j.chemgeo.2012.09.009)
- Le Losq C, Neuville DR, Florian P, Henderson GS, Massiot D (2014) Role of  $\text{Al}^{3+}$  on rheology and nano-structural changes of sodium silicate and aluminosilicate glasses and melts. *Geochim Cosmochim Acta* 126:495-517 doi: [10.1016/j.gca.2013.11.010](https://doi.org/10.1016/j.gca.2013.11.010)
- Le Losq C, Neuville DR, Florian P, Massiot D, Zhou Z, Chen W, Greaves GN (2017) Percolation channels: a universal idea to describe the atomic structure of glasses and melts. *Sci Rep* 7:16490 doi:[10.1038/s41598-017-16741-3](https://doi.org/10.1038/s41598-017-16741-3)
- Le Losq C, Berry AJ, Kendrick MA, Neuville DR, O'Neill HStC (2019) Determination of the oxidation state of iron in Mid-Ocean Ridge basalt glasses by Raman spectroscopy. *Am Mineral* 104:1032-1042 doi:[10.2138/am-2019-6887](https://doi.org/10.2138/am-2019-6887)
- Le Losq C, Cicconi MR, Greaves GN, Neuville DR (2019) Silicate Glasses. *In: Handbook of Glass*, Musgraves JD, Hu J, Calvez L (eds) Springer Nature, Switzerland pp 441-503 doi:[10.1007/978-3-319-93728-1](https://doi.org/10.1007/978-3-319-93728-1)
- Lee SK, Kim EJ (2015) Probing Metal-Bridging Oxygen and Configurational Disorder in Amorphous Lead Silicates: Insights from  $^{17}\text{O}$  Solid-State Nuclear Magnetic Resonance. *J Phys Chem C* 119:748-756 doi:[10.1021/jp509780f](https://doi.org/10.1021/jp509780f)

- Lee SK, Stebbins JF (2003) The distribution of sodium ions in aluminosilicate glasses: a high-field Na-23 MAS and 3Q MAS NMR study. *Geochim Cosmochim Acta* 67:1699-1709 doi:[10.1016/S0016-7037\(03\)00026-7](https://doi.org/10.1016/S0016-7037(03)00026-7)
- Le Roux S, Jund P (2010) Ring statistics analysis of topological networks: New approach and application to amorphous GeS<sub>2</sub> and SiO<sub>2</sub> systems. *Comp Mater Sci* 49:70-83 doi:[10.1016/j.commatsci.2010.04.023](https://doi.org/10.1016/j.commatsci.2010.04.023)
- Le Roux S, Petkov V (2010) ISAACS – interactive structure analysis of amorphous and crystalline systems. *J Appl Cryst* 43:181-185 doi:[10.1107/S0021889809051929](https://doi.org/10.1107/S0021889809051929)
- Levelut C, Gaimes N, Terki F, Cohen-Sohal G, Pelous J, Vacher R (1995) Glass-transition temperature: Relation between low-frequency dynamics and medium-range order. *Phys Rev B* 51:8606-8609 doi:[10.1103/PhysRevB.51.8606](https://doi.org/10.1103/PhysRevB.51.8606)
- Li D, Secco RA, Bancroft GM, Fleet ME (1995) Pressure induced coordination change of Al in silicate melts from Al K edge XANES of high pressure NaAlSi<sub>2</sub>O<sub>6</sub>-NaAlSi<sub>3</sub>O<sub>8</sub> glasses. *Geophys Res Lett* 22:3111-3114 doi:[10.1029/95GL03175](https://doi.org/10.1029/95GL03175)
- Li B, Ji C, Yang W, Wang J, Yang K, Xu R, Liu W, Cai Z, Chen J, Mao H-k (2018) Diamond anvil cell behavior up to 4 Mbar. *Proc Nat Acad Sci* 115:1713-1717 doi:[10.1073/pnas.1721425115](https://doi.org/10.1073/pnas.1721425115)
- Licheron M, Montouillout V, Millot F, Neuville DR (2011) Raman and <sup>27</sup>Al NMR structure investigations of aluminate glasses: (1-x)Al<sub>2</sub>O<sub>3</sub>- x MO, with M=Ca, Sr, Ba and 0.5 < x < 0.75). *J Non Cryst Solids* 257:2796-2801 doi:[10.1016/j.jnoncrysol.2011.03.001](https://doi.org/10.1016/j.jnoncrysol.2011.03.001)
- Liebermann RC (2011) Multi-anvil, high pressure apparatus: a half-century of development and progress. *High Press Res* 31:493-532 [10.1080/08957959.2011.618698](https://doi.org/10.1080/08957959.2011.618698)
- Liermann H-P, Morgenroth W, Ehnes A, Berghäuser A, Winkler B, Franz H, Weckert E (2010) The Extreme Conditions Beamline at PETRA III, DESY: Possibilities to conduct time resolved monochromatic diffraction experiments in dynamic and laser heated DAC. *J Phys: Conf Ser* 215:012029 doi:[10.1088/1742-6596/215/1/012029](https://doi.org/10.1088/1742-6596/215/1/012029)
- Lin J-F, Fukui H, Prendergast D, Okuchi T, Cai YQ, Hiraoka N, Yoo C-S, Trave A, Eng P, Hu MY, Chow P (2007) Electronic bonding transition in compressed SiO<sub>2</sub> glass. *Phys Rev B* 75:012201 doi:[10.1103/PhysRevB.75.012201](https://doi.org/10.1103/PhysRevB.75.012201)
- Liu H, Chen W, Pan R, Shan Z, Qiao A, Drewitt JWE, Hennem L, Jahn S, Langstaff DP, Chass GA, Tao H, Yue Y, Greaves GN (2020) From Molten Calcium Aluminates through Phase Transitions to Cement Phases. *Adv Sci* 7:1902209 doi:[10.1002/advs.201902209](https://doi.org/10.1002/advs.201902209)
- Louvel M, Drewitt JWE, Ross A, Thwaites R, Heinen BJ, Keeble DS, Beavers CM, Walter MJ, Anzellini S (2020) The HXD95: a modified Bassett-type hydrothermal diamond-anvil cell for *in situ* XRD experiments up to 5 GPa and 1300 K. *J Synchrotron Rad* 27:529-537 doi:[10.1107/S1600577519016801](https://doi.org/10.1107/S1600577519016801)
- Mao H-K, Mao WL (2007) Diamond-Anvil Cells and Probes for High *P-T* Mineral Physics Studies. *In: Treatise on Geophysics: Theory and Practice* (second edition) 2:263-291 doi:[10.1016/B978-044452748-6.00037-7](https://doi.org/10.1016/B978-044452748-6.00037-7)
- Magnien V, Neuville DR, Cormier L, Mysen BO, Richet P (2004) Kinetics of iron oxidation in silicate melts: A preliminary XANES study. *Chem Geol* 213:253-263 doi:[10.1016/j.chemgeo.2004.08.047](https://doi.org/10.1016/j.chemgeo.2004.08.047)
- Magnien V, Neuville DR, Cormier L, Roux J, Hazemann J-L, Pinet O, Richet P (2006) Kinetics of iron redox reactions: A high-temperature X-ray absorption and Raman spectroscopy study. *J Nucl Mater* 352:190-195 doi:[10.1016/j.jnucmat.2006.02.053](https://doi.org/10.1016/j.jnucmat.2006.02.053)
- Magnien V, Neuville DR, Cormier L, Roux J, Hazemann J-L, de Ligny D, Pascarelli S, Vickridge I, Pinet O, Richet P. (2008) Kinetics and mechanisms of iron redox reactions in silicate melts: The effects of temperature and alkali cations. *Geochim Cosmochim Acta* 72:157-2168 doi:[10.1016/j.gca.2008.02.007](https://doi.org/10.1016/j.gca.2008.02.007)
- Marruzzo A, Schirmacher W, Fratallocchi A, Ruocco G (2013) Heterogeneous shear elasticity of glasses: the origin of the boson peak. *Sci Rep* 3:1407 doi:[10.1038/srep01407](https://doi.org/10.1038/srep01407)
- Massiot D, Trumeau D, Touze B, Farnan I, Rifflet J-C, Douy A, Coutures J-P (1995) Structure and Dynamics of CaAl<sub>2</sub>O<sub>4</sub> from Liquid to Glass: A High-Temperature <sup>27</sup>Al NMR Time-Resolved Study *J Phys Chem* 99:16455-16459 doi:[10.1021/j100044a038](https://doi.org/10.1021/j100044a038)
- Masson O, Thomas P (2013) Exact and explicit expression of the atomic pair distribution function as obtained from X-ray total scattering experiments. *J. Appl. Cryst* 46:461-465 doi:[10.1107/S0021889812051357](https://doi.org/10.1107/S0021889812051357)
- Matson DW, Sharma SK, Philpotts JA (1983) The structure of high-silica alkali-silicate glasses. A Raman spectroscopic investigation. *J Non-Cryst Solids* 58:323-352 doi:[10.1016/0022-3093\(83\)90032-7](https://doi.org/10.1016/0022-3093(83)90032-7)

- McMillan P, Piriou B, Navrotsky A (1982) A Raman spectroscopic study of glasses along the joins silica-calcium aluminate, silica-sodium aluminate, and silica-potassium aluminate. *Geochim Cosmochim Acta* 46:2021-2037 doi:[10.1016/0016-7037\(82\)90182-X](https://doi.org/10.1016/0016-7037(82)90182-X)
- McMillan P, Piriou B (1982) The structures and vibrational spectra of crystals and glasses in the silica-alumina system. *J Non-Cryst Solids* 53:279-298 doi:[10.1016/0022-3093\(82\)90086-2](https://doi.org/10.1016/0022-3093(82)90086-2)
- McMillan P, Piriou B (1983) Raman spectroscopy of calcium aluminate glasses and crystals. *J Non-Cryst Solids* 55:221-242 doi:[10.1016/0022-3093\(83\)90672-5](https://doi.org/10.1016/0022-3093(83)90672-5)
- McMillan PF (1984) Structural studies of silicate glasses and melts – Applications and limitations of Raman spectroscopy. *Am Mineral* 69:622-644
- McMillan PF, Poe BT, Gillet P, Reynard B (1994) A study of SiO<sub>2</sub> glass and supercooled liquid to 1950 K via high-temperature Raman spectroscopy. *Geochim Cosmochim Acta* 58:3653-3664 doi:[10.1016/0016-7037\(94\)90156-2](https://doi.org/10.1016/0016-7037(94)90156-2)
- McMillan PF, Petuskey W, Cote B, Massiot D, Landron C, Coutures JP (1996) A structural investigation of CaO-Al<sub>2</sub>O<sub>3</sub> glasses via <sup>27</sup>Al MAS-NMR. *J Non-Cryst Solids* 195:261-71 doi:[10.1016/0022-3093\(95\)00536-6](https://doi.org/10.1016/0022-3093(95)00536-6)
- Mead RN, Mountjoy G (2006) A Molecular Dynamics Study of the Atomic Structure of (CaO)<sub>x</sub>(SiO<sub>2</sub>)<sub>1-x</sub> Glasses. *J Phys Chem B* 110:14273-14278 doi:[10.1021/jp0628939](https://doi.org/10.1021/jp0628939)
- Meade C, Hemley RJ, Mao HK (1992) High-pressure x-ray diffraction of SiO<sub>2</sub> glass. *Phys Rev Lett* 69:1387 doi:[10.1103/PhysRevLett.69.1387](https://doi.org/10.1103/PhysRevLett.69.1387)
- Mei Q, Benmore CJ, Weber JKR (2007) Structure of Liquid SiO<sub>2</sub>: A Measurement by High-Energy X-Ray Diffraction. *Phys Rev Lett* 98:057802 doi:[10.1103/PhysRevLett.98.057802](https://doi.org/10.1103/PhysRevLett.98.057802)
- Mei Q, Benmore CJ, Siewenie J, Weber JKR, Wilding M (2008a) Diffraction study of calcium aluminate glasses and melts: I. High energy x-ray and neutron diffraction on glasses around the eutectic composition. *J Phys Condens Matter* 20:245106 doi:[10.1088/0953-8984/20/24/245106](https://doi.org/10.1088/0953-8984/20/24/245106)
- Mei Q, Benmore CJ, Weber JKR, Wilding M, Kim J, Rix J (2008b) Diffraction study of calcium aluminate glasses and melts: II. High energy x-ray diffraction on melts. *J Phys Condens Matter* 20:245107 doi:[10.1088/0953-8984/20/24/245107](https://doi.org/10.1088/0953-8984/20/24/245107)
- Mei Q, Sinogeikin S, Shen G, Amin S, Benmore CJ, Ding K (2010) High-pressure x-ray diffraction measurements on vitreous GeO<sub>2</sub> under hydrostatic conditions. *Phys Rev B* 81:174113 doi:[10.1103/PhysRevB.81.174113](https://doi.org/10.1103/PhysRevB.81.174113)
- Meng Y, Shen G, Mao H-k (2006) Double-sided laser heating system at HPCAT for in situ x-ray diffraction at high pressures and high temperatures. *J Phys: Condens Matter* 18:S1097-S1103 doi:[10.1088/0953-8984/18/25/S17](https://doi.org/10.1088/0953-8984/18/25/S17)
- Mermet A, Duval E, Etienne S, G'Sell C (1996) Low frequency Raman scattering study of the nanostructure of plastically deformed polymer glasses. *J Non-Cryst Solids* 196:227-232 doi:[10.1016/0022-3093\(95\)00591-9](https://doi.org/10.1016/0022-3093(95)00591-9)
- Mezouar M, Le Bihan T, Libotte H, Le Godec Y, Häusermann (1999) Paris Edinburgh large-volume cell coupled with a fast imaging-plate system for structural investigation at high pressure and high temperature. *J Synchrotron Rad* 6:1115-1119 doi:[10.1107/S0909049599010651](https://doi.org/10.1107/S0909049599010651)
- Mezouar M, Faure P, Crichton W, Rambert N, Sitaud B, Bauchau S, Blattmann G (2002) Multichannel collimator for structural investigation of liquids and amorphous materials at high pressures and temperatures. *Rev Sci Instr* 73:3570-3574 doi:[10.1063/1.1505104](https://doi.org/10.1063/1.1505104)
- Morard G, Siebert J, Andrault D, Guignot N, Garbarino G, Guyot F, Antonangeli D (2013) The Earth's core composition from high pressure density measurements of liquid iron alloys. *Earth Planet Sci Lett* 373:169-178 doi:[10.1016/j.epsl.2013.04.040](https://doi.org/10.1016/j.epsl.2013.04.040)
- Morard G, Nakajima Y, Andrault D, Antonangeli D, Auzende AL, Boulard E, Cervera S, Clark AN, Lord OT, Siebert J, Svitlyk V, Garbarino G, Mezouar M (2017) Structure and Density of Fe-C Liquid Alloys Under High Pressure. *J Geophys Res Solid Earth* 122:7813-7823 doi:[10.1002/2017JB014779](https://doi.org/10.1002/2017JB014779)
- Morikawa H, Takagi Y, Ohno H (1982) Structural analysis of 2PbO·SiO<sub>2</sub> glass. *J Non-Cryst Solids* 53:173-182 doi:[10.1016/0022-3093\(82\)90027-8](https://doi.org/10.1016/0022-3093(82)90027-8)
- Morikawa H, Marumo F, Koyama T, Yamane M, Oyobe A (1983) Structural analysis of 12CaO.7Al<sub>2</sub>O<sub>3</sub> glass. *Journal Non-Cryst Solids* 56:355-360 doi:[10.1016/0022-3093\(83\)90493-3](https://doi.org/10.1016/0022-3093(83)90493-3)
- Moulton BJA, Henderson GS, Martinet C, Martinez V, Sonnevile C, de Ligny D (2019) Structure—longitudinal sound velocity relationships in glassy anorthite (CaAl<sub>2</sub>Si<sub>2</sub>O<sub>8</sub>) up to 20 GPa: An in situ Raman and Brillouin spectroscopy study. *Geochim Cosmochim Acta* 261:132-144 doi:[10.1016/j.gca.2019.06.047](https://doi.org/10.1016/j.gca.2019.06.047)
- Mountjoy G, Al-Hasni BM, Storey C (2011) Structural organisation in oxide glasses from molecular dynamics modelling. *J Non-Cryst Solids* 357:2522-2529 doi:[10.1016/j.jnoncrysol.2011.01.015](https://doi.org/10.1016/j.jnoncrysol.2011.01.015)



- Muniz RF, de Ligny D, Martinet C, Sandrini M, Medina AN, Rohling JH, Baesso ML, Lima SM, Andrade LHC, Guyot Y (2016) *In situ* structural analysis of calcium aluminosilicate glasses under high pressure. *J Phys Condens Matter* 28:315402 doi:[10.1088/0953-8984/28/31/315402](https://doi.org/10.1088/0953-8984/28/31/315402)
- Murakami M, Bass JD (2010) Spectroscopic Evidence for Ultrahigh-Pressure Polymorphism in SiO<sub>2</sub> Glass. *Phys Rev Lett* 104:025504 doi:[10.1103/PhysRevLett.104.025504](https://doi.org/10.1103/PhysRevLett.104.025504)
- Mysen BO, Seifert FA, Virgo D (1980) Structure and redox equilibria of iron-bearing silicate melts. *Am Mineral* 65:867-884
- Mysen BO, Virgo D, Kushiro I (1981) The structural role of aluminum in silicate melts - a Raman spectroscopic study at 1 atmosphere. *Am Mineral* 66:678-70
- Mysen BO, Finger LW, Virgo D, Seifert FA (1982a) Curve-fitting of Raman spectra of silicate glasses. *Am Min* 67:686-695
- Mysen BO, Virgo D, Seifert FA (1982b) The Structure of Silicate Melts: Implications for Chemical and Physical Properties of Natural Magma. *Rev Geophys Space Phys* 20:353-383 doi:[10.1029/RG020i003p00353](https://doi.org/10.1029/RG020i003p00353)
- Mysen BO, Virgo D, Seifert FA (1984) Redox equilibria of iron in alkaline earth silicate melts: relationships between melt structure, oxygen fugacity, temperature and properties of iron-bearing silicate liquids. *Am Mineral* 69:834-847.
- Mysen BO, Virgo D, Neumann E-R, Seifert FA (1985) Redox equilibria and the structural states of ferric and ferrous iron in melts in the system CaO-MgO-SiO<sub>2</sub>-Fe-O: relationships between redox equilibria, melt structure and liquidus phase equilibria. *Am Mineral* 70:317-331
- Mysen B. O., Frantz J. D. (1992) Raman spectroscopy of silicate melts at magmatic temperatures: Na<sub>2</sub>O-SiO<sub>2</sub>, K<sub>2</sub>O-SiO<sub>2</sub> and Li<sub>2</sub>O-SiO<sub>2</sub> binary compositions in the temperature range 25–1475°C, *Chem. Geol.* 96, 321-332 doi [10.1016/0009-2541\(92\)90062-A](https://doi.org/10.1016/0009-2541(92)90062-A)
- Mysen BO, Richet P (2005) *Silicate Glasses and Melts. Developments in Geochemistry Volume 10*, Elsevier, Holland, 1<sup>st</sup> edition.
- Mysen BO (2006) The structural behavior of ferric and ferrous iron in aluminosilicate glass near meta-aluminosilicate joins. *Geochim Cosmochim Acta* 70:2337-2353 doi:[10.1016/j.gca.2006.01.026](https://doi.org/10.1016/j.gca.2006.01.026)
- Nagashio K and Kuribayashi K (2004) Spherical Yttrium Aluminum Garnet Embedded in a Glass Matrix. *J Am Ceram Soc* 85:2353-2358 doi:[10.1111/j.1151-2916.2002.tb00459.x](https://doi.org/10.1111/j.1151-2916.2002.tb00459.x)
- Nakayama T (2002) Boson peak and terahertz frequency dynamics of vitreous silica. *Rep Prog Phys* 65:1195-1242 doi:[10.1088/0034-4885/65/8/203](https://doi.org/10.1088/0034-4885/65/8/203)
- Nayak MT, Desa JAE, Reddy VR, Nayak C, Bhattacharyya D, Jha SN (2019) Structures of silicate glasses with varying sodium and fixed iron contents. *J Non-Cryst Solids* 509:42-47 doi:[10.1016/j.jnoncrysol.2019.01.009](https://doi.org/10.1016/j.jnoncrysol.2019.01.009)
- Neuvill DR (2005) Structure and properties in (Sr,Na) silicate glasses and melts. *Phys Chem Glasses* 46:112-118
- Neuvill DR (2006) Viscosity, structure and mixing in (Ca, Na) silicate melts. *Chem Geol* 229:28-42 doi:[10.1016/j.chemgeo.2006.01.008](https://doi.org/10.1016/j.chemgeo.2006.01.008)
- Neuvill DR, Mysen BO (1996) Role of aluminum in the silicate network: In situ, high-temperature study of glasses and melts on the join SiO<sub>2</sub>-NaAlO<sub>2</sub>. *Geochim Cosmochim Acta* 60:1727-1737 doi:[10.1016/0016-7037\(96\)00049-X](https://doi.org/10.1016/0016-7037(96)00049-X)
- Neuvill DR, Cormier L, Massiot D (2004) Al environment in tectosilicate and peraluminous glasses: A <sup>27</sup>Al MQ-MAS NMR, Raman, and XANES investigation. *Geochim Cosmochim Acta* 68:5071-5079 doi: [10.1016/j.gca.2004.05.048](https://doi.org/10.1016/j.gca.2004.05.048)
- Neuvill DR, Cormier L, Massiot D (2006) Al coordination and speciation in calcium aluminosilicate glasses: Effects of composition determined by <sup>27</sup>Al MQ-MAS NMR and Raman spectroscopy. *Chem Geol* 229:173-185 doi:[10.1016/j.chemgeo.2006.01.019](https://doi.org/10.1016/j.chemgeo.2006.01.019)
- Neuvill DR, Cormier L, Montouillout V, Massiot D (2007) Local Al site distribution in aluminosilicate glasses by <sup>27</sup>Al MQMAS NMR. *J Non-Cryst Solids* 353:180-184 doi:[10.1016/j.jnoncrysol.2006.09.035](https://doi.org/10.1016/j.jnoncrysol.2006.09.035)
- Neuvill DR, Cormier L, Montouillout V, Florian P, Millot F, Rifflet JC, Massiot D (2008a) Structure of Mg- and Mg/Ca aluminosilicate glasses:<sup>27</sup>Al NMR and Raman spectroscopy investigations. *Am Mineral* 83:1721-1731 doi:[10.2138/am.2008.2867](https://doi.org/10.2138/am.2008.2867)
- Neuvill DR, Cormier L, Flank AM, de Ligny D, Roux J, Lagarde P (2008b) Environments around Al, Si and Ca in aluminate and aluminosilicate melts by x-ray absorption spectroscopy at high temperature. *Am Mineral* 93:228-234 doi:[10.2138/am.2008.2646](https://doi.org/10.2138/am.2008.2646)

- Neuvill DR, Henderson GS, Cormier L, Massiot D (2010) The structure of crystals, glasses, and melts along the CaO-Al<sub>2</sub>O<sub>3</sub> join: Results from Raman, Al L- and K-edge X-ray absorption, and <sup>27</sup>Al NMR spectroscopy. *Am Mineral* 95:1580-1589 doi:[10.2138/am.2010.3465](https://doi.org/10.2138/am.2010.3465)
- Neuvill DR, de Ligny D, Henderson GS (2014a) Advances in Raman Spectroscopy Applied to Earth and Material Sciences. *In: Spectroscopic Methods in Mineralogy and Materials Sciences*, Henderson GS, Neuvill DR, Downs RT (eds) *Rev Mineral Geochem* 78:509-541 doi:[10.2138/rmg.2013.78.13](https://doi.org/10.2138/rmg.2013.78.13)
- Neuvill D.R. Hennet L. Florian P. de Ligny D. (2014b) In situ High-Temperature Experiments. *In: Spectroscopic Methods in Mineralogy and Materials Sciences*, Henderson GS, Neuvill DR, Downs RT (eds) *Rev Mineral Geochem* 78:779-800 doi [10.2138/rmg.2013.78.19](https://doi.org/10.2138/rmg.2013.78.19)
- Nesbitt HW, Fleet ME (1981) An ion-association model for PbO-SiO<sub>2</sub> melts: interpretation of thermochemical, conductivity, and density data. *Geochim Cosmochim Acta* 45:235-244 doi:[10.1016/0016-7037\(81\)90168-X](https://doi.org/10.1016/0016-7037(81)90168-X)
- Nyrow A, Sternemann C, Wilke M, Gordon RA, Mende K, Yavaş H, Simonelli L, Hiraoka N, Sahle ChJ, Huotari S, Andreozzi GB, Woodland AB, Tolan M, Tse JS (2014) Iron speciation in minerals and glasses probed by M<sub>2/3</sub>-edge X-ray Raman scattering spectroscopy. *Contrib Mineral Petrol* 167:1012 doi:[10.1007/s00410-014-1012-8](https://doi.org/10.1007/s00410-014-1012-8)
- Novikov VN, Sokolov AP (1991) A correlation between low-energy vibrational spectra and first sharp diffraction peak in chalcogenide glasses *Solid State Commun* 77:243-247 doi:[10.1016/0038-1098\(91\)90341-R](https://doi.org/10.1016/0038-1098(91)90341-R)
- Novikov A, Neuvill DR, Hennet L, Thiaudière D, Gueguen Y, Florian P (2017) Al and Sr environment in tectosilicate glasses and melts: viscosity, Raman and NMR investigation. *Chem Geol* 461:115-127 doi:[10.1016/j.chemgeo.2016.11.023](https://doi.org/10.1016/j.chemgeo.2016.11.023)
- Ohira I, Kono Y, Shibasaki Y, Kenney-Benson C, Masuno A, Shen G (2019) Ultrahigh pressure structural changes in a 60 mol. % Al<sub>2</sub>O<sub>3</sub>-40 mol. % SiO<sub>2</sub> glass. *Geochem Perspect Lett* 10:41-45 doi:[10.7185/geochemlet.1913](https://doi.org/10.7185/geochemlet.1913)
- Ohno H, Nagasaki T, Igawa N, Kawamura H (1991) Neutron irradiation effects of PbO-SiO<sub>2</sub> glasses. *J Nucl Mater* 179:473-476 doi:[10.1016/0022-3115\(91\)90127-S](https://doi.org/10.1016/0022-3115(91)90127-S)
- Ohtani E, Taulelle F, Angell CA (1985) Al<sup>3+</sup> coordination changes in liquid aluminosilicates under pressure. *Nature* 314:78-81 doi:[10.1038/314078a0](https://doi.org/10.1038/314078a0)
- Ohtani E, Suzuki A, Ando R, Urakawa S, Funakoshi K, Katayama Y (2005) Viscosity and density measurements of melts and glasses at high pressure and temperature by using the multi-anvil apparatus and synchrotron X-ray radiation. *In: Advances in High-Pressure Technology for Geophysical Applications*, Chen J, Wang Y, Duffy TS, Shen G, Dobrzhinetskaya LF (eds) Elsevier, Holland, Chapter 10, 195-209 doi:[10.1016/B978-044451979-5.50012-0](https://doi.org/10.1016/B978-044451979-5.50012-0)
- O'Shaughnessy C, Henderson GS, Nesbitt HW, Bancroft GM, Neuvill DR (2017) Structure-property relations of caesium silicate glasses from room temperature to 1400 K: Implications from density and Raman spectroscopy. *Chem Geol* 461:82-95 doi:[10.1016/j.chemgeo.2016.11.028](https://doi.org/10.1016/j.chemgeo.2016.11.028)
- O'Shaughnessy C, Henderson GS, Nesbitt HW, Bancroft GM, Neuvill DR (2019) The influence of modifier cations on the Raman stretching modes of Q<sup>n</sup> species in alkali silicate glasses. *J Am Ceram Soc* 0:1-11 doi:[10.1111/jace.17081](https://doi.org/10.1111/jace.17081)
- Parshin DA (1993) Soft potential model and universal properties of glasses. *Physica Scripta* T49:180-185 doi:[10.1088/0031-8949/1993/T49A/030](https://doi.org/10.1088/0031-8949/1993/T49A/030)
- Pasquarello A, Car R (1998) Identification of Raman defect lines as signatures of ring structures in vitreous silica. *Phys Rev Lett* 80:5145-5147 doi:[10.1103/PhysRevLett.80.5145](https://doi.org/10.1103/PhysRevLett.80.5145)
- Petitgirard S, Salamat A, Beck P, Weck G, Bouvier P (2014) Strategies for *in situ* laser heating in the diamond anvil cell at an X-ray diffraction beamline. *J Synchrotron Rad* 21:89-96 doi:[10.1107/S1600577513027434](https://doi.org/10.1107/S1600577513027434)
- Phillips JC (1984) Microscopic origin of anomalously narrow Raman lines in network glasses. *J Non-Cryst Solids* 63:347-355 doi:[10.1016/0022-3093\(84\)90102-9](https://doi.org/10.1016/0022-3093(84)90102-9)
- Poe BT, McMillan PF, Coté B, Massiot D, Coutures J-P (1992) SiO<sub>2</sub>-Al<sub>2</sub>O<sub>3</sub> Liquids: In-Situ Study by High-Temperature <sup>27</sup>Al NMR Spectroscopy and Molecular Dynamics Simulation. *J Phys Chem* 96:8220-8224 doi:[10.1021/j100200a005](https://doi.org/10.1021/j100200a005)
- Poe BT, McMillan PF, Coté B, Massiot D, Coutures JP (1993) Magnesium and Calcium Aluminate Liquids: In Situ High-Temperature <sup>27</sup>Al NMR Spectroscopy. *Science* 259:786-788 doi:[10.1126/science.259.5096.786](https://doi.org/10.1126/science.259.5096.786)
- Poe B.T., McMillan P.F., Coté B., Massiot D. and Coutures J-P. (1994) Structure and Dynamics in Calcium Aluminate Liquids: High-Temperature <sup>27</sup>Al NMR and Raman Spectroscopy. *J Am Ceram Soc* 77:1832-1838 doi:[10.1111/j.1151-2916.1994.tb07058.x](https://doi.org/10.1111/j.1151-2916.1994.tb07058.x)



- Polian A, Grimsditch M (1990) Room-temperature densification of  $\alpha$ -SiO<sub>2</sub> versus pressure. *Phys Rev B* 41:6086-6087 doi:[10.1103/PhysRevB.41.6086](https://doi.org/10.1103/PhysRevB.41.6086)
- Polsky CH, Smith KH, Wolf GH (1999) Effect of pressure on the absolute Raman scattering cross section of SiO<sub>2</sub> and GeO<sub>2</sub> glasses. *J Non-Cryst Solids* 248:159-168 doi:[10.1016/S0022-3093\(99\)00238-0](https://doi.org/10.1016/S0022-3093(99)00238-0)
- Prescher C, Prakapenka VB, Stefanski J, Jahn S, Skinner LB, Wang Y (2017) Beyond sixfold coordinated Si in SiO<sub>2</sub> glass at ultrahigh pressures. *Proc Nat Acad Sci* 114:10041-10046 doi:[10.1073/pnas.1708882114](https://doi.org/10.1073/pnas.1708882114)
- Price DL, Moss SC, Reijers R., Saboungi M-L, Susman S (1989) Intermediate-range order in glasses and liquids. *J Phys: Condens Matter* 1:1005-1008 doi:[10.1088/0953-8984/1/5/017](https://doi.org/10.1088/0953-8984/1/5/017)
- Price DL (1996) Intermediate-range order in glasses. *Curr Opin Solid State Mater Sci* 1:572-577 doi:[10.1016/S1359-0286\(96\)80075-1](https://doi.org/10.1016/S1359-0286(96)80075-1)
- Price DL (2010) *High-Temperature Levitated Materials*. Cambridge University Press ISBN:1-139-48949-6
- Rahmani A, Benoit M, Benoit C (2003) Signature of small rings in the Raman spectra of normal and compressed amorphous silica: A combined classical and ab initio study. *Phys Rev B* 68:184202 doi:[10.1103/PhysRevB.68.184202](https://doi.org/10.1103/PhysRevB.68.184202)
- Richet P, Gillet P, Pierre A, Bouhifd MA, Daniel I, Fiquet G (1993) Raman spectroscopy, x-ray diffraction, and phase relationship determinations with a versatile heating cell for measurements up to 3600 K (or 2700 K in air). *J Appl Phys* 74:5451-5456 doi:[10.1063/1.354256](https://doi.org/10.1063/1.354256)
- Rigden SM, Ahrens TJ, Stolper EM (1984) Densities of Liquid Silicates at High Pressures. *Science* 226:1071-1074 doi:[10.1126/science.226.4678.1071](https://doi.org/10.1126/science.226.4678.1071)
- Roskosz M, Toplis MJ, Neuville DR, Mysen BO (2008) Quantification of the kinetics of iron oxidation in silicate melts using Raman spectroscopy and assessment of the role of oxygen diffusion. *Am Mineral* 93:1749-1759 doi:[10.2138/am.2008.2861](https://doi.org/10.2138/am.2008.2861)
- Rossano S, Balan E, Morin G, Bauer J-P, Calas G, Brouder C (1999) <sup>57</sup>Fe Mössbauer spectroscopy of tektites. *Phys Chem Mater* 26:530-538 doi:[10.1007/s002690050216](https://doi.org/10.1007/s002690050216)
- Rossano S, Ramos A, Delaye J-M, Creux S, Filippono A, Brouder C, Calas G (2000a) EXAFS and Molecular Dynamics combined study of CaO-FeO-2SiO<sub>2</sub> glass. New insight into site significance in silicate glasses. *Europhys Lett* 49:597-602 doi:[10.1209/epl/i2000-00192-1](https://doi.org/10.1209/epl/i2000-00192-1)
- Rossano S., Ramos A.Y. and Delaye J.-M. (2000b) Environment of ferrous iron in CaFeSi<sub>2</sub>O<sub>6</sub> glass; contributions of EXAFS and molecular dynamics. *J Non-Cryst Solids* 273:48-52 doi:[10.1016/S0022-3093\(00\)00124-1](https://doi.org/10.1016/S0022-3093(00)00124-1)
- Rossano S, Mysen B (2012) Raman Spectroscopy of Silicate Glasses and Melts in Geological Systems. *In: Raman spectroscopy applied to Earth sciences and cultural heritage*, Dubessy J, Caumon M-C, Rull F (eds) *EMU Notes in Mineralogy* 12:321-366 doi:[10.1180/EMU-notes.12.9](https://doi.org/10.1180/EMU-notes.12.9)
- Rouxel T, Ji H, Hammouda T, Moréac A (2008) Poisson's Ratio and the Densification of Glass under High Pressure. *Phys Rev Lett* 100:225501 doi:[10.1103/PhysRevLett.100.225501](https://doi.org/10.1103/PhysRevLett.100.225501)
- Rull F (2012) The Raman effect and the vibrational dynamics of molecules and crystalline solids. *In: Raman spectroscopy applied to Earth sciences and cultural heritage*, Dubessy J, Caumon M-C, Rull F (eds) *EMU Notes in Mineralogy* 12:1-60 doi:[10.1180/EMU-notes.12.1](https://doi.org/10.1180/EMU-notes.12.1)
- Sakamaki T, Wang Y, Park C, Yu T, Shen G (2012) Structure of Jadeite Melt at High Pressures up to 4.9 GPa. *J Appl Phys* 111:112623 doi:[10.1063/1.4726246](https://doi.org/10.1063/1.4726246)
- Sakamaki T, Suzuki A, Ohtani E, Terasaki H, Urakawa S, Katayama Y, Funakoshi K-I, Wang Y, Hernlund JW, Ballmer MD (2013) Ponded melt at the boundary between the lithosphere and asthenosphere. *Nat Geosci* 6:1041 doi:[10.1038/ngeo1982](https://doi.org/10.1038/ngeo1982)
- Sakamaki T, Wang Y, Park C, Yu T, Shen G (2014a) Contrasting behavior of intermediate-range order structures in jadeite glass and melt. *Phys Earth Planet Inter* 228:281-286 doi:[10.1016/j.pepi.2014.01.008](https://doi.org/10.1016/j.pepi.2014.01.008)
- Sakamaki T, Kono Y, Wang Y, Park C, Yu T, Jing Z, Shen G (2014b) Contrasting sound velocity and intermediate-range structural order between polymerized and depolymerized silicate glasses under pressure. *Earth Planet Sci Lett* 391:288-295 doi:[10.1016/j.epsl.2014.02.008](https://doi.org/10.1016/j.epsl.2014.02.008)
- Salmon PS (1994) Real space manifestation of the first sharp diffraction peak in the structure factor of liquid and glassy materials. *Proc R Soc Lond A* 445:351-365 doi:[10.1098/rspa.1994.0065](https://doi.org/10.1098/rspa.1994.0065)
- Salmon PS, Martin RA, Mason PE, Cuello GJ (2005) Topological versus chemical ordering in network glasses at intermediate and extended length scales. *Nature* 435:75-78 doi:[10.1038/nature03475](https://doi.org/10.1038/nature03475)
- Salmon PS, Barnes AC, Martin RA, Cuello GJ (2006) Glass Fragility and Atomic Ordering on the Intermediate and Extended Range. *Phys Rev Lett* 96:235502 doi:[10.1103/PhysRevLett.96.235502](https://doi.org/10.1103/PhysRevLett.96.235502)

- Salmon PS, Drewitt JWE, Whittaker DAJ, Zeidler A, Wezka K, Bull CL, Tucker MG, Wilding MC, Guthrie M, Marrocchelli D (2012) Density-driven structural transformations in network forming glasses: a high-pressure neutron diffraction study of GeO<sub>2</sub> glass up to 17.5 GPa. *J Phys: Condens Matter* 24:439601 doi:[10.1088/0953-8984/24/41/415102](https://doi.org/10.1088/0953-8984/24/41/415102)
- Salmon PS and Zeidler A (2013) Identifying and characterizing the different structural length scales in liquids and glasses: an experimental approach. *Phys Chem Chem Phys* 15:15286 doi:[10.1039/c3cp51741a](https://doi.org/10.1039/c3cp51741a)
- Sampath S, Benmore CJ, Lantzky KM, Neufeind J, Leinenweber K, Price DL, Yarger JL (2003) Intermediate-range Order in Permanently Densified GeO<sub>2</sub> Glass. *Phys Rev Lett* 90:115502 doi:[10.1103/PhysRevLett.90.115502](https://doi.org/10.1103/PhysRevLett.90.115502)
- Sanloup C, Drewitt JWE, Crépinsson C, Kono Y, Park C, McCammon C, Hennet L, Brassamin S, Bytchkov A (2013) Structure and density of molten fayalite at high pressure. *Geochim Cosmochim Acta* 118:118-128 doi:[10.1016/j.gca.2013.05.012](https://doi.org/10.1016/j.gca.2013.05.012)
- Sanloup C, Drewitt JWE, Konopkova Z, Dalladay-Simpson P, Morton DM, Rai N, van Westrenen W, Morgenroth W (2013b) Structural change in molten basalt at deep mantle conditions. *Nature* 503:104-107 doi:[10.1038/nature12668](https://doi.org/10.1038/nature12668)
- Sarnthein J, Pasquarello A, Car R (1997) Origin of the High-Frequency Doublet in the Vibrational Spectrum of Vitreous SiO<sub>2</sub>. *Science* 275:1925-1927 doi: [10.1126/science.275.5308.1925](https://doi.org/10.1126/science.275.5308.1925)
- Sato T, Funamori N (2008) Sixfold-Coordinated Amorphous Polymorph of SiO<sub>2</sub> under High Pressure. *Phys rev Lett* 101:255502 doi: [10.1103/PhysRevLett.101.255502](https://doi.org/10.1103/PhysRevLett.101.255502)
- Sato T, Funamori N (2010) High-pressure structural transformation of SiO<sub>2</sub> glass up to 100 GPa. *Phys Rev B* 82:184102 doi:[10.1103/PhysRevB.82.184102](https://doi.org/10.1103/PhysRevB.82.184102)
- Schirmacher W, Ruocco G, Scopigno T (2007) Acoustic Attenuation in Glasses and its Relation with the Boson Peak. *Phys Rev Lett* 98:025501 doi:[10.1103/PhysRevLett.98.025501](https://doi.org/10.1103/PhysRevLett.98.025501)
- Schirmacher W (2013) The boson peak. *Physica Status Solidi (b)* 250:937-253 doi:[10.1002/pssb.201248544](https://doi.org/10.1002/pssb.201248544)
- Schirmacher W, Scopigno T, Ruocco G (2015) Theory of vibrational anomalies in glasses. *J Non-Cryst Solids* 407:133-140 doi:[10.1016/j.jnoncrysol.2014.09.054](https://doi.org/10.1016/j.jnoncrysol.2014.09.054)
- Sears VF (1992) Neutron scattering lengths and cross sections. *Neutron News* 3:26-37 doi:[10.1080/10448639208218770](https://doi.org/10.1080/10448639208218770)
- Seifert F, Mysen BO, Virgo D (1982) 3-dimensional network structure of quenched melts (glass) in the systems SiO<sub>2</sub>-NaAlO<sub>2</sub>, SiO<sub>2</sub>-CaAl<sub>2</sub>O<sub>4</sub> and SiO<sub>2</sub>-MgAl<sub>2</sub>O<sub>4</sub>. *Am Mineral* 67:696-717
- Shannon RD (1976) Revised Effective Ionic Radii and Systematic Studies of Interatomic Distances in Halides and Chalcogenides. *Acta Cryst A* 32:751-767 doi:[10.1107/S0567739476001551](https://doi.org/10.1107/S0567739476001551)
- Sharma SK, Mammone JF, Nicol MF (1981) Raman investigation of ring configurations in vitreous silica. *Nature* 292:140-141 doi:[10.1038/292140a0](https://doi.org/10.1038/292140a0)
- Shen G, Rivers ML, Wang Y, Sutton SR (2001) Laser heated diamond cell system at the Advanced Photon Source for in situ x-ray measurements at high pressure and temperature. *Rev Sci Instr* 72:1273-1282 doi:[10.1063/1.1343867](https://doi.org/10.1063/1.1343867)
- Shen G, Prakapenka VB, Rivers ML, Sutton SR (2003) Structural investigation of amorphous materials at high pressures using the diamond anvil cell. *Rev Sci Instr* 74:3021-3026 doi:[10.1063/1.1574394](https://doi.org/10.1063/1.1574394)
- Shen GY, Prakapenka VB, Rivers ML, Sutton SR (2004) Structure of liquid iron at pressures up to 58 GPa. *Phys Rev Lett* 92:185701 doi:[10.1103/PhysRevLett.92.185701](https://doi.org/10.1103/PhysRevLett.92.185701)
- Shen G, Mei Q, Prakapenka VB, Lazor P, Sinogeikin S, Meng Y, Park C (2011) Effect of helium on structure and compression behavior of SiO<sub>2</sub> glass. *Proc Nat Acad Sci* 108:6004-6007 doi:[10.1073/pnas.1102361108](https://doi.org/10.1073/pnas.1102361108)
- Shi Y, Neufeind J, Page K, Lamberson LA, Smith NJ, Tandia A, Song AP (2019) Ring size distribution in silicate glasses revealed by neutron scattering first sharp diffraction peak analysis. *J Non-Cryst Solids* 516:71-81 doi: [10.1016/j.jnoncrysol.2019.03.037](https://doi.org/10.1016/j.jnoncrysol.2019.03.037)
- Shi C, Alderman OLG, Berman D, Du J, Neufeind J, Tamalonis A, Weber JKR, You J, Benmore CJ (2019) The Structure of Amorphous and Deeply Supercooled Liquid Alumina. *Front. Mater.* 6:38 doi:[10.3389/fmats.2019.00038](https://doi.org/10.3389/fmats.2019.00038)
- Shibazaki Y, Kono Y, Shen G (2019) Compressed glassy carbon maintaining graphite-like structure with linkage formation between graphene layers. *Sci Rep* 9:7531 doi:[10.1038/s41598-019-43954-5](https://doi.org/10.1038/s41598-019-43954-5)
- Skinner LB, Barnes AC, Salmon PS, Crichton WA (2008) *J Phys: Condens Matter* 20:205103 doi: [10.1088/0953-8984/20/20/205103](https://doi.org/10.1088/0953-8984/20/20/205103)

- Skinner LB, Benmore CJ, Weber JKR, Tumber S, Lazareva L, Neufeind J, Santodonato L, Du J, Parise JB (2012a) Structure of Molten CaSiO<sub>3</sub>: Neutron Diffraction Isotope Substitution with Aerodynamic Levitation and Molecular Dynamics Study. *J Phys Chem B* 116: 13439-13447 doi:[10.1021/jp3066019](https://doi.org/10.1021/jp3066019)
- Skinner L.B., Barnes A.C., Salmon P.S., Fischer H.E., Drewitt J.W.E., Honkimäki V. (2012b) Structure and triclustering in Ba-Al-O glass. *Physical Review B*, 85:064201 doi:[10.1103/PhysRevB.85.064201](https://doi.org/10.1103/PhysRevB.85.064201)
- Skinner LB, Benmore CJ, Weber JKR, Wilding MC, Tumber SK, Parise JB (2013a) A time resolved high energy x-ray diffraction study of cooling liquid SiO<sub>2</sub>. *Phys Chem Chem Phys* 15: 8566-8572 doi:[10.1039/C3CP44347G](https://doi.org/10.1039/C3CP44347G)
- Skinner LB, Barnes AC, Salmon PS, Hennet L, Fischer HE, Benmore CJ, Kohara S, Weber JKR, Bytchkov A, Wilding MC, Parise JB, Farmer TO, Pozdnyakova I, Tumber SK, Ohara K (2013b) Joint diffraction and modelling approach to the structure of liquid alumina. *Phys Rev B* 87:024201 doi:[10.1103/PhysRevB.87.024201](https://doi.org/10.1103/PhysRevB.87.024201)
- Spiekermann, G, Steele-MacInnis, M, Kowalski, PM, Schmidt, C, and Jahn S (2013) Vibrational properties of silica species in MgO-SiO<sub>2</sub> glasses obtained from ab initio molecular dynamics. *Chem Geol* 346:22-33 doi:[10.1016/j.chemgeo.2012.08.020](https://doi.org/10.1016/j.chemgeo.2012.08.020)
- Spiekermann G, Harder M, Gilmore K, Zalden P, Sahle CJ, Petitgirard S, Wilke M, Biedermann N, Weis C, Morgenroth W, Tse JS, Kulik E, Nishiyama N, Yavaş H, Sternemann C (2019) Persistent Octahedral Coordination in Amorphous GeO<sub>2</sub> Up to 100 GPa by K $\beta$  X-Ray Emission Spectroscopy. *Phys Rev X* 9:011025 doi:[10.1103/PhysRevX.9.011025](https://doi.org/10.1103/PhysRevX.9.011025)
- Soignard E, Benmore CJ, Yarger JL (2010) A perforated diamond anvil cell for high-energy x-ray diffraction of liquids and amorphous solids at high pressure. *Rev Sci Instr* 81:035110 doi:[10.1063/1.3356977](https://doi.org/10.1063/1.3356977)
- Sokolov AP, Kisluk A, Soltwisch M, Quitmann D (1992) Medium-Range Order in Glasses: Comparison of Raman and Diffraction Measurements. *Phys Rev Lett* 69:1540-1543 doi:[10.1103/PhysRevLett.69.1540](https://doi.org/10.1103/PhysRevLett.69.1540)
- Sokolov AP (1998) Vibrations at the boson peak: random- and coherent-phase contributions. *J Phys:Condens Matter* 11:A213-A218 doi:[10.1088/0953-8984/11/10A/017](https://doi.org/10.1088/0953-8984/11/10A/017)
- Spiekermann G, Harder M, Gilmore K, Zalden P, Sahle ChJ, Petitgirard S, Wilke M, Biedermann N, Weis C, Morgenroth W, Tse JS, Kulik E, Nishiyama N, Yavaş H, Sternemann (2019) Persistent Octahedral Coordination in Amorphous GeO<sub>2</sub> Up to 100 GPa by K $\beta$  X-Ray Emission Spectroscopy. *Phys Rev X* 9:011025 doi:[10.1103/PhysRevX.9.011025](https://doi.org/10.1103/PhysRevX.9.011025)
- Stavrou E, Tsiantos C, Tsofouridou RD, Kriptou S, Kontos AG, Raptis C, Capoen B, Bouazaoui M, Turrell S, Khatir S (2010) Raman scattering boson peak and differential scanning calorimetry studies of the glass transition in tellurium-zinc oxide glasses. *J Phys: Condens Matter* 22:195103 doi:[10.1088/0953-8984/22/19/195103](https://doi.org/10.1088/0953-8984/22/19/195103)
- Stebbins JF (1991) NMR evidence for five-coordinated silicon in a silicate glass at atmospheric pressure. *Nature* 351:638-639 doi:[10.1038/351638a0](https://doi.org/10.1038/351638a0)
- Stebbins JF, Oglesby JV, Xu Z (1997) Disorder among network-modifier cations in silicate glasses: New constraints from triple-quantum <sup>17</sup>O NMR. *Am Mineral* 82:1116-1124 doi:[10.2138/am-1997-11-1209](https://doi.org/10.2138/am-1997-11-1209)
- Stebbins JF, Poe BT (1999) Pentacoordinate silicon in high-pressure crystalline and glassy phases of calcium disilicate (CaSi<sub>2</sub>O<sub>5</sub>). *Geophys Res Lett* 26:2521-2523 doi:[10.1029/1999GL008364](https://doi.org/10.1029/1999GL008364)
- Stolper E, Walker D, Hager BH, Hays JF (1981) Melt Segregation from Partially Molten Source Regions: The Importance of Melt Density and Source Region Size. *J Geophys Res* 86:6261-6271 doi:[10.1029/JB086iB07p06261](https://doi.org/10.1029/JB086iB07p06261)
- Susman S, Volin KJ, Price DL, Grimsditch M, Rino JP, Kalia RK, Vashishta P, Gwanmesia G, Wang Y, Liebermann RC (1991) Intermediate-range order in permanently densified vitreous SiO<sub>2</sub>. A neutron-diffraction and molecular-dynamics study. *Phys Rev B* 43:1194-1197 doi:[10.1103/PhysRevB.43.1194](https://doi.org/10.1103/PhysRevB.43.1194)
- Takaishi T, Takahashi M, Jin J, Uchino T, Yoko T, Takahashi M (2005) Structural study on PbO-SiO<sub>2</sub> glasses by x-ray and neutron diffraction and <sup>29</sup>Si MAS NMR Measurements. *Journal of the American Ceramic Society*, 88: 1591-1596 doi:[10.1111/j.1551-2916.2005.00297.x](https://doi.org/10.1111/j.1551-2916.2005.00297.x)
- Takahashi Y, Osada M, Masai H, Fujiwara T (2009) Crystallization and nanometric heterogeneity in glass: In situ observation of the boson peak during crystallization. *Phys Rev B* 79:214204 doi:[10.1103/PhysRevB.79.214204](https://doi.org/10.1103/PhysRevB.79.214204)
- Tangeman JA, Philips BL, Nordine PC, Weber JKR (2004) Thermodynamics and structure of single- and two-phase yttria-alumina glasses. *J Phys Chem B* 108:10663-10671 doi:[10.1021/jp027779e](https://doi.org/10.1021/jp027779e)

- Taraskin SN, Elliott SR (1997) Nature of vibrational excitations in vitreous silica. *Phys Rev B* 56:8605-8622 doi:[10.1103/PhysRevB.56.8605](https://doi.org/10.1103/PhysRevB.56.8605)
- Taraskin SN, Elliot SR (1999) Low-frequency vibrational excitations in vitreous silica: the Ioffe–Regel limit. *J Phys Condens Matter* 11:A219-A227 doi:[10.1088/0953-8984/11/10A/018](https://doi.org/10.1088/0953-8984/11/10A/018)
- Taraskin SN, Elliott S, Loh YH, Nataranjan G (2001) Origin of the Boson Peak in Systems with Lattice Disorder. *Phys Rev Lett* 86:1255-1261 doi:[10.1103/PhysRevLett.86.1255](https://doi.org/10.1103/PhysRevLett.86.1255)
- Thomas BWM, Mead RN, Mountjoy G (2006) A molecular dynamics study of the atomic structure of  $(\text{CaO})_x(\text{Al}_2\text{O}_3)_{1-x}$  glass with  $x = 0.625$  close to the eutectic. *J Phys: Condens Matter* 18:4697-4708 doi:[10.1088/0953-8984/18/19/021](https://doi.org/10.1088/0953-8984/18/19/021)
- Toplis MJ, Kohn SC, Smith ME, Poplett IJF (2000) Fivefold-coordinated aluminum in tectosilicate glasses observed by triple quantum MAS NMR. *Am Mineral* 85:1556-1560 doi:[10.2138/am-2000-1031](https://doi.org/10.2138/am-2000-1031)
- Trachenko K, Dove MT (2002) Densification of silica glass under pressure. *J Phys: Condens Matter* 14:7449 doi:[10.1088/0953-8984/14/32/304](https://doi.org/10.1088/0953-8984/14/32/304)
- Umari P, Pasquarello A (2002) Modeling of the Raman spectrum of vitreous silica: concentration of small ring structures. *Physica B* 316-317:572-574 doi:[10.1016/S0921-4526\(02\)00576-8](https://doi.org/10.1016/S0921-4526(02)00576-8)
- Umari P, Gonze X, Pasquarello A (2003) Concentration of Small Ring Structures in Vitreous Silica from a First-Principles Analysis of the Raman Spectrum. *Phys Rev Lett* 90:867-755 doi:[10.1103/PhysRevLett.90.027401](https://doi.org/10.1103/PhysRevLett.90.027401)
- Vaccari M, Aquilanti G, Pascarelli S, Mathon O (2009) A new EXAFS investigation of local structural changes in amorphous and crystalline  $\text{GeO}_2$  at high pressure. *J Phys Condens Matter* 21:145403 doi:[10.1088/0953-8984/21/14/145403](https://doi.org/10.1088/0953-8984/21/14/145403)
- Virgo D, Mysen BO (1985) The structural state of iron in oxidized vs. reduced glasses at 1 atm: A  $^{57}\text{Fe}$  Mössbauer study. *Phys Chem Min* 12:65-76 doi:[10.1007/BF01046829](https://doi.org/10.1007/BF01046829)
- Waasmaier D, Kirfel A (1995) New analytical scattering-factor functions for free atoms and ions. *Acta Cryst. A* 51:416-431 doi:[10.1107/S0108767394013292](https://doi.org/10.1107/S0108767394013292)
- Wang Z, Cooney TF, Sharma SK (1993) High temperature structural investigation of  $\text{Na}_2\text{O}\cdot 0.5\text{Fe}_2\text{O}_3\cdot 3\text{SiO}_2$  and  $\text{Na}_2\text{O}\cdot \text{FeO}\cdot 3\text{SiO}_2$  melts and glasses. *Contrib Mineral Pet* 115:112-122 doi:[10.1007/BF00712983](https://doi.org/10.1007/BF00712983)
- Wang Z, Cooney TF, Sharma SK (1995) In situ structural investigation of iron-containing silicate liquids and glasses. *Geochim Cosmochim Acta* 59:1571-1577 doi:[10.1016/0016-7037\(95\)00063-6](https://doi.org/10.1016/0016-7037(95)00063-6)
- Wang Y, Sakamaki T, Skinner LB, Jing Z, Yu T, Kono Y, Park C, Shen G, Rivers ML, Sutton SR (2013) Atomistic insight into viscosity and density of silicate melts under pressure. *Nature Commun* 5:3241 doi:[10.1038/ncomms4241](https://doi.org/10.1038/ncomms4241)
- Wang Y, Hong L, Wang Y, Schirmacher W, Zhang J (2018) Disentangling boson peaks and Van Hove singularities in a model glass. *Phys Rev B* 98:174207 doi:[10.1103/PhysRevB.98.174207](https://doi.org/10.1103/PhysRevB.98.174207)
- Warren BE (1934a) Identification of crystalline substances by means of x-rays. *J Am Ceram Soc* 17: 73-77 doi:[10.1111/j.1151-2916.1934.tb19287.x](https://doi.org/10.1111/j.1151-2916.1934.tb19287.x)
- Warren BE (1934b) The diffraction of x-rays in glass. *Phys Rev B* 45:657-661 doi:[10.1103/PhysRev.45.657](https://doi.org/10.1103/PhysRev.45.657)
- Warren BE (1934c) X-ray determination of the structure of glass. *J Am Ceram Soc* 17:249-254 doi:[10.1111/j.1151-2916.1934.tb19316.x](https://doi.org/10.1111/j.1151-2916.1934.tb19316.x)
- Warren BE, Krutter H, Morningstar O (1936) Fourier analysis of x-ray patterns of vitreous  $\text{SiO}_2$  and  $\text{B}_2\text{O}_3$ . *Journal of the American Ceramic Society* 19:202-206 doi:[10.1111/j.1151-2916.1992.tb05433.x](https://doi.org/10.1111/j.1151-2916.1992.tb05433.x)
- Waseda Y, Toguri JM (1978) The Structure of the Molten  $\text{FeO}\text{-SiO}_2$  System. *Metall Trans B* 9:595-601 doi:[10.1007/BF03257207](https://doi.org/10.1007/BF03257207)
- Waseda Y, Shiraishi Y, Toguri JM (1980) The Structure of the Molten  $\text{FeO}\text{-Fe}_2\text{O}_3\text{-SiO}_2$  System by X-ray Diffraction. *Trans Jpn Inst Met* 21:51-62 doi:[10.2320/matertrans1960.21.51](https://doi.org/10.2320/matertrans1960.21.51)
- Watanuki T, Shimomura O, Yagi T, Kondo T, Isshiki M (2001) Construction of laser-heated diamond anvil cell system for in situ x-ray diffraction study at SPring-8. *Rev Sci Instr* 72:1289-1292 doi:
- Waychunas GA, Brown Jr GE, Ponader CW, Jackson WE (1988) Evidence from X-ray absorption for network-forming  $\text{Fe}^{2+}$  in molten alkali silicates. *Nature* 332:251-253 doi:[10.1038/332251a0](https://doi.org/10.1038/332251a0)
- Weber JKR, Benmore CJ, Tangeman JA, Siewenie J, Hiera KJ (2003) Structure of Binary  $\text{CaO}\text{-Al}_2\text{O}_3$  and  $\text{SrO}\text{-Al}_2\text{O}_3$  Liquids by Combined Levitation-Neutron Diffraction. *J Neutron Res* 11:113-121 doi:[10.1080/1023816031000099746](https://doi.org/10.1080/1023816031000099746)
- Weber JKR, Abadie JG, Hixson AD, Nordine PC, Jerman GA (2004a) Glass Formation and Polyamorphism in Rare-Earth Oxide–Aluminum Oxide Compositions. *J Am Ceram Soc* 83:1868-1872



- doi:[10.1111/j.1151-2916.2000.tb01483.x](https://doi.org/10.1111/j.1151-2916.2000.tb01483.x)
- Weber JKR, Benmore CJ, Siewenie J, Urquidi J, Key TS (2004b) Structure and bonding in single- and two-phase alumina-based glasses. *Phys Chem Chem Phys* 6:2480-2483 doi:[10.1039/B314957A](https://doi.org/10.1039/B314957A)
- Weigel C, Cormier L, Galois L, Calas G (2006) Determination of Fe<sup>3+</sup> sites in a NaFeSi<sub>2</sub>O<sub>6</sub> glass by neutron diffraction with isotopic substitution coupled with numerical simulation. *Appl Phys Lett* 89:141911 doi:[10.1063/1.2359532](https://doi.org/10.1063/1.2359532)
- Weigel C, Cormier L, Calas G, Galois L, Bowron DT (2008a) Intermediate-range order in the silicate network glasses NaFe<sub>x</sub>Al<sub>1-x</sub>Si<sub>2</sub>O<sub>6</sub> (x=0,0.5,0.8,1): A neutron diffraction and empirical potential structure refinement modeling investigation. *Phys Rev B* 78:064202 doi:[10.1103/PhysRevB.78.064202](https://doi.org/10.1103/PhysRevB.78.064202)
- Weigel C, Cormier L, Calas G, Galois L, Bowron DT (2008b) Nature and distribution of iron sites in a sodium silicate glass investigated by neutron diffraction and EPSR simulation. *J Non-Cryst Solids* 354:5378-5385 doi:[10.1016/j.jnoncrsol.2008.09.030](https://doi.org/10.1016/j.jnoncrsol.2008.09.030)
- Wilding M, Bingham PA, Wilson M, Kono Y, Drewitt JWE, Brooker RA, Parise JB (2019) CO<sub>3+1</sub> network formation in ultra-high pressure carbonate liquids. *Sci Rep* 9:15416 doi:[10.1038/s41598-019-51306-6](https://doi.org/10.1038/s41598-019-51306-6)
- Wilke M, Farges F, Partzsch GM, Schmidt C, Behrens H (2007) Speciation of Fe in silicate glasses and melts by in-situ XANES spectroscopy. *Am Mineral* 92:44-56 doi:[10.2138/am.2007.1976](https://doi.org/10.2138/am.2007.1976)
- Wezka K, Salmon PS, Zeidler A, Whittaker DAJ, Drewitt JWE, Klotz S, Fischer HE, Marrocchelli D (2012) Mechanisms of network collapse in GeO<sub>2</sub> glass: high-pressure neutron diffraction with isotope substitution as arbitrator of competing models. *J Phys: Condens Matter* 24:502101 doi:[10.1088/0953-8984/24/50/502101](https://doi.org/10.1088/0953-8984/24/50/502101)
- Wilding MC, McMillan PF, Navrotsky A (2002) Thermodynamic and structural aspects of the polyamorphic transition in yttrium and other rare-earth aluminate liquids. *Physica A* 314:379-390 doi:[10.1016/S0378-4371\(02\)01045-2](https://doi.org/10.1016/S0378-4371(02)01045-2)
- Wilding MC, Wilson M, McMillan PF (2005) X-ray and neutron diffraction studies and MD simulation of atomic configurations in polyamorphic Y<sub>2</sub>O<sub>3</sub>-Al<sub>2</sub>O<sub>3</sub> systems. *Phil Trans Royal Soc A* 363:589-607 doi:[10.1098/rsta.2004.1510](https://doi.org/10.1098/rsta.2004.1510)
- Wilding MC, Benmore CJ, Weber JKR (2010) Changes in the local environment surrounding magnesium ions in fragile MgO-SiO<sub>2</sub> liquids. *Europhys Lett* 89:26005 doi:[10.1209/0295-5075/89/26005](https://doi.org/10.1209/0295-5075/89/26005)
- Wilding MC, Wilson M, McMillan PF, Benmore CJ, Weber JKR, Deschamps T, Champagnon B (2015) Structural properties of Y<sub>2</sub>O<sub>3</sub>-Al<sub>2</sub>O<sub>3</sub> liquids and glasses: An overview. *J Non-Cryst Solids* 407:228-234 doi:[10.1016/j.jnoncrsol.2014.09.044](https://doi.org/10.1016/j.jnoncrsol.2014.09.044)
- Wilke M, Partzsch GM, Bernhardt R, Lattard D (2004) Determination of the iron oxidation state in basaltic glasses using XANES at the K-edge. *Chem Geol* 213:71-87 doi:[10.1016/j.chemgeo.2005.03.004](https://doi.org/10.1016/j.chemgeo.2005.03.004)
- Wilke M (2005) Fe in magma – An overview. *Ann Geophys* 48:609-617 doi:[10.4401/ag-3222](https://doi.org/10.4401/ag-3222)
- Wilke M, Farges F, Partzsch GM, Schmidt C, Behrens H (2007) Speciation of Fe in silicate glasses and melts by in-situ XANES spectroscopy. *Am Mineral* 92:44-56 doi:[10.2138/am.2007.1976](https://doi.org/10.2138/am.2007.1976)
- Wilson M, McMillan PF (2004) Interpretation of x-ray and neutron diffraction patterns for liquid and amorphous yttrium and lanthanum aluminum oxides from computer simulation. *Phys Rev B* 69:054206 doi:[10.1103/PhysRevB.69.054206](https://doi.org/10.1103/PhysRevB.69.054206)
- Williams Q, Jeanloz R (1988) Spectroscopic Evidence for Pressure-Induced Coordination Changes in Silicate Glasses and Melts. *Science* 239:902-905 doi:[10.1126/science.239.4842.902](https://doi.org/10.1126/science.239.4842.902)
- Worrell CA, Henshall T (1978) Vibrational spectroscopic studies of some lead silicate glasses. *J Non-Cryst Solids* 29:283-299 doi:[10.1016/0022-3093\(78\)90150-3](https://doi.org/10.1016/0022-3093(78)90150-3)
- Wright AC, Clarke SJ, Howard CK, Bingham PA, Forder SD, Holland D, Martlew D, Fischer HE (2014) The environment of Fe<sup>2+</sup>/Fe<sup>3+</sup> cations in a soda–lime–silica glass. *Phys Chem Glasses: Eur J Glass Sci Technol B* 55:243-252
- Wu Z, Bonnin-Mosbah M, Duraud JP, Métrich N, Delaney JS (1999) XANES studies of Fe-bearing glasses. *J Synchrotron Rad* 6:344-346 doi:[10.1107/S0909049598015969](https://doi.org/10.1107/S0909049598015969)
- Xue X, Kanzaki M, Trønnes RG, Stebbins JF (1989) Silicon Coordination and Speciation Changes in a Silicate Liquid at High Pressures. *Science* 245:962-964 doi:[10.1126/science.245.4921.962](https://doi.org/10.1126/science.245.4921.962)
- Yamada A, Inoue T, Urakawa S, Funakoshi K-I, Funamori N, Kikegawa T, Ohfuji H, Irifune T (2007) In situ X-ray experiment on the structure of hydrous Mg-silicate melt under high pressure and high temperature. *Geophys Res Lett* 34:L10303 doi:[10.1029/2006GL028823](https://doi.org/10.1029/2006GL028823)

- Yamada A, Wang Y, Inoue T, Yang W, Park C, Yu T, Shen G (2011) High-pressure x-ray diffraction studies on the structure of liquid silicate using a Paris–Edinburgh type large volume press. *Rev Sci Instr* 82:015103 doi:[10.1063/1.3514087](https://doi.org/10.1063/1.3514087)
- Yarger JL, Smith KH, Nieman RA, Diefenbacher J, Wolf GH, Poe BT, McMillan PF (1995) Al Coordination Changes in High-Pressure Aluminosilicate Liquids. *Science* 270:1964-1967 doi:[10.1126/science.270.5244.1964](https://doi.org/10.1126/science.270.5244.1964)
- Zahra AM, Zahra CY, Piriou B (1993) DSC and Raman studies of lead borate and lead silicate glasses. *J Non-Cryst Solids* 155:45–55 doi:[10.1016/0022-3093\(93\)90470-I](https://doi.org/10.1016/0022-3093(93)90470-I)
- Zeidler A, Drewitt JWE, Salmon PS, Barnes AC, Crichton WA, Klotz S, Fischer HE, Benmore CJ, Ramos S, Hannon AC (2009) Establishing the structure of GeS<sub>2</sub> at high pressures and temperatures: a combined approach using x-ray and neutron diffraction. *J Phys: Condens Matter* 21:474217 doi:[10.1088/0953-8984/21/47/474217](https://doi.org/10.1088/0953-8984/21/47/474217)
- Zeidler A, Wezka K, Rowlands RF, Whittaker DAJ, Salmon PS, Polidori A, Drewitt JWE, Klotz S, Fischer HE, Wilding MC, Bull CL, Tucker MG, Wilson M (2014) High-Pressure Transformation of SiO<sub>2</sub> Glass from a Tetrahedral to an Octahedral Network: A Joint Approach Using Neutron Diffraction and Molecular Dynamics. *Phys Rev Lett* 113:135501 doi:[10.1103/PhysRevLett.113.135501](https://doi.org/10.1103/PhysRevLett.113.135501)
- Zeidler A, Salmon PS, Skinner LB (2014) Packing and the structural transformations in liquid and amorphous oxides from ambient to extreme conditions. *Proc Nat Acad Sci* 111:10045-10048 doi:[10.1073/pnas.1405660111](https://doi.org/10.1073/pnas.1405660111)
- Zeidler A, Salmon PS (2016) Pressure-driven transformation of the ordering in amorphous network-forming materials. *Phys Rev B* 93:214204 doi:[10.1103/PhysRevB.93.214204](https://doi.org/10.1103/PhysRevB.93.214204)
- Zha C-s, Hemley RJ, Mao H-k, Duffy TS, Meade C (1994) Acoustic velocities and refractive index of SiO<sub>2</sub> glass to 57.5 GPa by Brillouin scattering. *Phys Rev B* 50:13105-13112 doi:[10.1103/PhysRevB.50.13105](https://doi.org/10.1103/PhysRevB.50.13105)
- Zhai S, Ito E (2011) Recent advances of high-pressure generation in a multianvil apparatus using sintered diamond anvils. *Geosci Front* 2:101-106 doi:[10.1016/j.gsf.2010.09.005](https://doi.org/10.1016/j.gsf.2010.09.005)
- Zhang HL, Hirschmann MM, Cottrell E, Newville M, Lanzirotti A (2016) Structural environment of iron and accurate determination of Fe<sup>3+</sup>/ΣFe ratios in andesitic glasses by XANES and Mössbauer spectroscopy. *Chem Geol* 428:48-58 doi:[10.1016/j.chemgeo.2016.02.022](https://doi.org/10.1016/j.chemgeo.2016.02.022)